



**DEVELOPMENT OF AMPEROMETRIC BIOSENSOR WITH  
CYCLOPENTADIENYL RUTHENIUM(II) THIOLATO *SCHIFF* BASE SELF-  
ASSEMBLED MONOLAYER (SAM) ON GOLD**

**LAWRENCE AWA TICHA**

**A thesis submitted in fulfilment of the requirements for the degree of  
Magister Scientiae in Chemistry**

Department of Chemistry

University of the Western Cape

DATE: November 2007

Supervisors:

Professor Priscilla Baker

And

Professor Emmanuel I. Iwuoha

## **DECLARATION**

I declare that “*Development of amperometric biosensor with cyclopentadienyl ruthenium (II) thiolato Schiff base self-assembled monolayer (SAM) on gold*” is my own work, that it has not been submitted for any other degree examination in any other university, and that all the sources I have used or quoted have been indicated and acknowledged by complete references.

**LAWRENCE AWA TICHA**



.....

*Signature*

## **ACKNOWLEDGEMENTS**

**I express profound gratitude to the Almighty God for the gift of life, and opportunity for the fulfillment of ambitions.**

**My parents Mr. and Mrs. Ticha, for my forthright upbringing and legacy of self-belief, my late grand mother, Ma Monica Tewah; may her soul rest in peace.**

**My supervisors, Dr. P. Baker and Prof. Emmanuel I. Iwuoha for their camaraderie and financial leverage in actualizing this research. Without your advice and support, this project wouldn't have been realized. THANK YOU.**

**To all the loving people of the Sensor Research Laboratory for constant support and encouragement.**

**To Dr. Salam Titinchi and Dr. Hanna Abbo of the organometallic group for advice and direction, thank you.**

**To the staff of the Science Faculty in general and the Chemistry department in particular for allowing this research to be carried out.**

**To my wife Mrs. Ticha Victoire Meshi for her understanding, love and support – you are wonderful darling.**

**To Mr. Esau Muluh Ticha, Ticha Ignatius Khan, Ticha Odilia Fri and Ticha Loveline Tse.**

**Without your constant motivations, this dream would not have been realized; thank you.**

**A special thanks to the National Research foundation (NRF) of South Africa for financial support.**

## TABLE OF CONTENTS

<b>Contents:</b>	<b>Page No</b>
<b>Title page</b>	i
<b>Declaration</b>	ii
<b>Acknowledgements</b>	iii
<b>Table of contents</b>	iv-viii
<b>List of scheme</b>	x
<b>List of figures</b>	ix-xii
<b>List of tables</b>	vii
<b>Keywords</b>	vii
<b>Research Outcomes</b>	xiv
<b>Abstract</b>	xv
 <b>CHAPTER ONE</b>	
1.1 General Introduction	1-2
1.2 Some Applications of Self-Assembled monolayers (SAMs)	2
1.2.1 SAMs as Etch Resists	2
1.2.2 SAMs as Barriers to Electron Transport	3
1.2.3 SAMs for Electrochemistry	3-4
1.3 Transition Metal Thiolates	5
1.4 Rationale and Objectives	6



1.5 Aim of Study	7
1.6 Mile Stones	8
<b>CHAPTER TWO</b>	<b>9</b>
2.1 Literature Review	9
2.1.1 Introduction	9
2.2 Biosensor	10
2.2.1 Components of a Biosensors	10-13
2.2.2 Mediators	13-15
2.3 Enzymes	16
2.3.1 Factors Affecting enzyme Activity	16
2.3.1.1 Enzyme and Substrate concentration	16
2.3.1.2 Temperature and pH	16-17
2.3.2 Amperometric Detection	17-18
2.4 Immobilization Techniques	19-20
2.4.1 Cross-linking	20-20
2.4.2 Covalent Binding	22-23
2.4.3 Physical Adsorption	23-24
2.4.4 Behaviour of Immobilized Enzymes	25
2.4.5 Stability of Immobilized Enzymes	25
2.4.6 Kinetic Parameters of Immobilized enzymes	25-26
2.4.7 Peroxidases	27
2.5 Self-Assembled Monolayer (SAM)	28-29



2.5.1 Preparation of SAMs	30-31
2.5.2 The Role of Solvents in SAM Preparation	31-33
2.5.3 Effect of Temperature on SAMs formation	33
2.5.4 Concentration and Immersion Time	34
2.5.5 The Purity of Thiol Solution	35
2.5.6 Why a Clean Substrate?	35-36
2.5.7 Rationale for the Choice of gold as Standard	36-37
2.5.8 Nature of the Metal SAM Interface	37-38
2.5.9 Thermodynamic Analysis of the Gold Thiolate Bonds	38-39
2.5.10 Mechanisms of Self-assembled Monolayers	40
2.5.11 Defects Found in SAMs	42
2.5.12 Rationale for SAMs Modification	43-44
2.6 Pulse Voltammetric Techniques	45-46
2.6.1 Cyclic Voltammetry (CV)	46-50
2.6.2 Differential Pulse Voltammetry (DPV)	50-51
2.6.3 Osteryoung Square Wave Voltammetry (OSWV)	52-53
<b>CHAPTER THREE</b>	<b>54</b>
3.1 Synthesis and Characterization of Cyclopentadienylruthenium(II) Thiolato Schiff Base Complex	54
3.1.1 Introduction	54
3.2 Experimental	54
3.2.1 Materials	54-55

3.2.2 Instrumentation	55
3.2.3 Buffers and Solutions	55
3.3 Methodology	55
3.3.1 Synthesis of OHCC <sub>6</sub> H <sub>4</sub> O(CH <sub>2</sub> ) <sub>2</sub> SMe	56
3.3.2 Synthesis of HSC <sub>6</sub> H <sub>4</sub> NC(H)C <sub>6</sub> N <sub>4</sub> O(CH <sub>2</sub> ) <sub>2</sub> SMe	57
3.3.3 Synthesis of	
[Ru(SC <sub>6</sub> H <sub>4</sub> NC(H)C <sub>6</sub> H <sub>4</sub> OCH <sub>2</sub> CH <sub>2</sub> SMe)(η <sup>5</sup> -C <sub>2</sub> H <sub>5</sub> ) <sub>2</sub>	57-58
3.4 Immobilization of cyclopentadienylruthenium(II)thiolato Schiff base on gold electrode	58
3.5 Immobilization of protein (HRP) on SAM	59
3.5.1 Electrochemical Characterization of cyclopentadienylruthenium(II) thiolato Schiff base complex in solution	61
3.5.2 Electrochemical characterization of the Schiff base complex on gold electrode	61
3.6 Electrochemical measurements	62-63
<b>CHAPTER FOUR</b>	<b>64</b>
4 Results and Discussions	64
4.1 Synthesis of 4-alkoxybenzaldehyde, OHCC <sub>6</sub> H <sub>4</sub> O(CH <sub>2</sub> ) <sub>2</sub> SMe	64-65
4.2 Synthesis of Schiff base ligand, HSC <sub>6</sub> H <sub>4</sub> NC(H)C <sub>6</sub> N <sub>4</sub> O(CH <sub>2</sub> ) <sub>2</sub> SMe	65-67
4.3 Synthesis of cyclopentadienyl ruthenium (II) thiolato Schiff base complex,	
[Ru(SC <sub>6</sub> H <sub>4</sub> NC(H)C <sub>6</sub> H <sub>4</sub> OCH <sub>2</sub> CH <sub>2</sub> SMe)(η <sup>5</sup> -C <sub>2</sub> H <sub>5</sub> ) <sub>2</sub>	69-70
4.4 Electrochemical characterization of cyclopentadienyl ruthenium (II) thiolato Schiff base complex in solution	72-77

4.5 Characterization of $[\text{Ru}(\text{SC}_6\text{H}_4\text{NC}(\text{H})\text{C}_6\text{H}_4\text{OCH}_2\text{CH}_2\text{SME})(\eta^5\text{-C}_2\text{H}_5)_2]$ on gold	78-85
4.5.1 Stability of SAM	86
4.6 Scanning Electron Microscopy Analysis	87
4.7 Electrocatalytic reduction of peroxides at the Au//SAM/HRP-modified electrode	89-90
4.7.1 Electrocatalytic reduction of peroxides using CV at the Au//SAM/HRP-modified electrode	91
4.7.2 Electrocatalytic reduction of peroxides using OSWV at the Au//SAM/HRP-modified electrode	94-101
4.8 Conclusion	102-103
4.9 References	105-110





## **LIST OF FIGURES:**

**Fig. 2. 1:** Schematic diagram of a typical biosensor set-up

**Fig. 2.2:** A diagrammatic illustration of the mechanism of self-assembled monolayer formation.  
The initial adsorption is fast (seconds) while the final (organization) phase takes >15 h.

**Fig. 2.3:** A typical cyclic voltammogram showing anodic ( $E_{p,a}$ ) and cathodic ( $E_{p,c}$ ) peaks, together with anodic ( $i_{p,a}$ ) and cathodic ( $i_{p,c}$ ) peak currents.

**Fig. 2.4:** Potential wave form for differential pulse voltammetry

**Fig. 2.5:** A typical differential pulse voltammogram

**Fig. 2.6:** Potential wave form for square wave voltammetry

**Fig. 2.7:** A typical square wave voltammogram

**Fig. 3.1:** A typical set-up of an electrochemical cell showing the working (WE), reference (RE), counter (auxiliary)(CE) electrodes and a degassing pipe (P)

**Fig. 4.1a** .Infrared spectrum of the Schiff base ligand. The absence of the carbonyl peak at  $1730\text{ cm}^{-1}$  and the presence of the imine peak at  $1590.83\text{ cm}^{-1}$  indicate the formation of the Schiff base ligand

**Fig. 4.1a**  $^1\text{NMR}$  of 4-alkoxybenzaldehyde (b)  $^1\text{NMR}$  of Schiff base ligand

**Fig. 4:** Cyclic voltammograms of a  $2 \times 10^{-3}\text{ M}$

$[\text{Ru}(\text{SC}_6\text{H}_4\text{NC}(\text{H})\text{C}_6\text{H}_4\text{OCH}_2\text{CH}_2\text{SME})(\eta^5\text{-C}_2\text{H}_5)_2]$  on a bare gold electrode

containing 0.1 M TBATFB at a potential window of

(a) -800 mV/s to +800 mV/s and (b) -200 mV/s to +600 mV/s at a scan rate of 50 mV/s

**Fig. 4.4a:** Plot of  $v^{-1/2}$  vs. anodic peak current; the high correlation ( $r^2 = 0.988$ ) indicating electron diffusion limited response of the Au//SAM electrode

**Fig. 4.4b:** Reversibility plots for the voltammograms of  $2 \times 10^{-3}$  M

$[\text{Ru}(\text{SC}_6\text{H}_4\text{NC}(\text{H})\text{C}_6\text{H}_4\text{OCH}_2\text{CH}_2\text{SME})(\eta^5\text{-C}_2\text{H}_5)_2]$  from -200 to +600 mV/s.

The scan rate was varied from 5 to 300 mV/s. All other conditions are as in fig. 4.3b.

The superimposition of the plots demonstrate the reversibility of the  $\text{Ru}^{\text{III}}/\text{Ru}^{\text{II}}$  redox couple

**Fig. 4.5:** Bare Au (broken line) and Au + SAM (smooth line) in 0.1 M PBS. SAM formation on the gold electrode was indicated by a significant suppression of the oxygen redox peak of the gold electrode. No electronic communication was observed between the Au//SAM and the solution, hence the surface of the gold electrode was completely covered by the SAM, excluding ions and water from the underlying gold electrode

**Fig. 4.5.1:** Schematic representation of a single molecule, showing self-assembled monolayer formation through covalent bond formation between the thiol-end group and the Gold-electrode surface

**Fig. 4.5.2:** Cyclic voltammograms of the NaOH-treated SAM-modified gold electrode

in 0.1 M phosphate, pH 6.9 at a scan rate of 50 mV/s.

Before and after cycling in 0.1 NaOH

**Fig. 4.5.3:** (a) Plot of formal potentials vs. pH at a scan rate of  $50 \text{ mVs}^{-1}$ . pH was

varied from 3.3 to 9.3 with a slope of  $-34 \text{ mV pH}^{-1}$ , demonstrating a

two electron, one proton redox process. (b) OSWV voltammograms as a function of pH.

The electrode was held at a constant potential of 200 mV.

**Fig. 4.6.1:** Cyclic voltammograms (5 mV/s scan rate) of SAM//HRP-modified

Au electrode in 0.1 M phosphate buffer, pH 6.8 for  
0  $\mu\text{M}$ , 0.1  $\mu\text{M}$ , 0.2  $\mu\text{M}$  and 0.3  $\mu\text{M}$   $\text{H}_2\text{O}_2$  under anaerobic conditions

**Fig. 4.6.2:** Cyclic voltammograms (5 mV/s scan rate) of SAM//HRP-modified  
Au electrode in 0.1 M phosphate buffer, pH 6.8 for  
0  $\mu\text{M}$ , 0.1  $\mu\text{M}$ , 0.2  $\mu\text{M}$  and 0.3  $\mu\text{M}$  Cumene hydroperoxide under anaerobic conditions

**Fig. 4.6.3:** Cyclic voltammograms (5 mV/s scan rate) of SAM//HRP-modified  
Au electrode in 0.1 M phosphate buffer, pH 6.8 for  
0  $\mu\text{M}$ , 0.1  $\mu\text{M}$ , 0.2  $\mu\text{M}$  and 0.3  $\mu\text{M}$  Tert- butyl hydroperoxide under anaerobic conditions

**Fig. 4.6.4:** OSWV (4 mV step potential, 25 mV amplitude, 15 Hz frequency)  
voltammograms of Au//SAM/HRP-modified electrode in  
0.1 M phosphate buffer, pH 6.8 for 0.00  $\mu\text{M}$ , 0.10  $\mu\text{M}$ , 0.20  $\mu\text{M}$  and 0.03  $\mu\text{M}$   $\text{H}_2\text{O}_2$   
under anaerobic conditions.

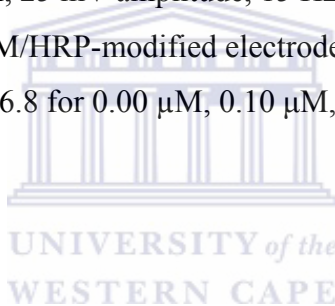


**Fig. 4.6.5:** OSWV (4 mV step potential, 25 mV amplitude, 15 Hz frequency)  
voltammograms of Au//SAM/HRP-modified electrode in 0.1 M phosphate buffer,  
pH 6.8 for 0.00  $\mu\text{M}$ , 0.10  $\mu\text{M}$ , 0.20  $\mu\text{M}$  and 0.30  $\mu\text{M}$  Cumene hydroperoxide  
under anaerobic conditions

**Fig 4.6.7:** Calibration curve of hydrogen peroxide biosensor illustrating the  
linear range (inset) of the biosensor with a detection limit of 6.45  $\mu\text{M}$  and  $r^2 = 0.991$

**Fig 4.6.8:** Calibration curve of cumene hydro peroxide biosensor illustrating the  
linear range (inset) of the biosensor with a detection limit of 6.92  $\mu\text{M}$  and  $r^2 = 0.988$ .

**Fig 4.6.9:** Calibration curve of Tert-butyl hydroperoxide biosensor illustrating the  
linear range (inset) of the biosensor with a detection limit of 7.01  $\mu\text{M}$  and  $r^2 = 0.985$ .

## LIST OF TABLES

**Table 2.1:** Examples of biosystem-transducer, measurement mode and potential applications

**Table 2.2:** Examples of head groups and substrates used in forming SAMs on metals, Oxides and Semiconductors

**Table 4.1:** Peroxides and their respective biosensor analyses



## LIST OF SCHEMES

**Scheme 1:** Reaction scheme for the synthesis of

[Ru(SC<sub>6</sub>H<sub>4</sub>NC(H)C<sub>6</sub>H<sub>4</sub>OCH<sub>2</sub>CH<sub>2</sub>SMe)(η<sup>5</sup>-C<sub>2</sub>H<sub>5</sub>)<sub>2</sub>] complex via Williamson and Schiff base condensation reaction. Compounds (a) OHCC<sub>6</sub>H<sub>4</sub>O(CH<sub>2</sub>)<sub>2</sub>Sme, (b) HSC<sub>6</sub>H<sub>4</sub>NC(H)C<sub>6</sub>N<sub>4</sub>O(CH<sub>2</sub>)<sub>2</sub>SMe and (c)) [Ru(SC<sub>6</sub>H<sub>4</sub>NC(H)C<sub>6</sub>H<sub>4</sub>OCH<sub>2</sub>CH<sub>2</sub>SMe)(η<sup>5</sup>-C<sub>2</sub>H<sub>5</sub>)<sub>2</sub>

**Fig. 4.2:** A schematic illustration of the electrocatalytic reduction of peroxides at the Au//SAM/HRP-modified gold electrode.

## **KEY WORDS**

Self-assembled monolayer (SAM)

Cyclopentadienylruthenium(II) thiolato Schiff base

Biosensors

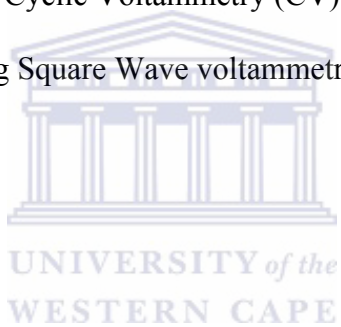
Electrostatic doping

Horseradish peroxidase

Peroxides

Cyclic Voltammetry (CV)

Osteryoung Square Wave voltammetry (OSWV)



## RESEARCH OUTCOMES

Amperometric Biosensors with cyclopentadienylruthenium(II) Thiolato Schiff base Self-Assembled monolayer on Gold.

L.A. Ticha, PGL Baker, Amir Al-Ahmed, Hana S. Abbo, Salam J.J. Titinchi, E.I. Iwuoha  
*SensorLab, Department of Chemistry, University of the Western Cape, Bellville 7535, South Africa.*  
**(Student poster presentation winner at the 38<sup>th</sup> National Convention of the South African Chemical Institute (SACI), Durban, 3-12 December 2006).**

A novel Organic Peroxide Biosensor via the Direct Electrochemistry of Horseradish Peroxidase (HRP) Immobilized on a Cyclopentadienyl ruthenium (II) thiolato Schiff base self-assembled mono layer (SAM) on Gold.

L.A. Ticha, PGL Baker, T.T. Waryo, E.I. Iwuoha  
*Sensor Lab., Department of Chemistry, University of the Western Cape, Bellville 7535, South Africa.*  
**(Poster presented at the Southern and Eastern Network of Analytical Chemist (SEANAC), Gaborone, Botswana 15-18 July 2007)**

Electrocatalytic Responses of novel cyclopentadienylruthenium(II) Thiolato Schiff base Self-Assembled mono layer on Gold.

L.A. Ticha, Priscilla G.L. Baker, Hanna S. Abbo, Salam J.J. Titinchi, Emmanuel I. Iwuoha  
*SensorLab, Department of Chemistry, University of Western Cape,*  
*Private Bag X17, Bellville 7535, Cape Town, South Africa* **(Paper submitted to Sensors)**

## ABSTRACT

A novel cyclopentadienylruthenium(II) thiolato Schiff base,  $[\text{Ru}(\text{SC}_6\text{H}_4\text{NC}(\text{H})\text{C}_6\text{H}_4\text{OCH}_2\text{CH}_2\text{SMe})(\eta^5\text{-C}_2\text{H}_5)_2]$  was synthesized and deposited as a self-assembled monolayer (SAM) on a gold electrode. Effective electronic communication between the Ru(II) centers and the gold electrode was established by electrostatically cycling the Schiff base-doped gold electrode in 0.1 M NaOH from -200 mV to +600 mV. The SAM-modified gold electrode (Au/SAM) exhibited quasi-reversible electrochemistry. The integrity of this electro-catalytic SAM, with respect to its ability to block and electro-catalyze certain Faradaic processes, was interrogated using Cyclic and Osteryoung Square Wave voltammetric experiments. The formal potential,  $E^0$ , varied with pH to give a slope of about -34 mV  $\text{pH}^{-1}$ . The surface concentration,  $\Gamma$ , of the ruthenium redox centers was found to be  $1.591 \times 10^{-11} \text{ mol cm}^{-2}$ . By electrostatically doping the Au/SAM/Horseradish peroxidase at an applied potential of +700 mV vs Ag/AgCl, a biosensor was produced for the amperometric analysis of hydrogen peroxide, cumene hydroperoxide and tert-butylhydroperoxide. The electrocatalytic-type biosensors displayed typical Michaelis-Menten kinetics with their limits of detection of 6.45  $\mu\text{M}$ , 6.92  $\mu\text{M}$  and 7.01  $\mu\text{M}$  for hydrogen peroxide, cumene hydroperoxide and tert-butylhydroperoxide respectively.

# **CHAPTER ONE**

## **1.1 General Introduction:**

The concept of modified electrodes is one of the exciting developments in the field of electroanalytical chemistry. Different strategies have been employed for the modification of the electrode surface. Molecules that adsorb strongly to a surface and have shapes that pack well in two dimensions are used to form self-assembled monolayer (SAM). Chemical systems that exhibit self-assembly include thiols, disulfides and sulfides on gold [1, 2], silanes on silicon dioxides, fatty acids on metal oxide surfaces, phosphonates on phosphonate surfaces, and isocyanides on platinum [3]. Of all the types of self-assembled monolayers that have been studied, two systems have shown the greatest promise for providing an organic surface with a uniform chemical structure: adsorption of organosulfur compounds on noble metals such as gold, silver and reaction of alkyltrichlorosilanes with silicon or glass [4-6]. Exposure of a gold surface to a dilute solution (1.0 mM) of *n*-alkanethiol results in a chemisorbed monolayer that is densely packed in two dimensions and excludes ions and water from the underlying gold electrode [7,8]. The thermodynamically favorable formation of the gold-thiolate bond makes the gold-thiol system ideal for monolayer self assembly schemes, and the stability of that bond over a wide range of applied potential makes such a system suitable for electrochemical studies. Self-assembly chemistry offers advantages over other approaches to electrode surface modification such as polymer films, which are usually much thicker and have considerable tertiary structure, and transferred Langmuir-Blodgett (LB) films, which often contain many defects and can be intrinsically unstable. The main motivations behind the modification of the electrode surface are:



- 1- Improved electrocatalysis
- 2- Freedom from surface fouling and
- 3- Prevention of undesirable reactions competing kinetically with the desired electrode process.

## **1.2. Some applications of self-assembled monolayers (SAMs):**

### **1.2.1. SAMs as Etch Resists:**

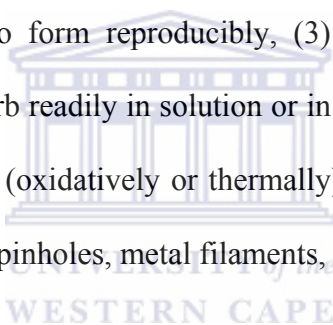
Hydrophobic SAMs formed from long-chain alkanethiols ( $n > 16$ ) can protect metal films from corrosion by aqueous wet-chemical etchants [9]. Combining this ability with techniques for generating inplane patterns of thiols makes it possible to fabricate micro- and nanostructures composed of gold, silver, copper, palladium, platinum, and gold/palladium alloys. Some of the parameters that determine the minimum critical dimensions and quality (as measured by the density of pinhole defects on etching and on the edge roughness) of the structures are the composition of the SAM, the density of defects in the SAM, the selectivity of the wet chemical etchant, and the morphology of the thin film. The addition of amphiphiles, such as octanol, or use of polymeric complexing agents, such as polyethyleneimine, decreases the number of pits and pinholes

produced in the surfaces of etched structures, controls the vertical profile of the edges of etched features, and enables the use of SAMs as resists to pattern thick electrodeposited films.

### **1.2.2. SAMs as Barriers to Electron Transport:**

Processes that transfer electrons from one location to another over nanometer-scale distances (1-100 nm) are fundamental to important redox processes in biology (photosynthesis, respiration)

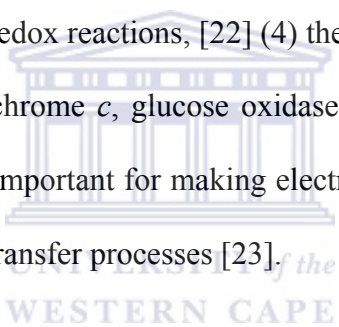
[10] and to the operation of a wide range of devices, including photovoltaics, transistors, and catalysts [11-13]. The mechanisms of electron transfer in bulk materials (such as metals and semiconductors) and in homogeneous solutions of coupled redox species are reasonably well-understood [14]. Charge-transfer processes in biological systems are, however, often mediated by organic molecules, and future electronic systems may also involve electron transport through organic matter. The relationships between molecular and solid-state structure and the mechanisms for charge transfer in these types of systems are not well-established [15, 16]. SAMs can provide a clear understanding of these systems since: - (1) they are essentially dielectric layers with relatively few defects and structures that can be controlled through molecular synthesis, (2) they are easy to form reproducibly, (3) they form highly ordered and dense structures, (4) they do not desorb readily in solution or in a vacuum. Their disadvantages are that they are not particularly stable (oxidatively or thermally), especially relative to silicon dioxide, and show a number of defects (pinholes, metal filaments, etc.).



### **1.2.3. SAMs for Electrochemistry:**

Chemical modification of an electrode for electrochemistry makes it possible to generate barrier layers. These layers prevent free diffusion of electroactive species to the surface of the electrode [17]. SAMs are more convenient (and more effective) choices for modifying electrodes in electrochemistry than Langmuir-Blodgett (LB) films or nonspecific physisorbed films because they form spontaneously, are easy to handle mechanically, and are relatively stable in solutions of electrolytes, that is, they do not desorb readily. There are two experimental configurations used commonly in electrochemistry for studying electron transfer processes with SAM-modified electrodes. One strategy uses a thick (1-2 nm), hydrophobic SAM to block a redox species

(dissolved in the surrounding electrolyte solution) from diffusing to the surface of the electrode itself [18]. A second approach uses a mixed SAM where one molecular component terminates with an electroactive group (for example, ferrocene or ruthenium pentaamine); the immobilization of the redox species on the SAM minimizes effects of diffusion in the measured current responses. [19,20]. Some of the charge-transfer phenomena studied with these SAM-modified electrodes include (1) the parameters (distance from the surface, electrolyte, temperature, metal) affecting electron transfer through alkane chains [21] and through unsaturated chains (e.g., polyphenylene vinylene, polyphenylene ethynylene), (2) coupled electron-proton-transfer reactions, (3) the effect of solvation of electroactive species in hydrophobic environments on redox reactions, [22] (4) the effect of orientation and conformation of electroactive proteins (cytochrome *c*, glucose oxidase, peroxidases) on the rates of electron transfer across SAMs-a factor important for making electrochemical sensors to detect enzymatic activity and studying electron-transfer processes [23].



### **1.3. Transition metal thiolates:**

Thiolates are presently a subject of great interest in the chemistry of complexes involving transition-metal elements and soft ligands. The manifold electronic and steric capabilities offered by the monodentate ligands  $\text{RS}^-$  and the bidentate chelate ligands  $\text{SRS}^-$  have been used to stabilize a broad spectrum of mononuclear, oligomeric, and polymeric complexes with remarkable structures and properties. Sulfides (thiolates) are powerful bridging ligands,

particularly for low-oxidation state metal centers. Thiolate ligands ( $L_nM-SR$ ) in particular have been well documented over the last several decades [24]. It is well-documented that transition metals easily undergo redox processes by donating or accepting electrons by virtue of the fact that they are capable of exhibiting multiple oxidation states [25]. Thiolates and mixed sulfide-thiolates of the late open and closed-shell 3d metals (Fe, Co, Ni, Cu, Zn) and some of their homologues (Au, Cd, Hg), as well as of Mo, Ru are of particular importance as model complexes for biologically important metal centers coordinated sulfur.

The above mentioned transition metals would be suitable candidates for electrochemical investigations as the voltage/potential required to access their different oxidation states is easy to achieve. It is also expected that there would be a minimal signal interference attributed to the electrochemical behavior of  $H_2O$ ,  $H_2O_2$ ,  $H_2$ , and  $O_2$  whose redox species are formed at very positive/negative potentials and is outside the range of the potential window of these metals. Thus, this allows us to evaluate the electrocatalytic response of horseradish peroxidase to peroxides when immobilized on the thiolato Schiff base self-assembled monolayer on a gold electrode.

#### **1.4. Rationale and Objectives:**

Peroxides pose a special threat to the environmental. Organic peroxides can be severe fire and explosion hazard. These peroxides are commonly used in household bleaching, in deodorants, sewerage treatment and as disinfectants. Exposure to hydrogen peroxide takes place through inhalation of damp or mist air, through food uptake and through skin or eye contact. Hydrogen peroxide can irritate the eyes, skin and mucous membranes. Exposure of the eyes to concentrations of 5% or more can result in permanent eye damage. Tests with laboratory animals

from the American International Agency on Cancer Research (IARC) show that hydrogen peroxide can be carcinogenic to animals. Laboratory tests with bacteria show that it is mutagenic; it changes and damages DNA. When humans inhale hydrogen peroxide, it causes lung irritation. Skin exposure causes painful blisters, burns and skin whitening. Organs that are extra susceptible to hydrogen peroxide exposure are the lungs, the intestines, the thymus, the liver and the kidney.

Usually, the detection and quantification of peroxides in the industrial effluents is conducted through volumetric, colorimetric and chemiluminescence techniques which are complex, time consuming, and are prone to interferences. Because of their high specificity, selectivity, sensitivity, rapid response and portability with user-friendly operational technology requiring minimal or no technical handling, amperometric biosensors are providing a suitable alternative. The hydrogen peroxide SAM-based nano-biosensor will provide a quicker alternative analytical procedure for the detection of peroxides. Furthermore, the biosensor will be in a single test-use format, thus eradicating the possibility of transducer fouling.

### **1.5. Aim of the study:**

This research envisages the fabrication of a novel high performance electrocatalytic nano-biosensor with an enzyme, horseradish peroxidase (HRP) encapsulated in organometallic thiolato Schiff base complex self-assembled monolayer on gold electrode. Cyclopentadienylruthenium (II) thiolato base complex will be used as a model complex. The Schiff base complex will be synthesized by the Williamson reaction followed by a Schiff base condensation reaction. The self-assembly of the complex on a gold electrode will be achieved in appropriate solvent medium (dichloromethane) through the sulfur of the methyl sulfide end

group. The novelty of this technique is that the thiolato Schiff base self-assembled monolayer (SAM) will be electroactive and as well as designed to encapsulate horseradish peroxidase (HRP) within the nano-scale monolayer. The interaction between the enzyme and organic and inorganic peroxides will be investigated.



### **1.6. Mile stones:**

The following milestones are envisaged in this research:-

1. Synthesis, instrumental as well as electrochemical characterization of organo-ruthenium thiolato Schiff base complex.
2. Development and optimization of biosensors with the thiolato Schiff base self-assembled monolayer (SAM) and horseradish peroxidase.
3. Spectroelectrochemical and voltammetric interrogation of the biosensor.
4. Kinetic modeling of the biosensor.



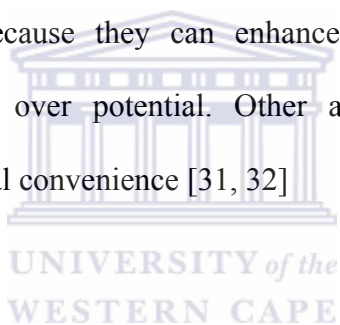
## **CHAPTER TWO**

### **2.1.LITERATURE REVIEW**

#### **2.1.1. Introduction:**

Amperometric biosensors have been used in versatile fields ranging from clinical diagnostics to environmental analysis and even to the diction of chemical and biological warfare [26]. Immobilizations of biomolecule using suitable electrochemical materials play a crucial role in the construction of biosensors [27, 28]. Main strategies of biomolecules immobilization are

physical adsorption, cross-linking, covalent bonding, and entrapment in gels or membranes, amongst other techniques [29]. The term ‘self-assembly’ involves the arrangement of atoms and molecules into an ordered or even aggregate of functional entities without the intervention of mankind towards an energetically stable form. Self-assembled monolayer (SAM) formation induced by strong chemisorptions between the substrate and head group of selected organic molecules provide one of the most elegant approaches towards making ultra thin organic films with controlled thickness [30]. One of the most widely used systems in SAM formation is the adsorption of sulphur derivatives (thiols, disulfides) on gold. Self-assembled monolayers of organosulfur compounds on gold electrodes are very promising for the construction of electrochemical biosensors because they can enhance selectivity and sensitivity, improve response time, and decrease over potential. Other advantages of SAMs include simple instrumentation, and operational convenience [31, 32]



## **2.2. Biosensors:**

A biosensor is an analytical tool consisting of a biologically active material used in close conjunction with a device that will convert a biochemical signal into a quantifiable electrical signal. Biosensors have many advantages, such as simple and low-cost instrumentation, fast response times, and minimum sample pretreatment. The most widespread example of a commercial biosensor is the blood glucose biosensor, which uses an enzyme to break blood glucose down. In so doing, it transfers an electron to an electrode and this is converted into a measure of blood glucose concentration. Many of today’s biosensors applications are similar, in that they use organisms which respond to toxic substances at a much lower level than us



(humans) to warn us of their (toxins) presence. These devices can be used both in environmental monitoring and in water treatment facilities.

### 2.2.1. Components of a biosensor:

A biosensor has two main components: a **receptor** and a **detector**. The receptor is responsible for the selectivity of the sensor. Examples of which are enzymes, antibodies, and lipid layers. The detector, which plays the role of a transducer, translates the physical or chemical change by recognizing the analyte and relaying it through an electrical signal. It must be noted here that the detector is not selective. It can be a pH or an oxygen electrode. The biosensor device incorporates a biological sensing element with a traditional transducer. The biological-sensing element selectively recognizes a particular biological molecule through a reaction, specific adsorption, or other physical or chemical process, and the transducer converts the result of this recognition into a measurable signal, which can be quantified. Common transduction systems are optical, electro optical, or electrochemical; these offers many opportunities to tailor biosensors for specific applications [33]. For instance, the glucose concentration in a blood sample can be measured directly by a biosensor which is specific for blood glucose by simply dipping the sensor into the sample. *Fig 2.1* is schematic diagram of a typical biosensor set-up.

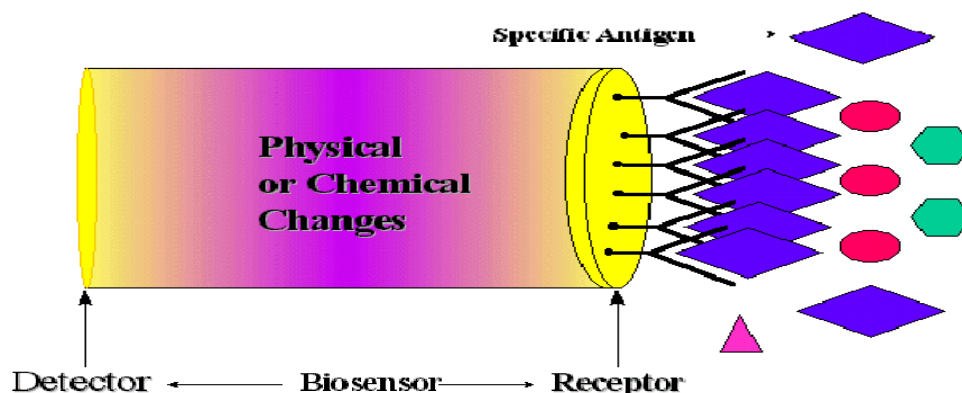


***Fig.2. 1: Schematic diagram of a typical biosensor set-up***

Almost all types of biological reactions be it chemical or affinity can be exploited for biosensors. The concept commonly used to explain this is shape-specific which is the basis of high sensitivity and selectivity of biological molecules, especially antigen-antibody systems. The analyte molecule has a complementary structure to the antibody, and the bound pair is in a lower energy state than the two separate molecules, providing a strong bond which is difficult to break. *Table 2.1* highlights some commonly encountered examples of biosystem-transducer combinations in terms of transducer, measurement mode and potential application.

**Table 2.1: Examples of biosystem-transducer, measurement mode and potential applications**

Amperometric biosensors combine the selectivity of an enzyme reaction with the sensitivity of amperometric detection. In operation, these biosensors make use of an enzyme to convert an analyte into an electroactive product, which is then transduced into a quantifiable amperometric response by an electrode. A lot of sophistication is associated with these biosensors defined by the manner in which the enzyme reaction is transduced to the amperometric response. The latest

<b>TRANSDUCER SYSTEM</b>	<b>MEASUREMENT MODE</b>	<b>TYPICAL APPLICATIONS</b>
<b>Ion-selective Electrode</b>	<b>Potentiometric</b>	<b>Ions in biological media, enzyme electrode</b>
<b>Gas-sensing Electrodes</b>	<b>Potentiometric</b>	<b>Gases, enzymes, organelles, cell or tissue electrodes</b>
<b>Field-Effect Transistors</b>	<b>Potentiometric</b>	<b>Ions, gases, enzyme substrates, immunological analytes</b>
<b>Optoelectronic and Fibre-optic Devices</b>	<b>Optical</b>	<b>pH; enzymes; immunological analytes</b>
<b>Thermistors</b>	<b>Calorimetric</b>	<b>Enzymes, organelles, gases, pollutants, antibiotics, vitamins</b>
<b>Enzyme Electrodes</b>	<b>Amperometric</b>	<b>Enzymes, immunological systems</b>
<b>Conductimeter</b>	<b>Conductance</b>	<b>Enzyme substrates</b>
<b>Piezoelectric Crystals</b>	<b>Acoustic (mass)</b>	<b>Volatile gases and vapors, antibodies</b>

gen  
erati  
on  
of  
bios  
ens  
ors  
is  
char  
acte  
rize  
d by  
“wir  
ed”  
enz

ymes, in which the enzymatic reaction is directly transduced to the amperometric response by means of a molecular wire that connects the enzyme to the electrode.

Although  $H_2O_2$  is rarely an analyte of primary interest, diagnostic assays often require  $H_2O_2$  detection. Equally important, the characteristics of  $H_2O_2$  biosensors can facilitate several unique applications, including the adaptation of wired-enzyme to an electrochemical affinity assay. The main objective of our research is to construct an amperometric biosensor with the aid of an enzyme (horseradish peroxidase) for the analysis of  $H_2O_2$  and extrapolate to the analysis of organic peroxides.

### **2.2.2 Mediators:**

Electron-transfer processes between the active site of an (immobilized) enzyme and the electrode surface play a crucial role in how an amperometric biosensor effectively carries out its function of measuring substrate-dependent currents. Owing to the fact that enzyme-integrated active sites are often insulated by a protein shell, direct electron communication becomes difficult. Thus, alternative electron-transfer pathways, examples of which are free-diffusing low-molecular weight redox-active molecules, have been demonstrated [34]. These redox-mediators have outstanding advantages:

- They offer a fast electron-transfer rate ( $K_{ET}$ ) with both the active site of the enzyme and the electrode surface
- A low redox potential in order to avoid co-oxidation or co-reduction of interfering compounds
- Sufficient chemical stability of the oxidized and the reduced forms

- A low reorganization energy to allow fast electron transfer even over significant electron-transfer distances.

In most cases, the possibility of an interaction between a specific enzyme and a redox mediator is investigated by means of voltammetry of the dissolved enzyme in the presence of the mediator and saturation concentrations of the enzyme's substrate. In the absence of the substrate, only the redox wave of the mediator is observed, while in the presence of the substrate, a typical Electrocatalytic voltammogram is recorded from which the electron-transfer rate between enzyme and redox mediator can be deduced [35]. However, even with the use of small electrochemical cells, the loss of the often valuable mediator compounds and, concomitantly, the loss of the enzyme do not allow a thorough investigation of a specific redox mediator with a number of enzymes, using a variety of different electrolyte solutions, pH values amongst others. Most of the presently applied redox mediators suffer from low stability, slow electron-transfer rate especially with some, or poor solubility in aqueous electrolytic which is indispensable for the preservation of enzymatic activity. Transition-metal complexes have proven to be suitable redox mediators with a variety of enzymes. They offer certain adaptability due to the possibilities of varying the ligand shell of the central metal [36] and hence modulating the redox potential, the charge, and the interaction potential with a specific enzyme.

In recent years, osmium and ruthenium complexes have been evaluated with respect to their ability to act as redox mediators with different oxidoreductases. Ruthenium complexes of the form  $[\text{Ru}(\text{LL})_2\text{X}_2]$ , where LL is 1,2-bipyridine or 1,10-phenanthroline and X is an acido ligand, were found to undergo rapid interaction with some oxidoreductases, such as FAD-dependent glucose oxidase (GOX), and horseradish peroxidase (HRP) [37]. In addition, these mediators could be bound to the surface of the redox protein by means of ligand exchange reactions with

protein bound-bound histidine residues. The obtained mediator-modified enzyme electrode showed improved electron-transfer rates compared with the native enzyme [38-39]. In this study, a novel cyclopentadienylruthenium (II) thiolato Schiff base complex was synthesized and deposited on a gold disc electrode as a self-assembled monolayer. This was motivated by the complex's thiolato end group affinity for gold. A model enzyme, horseradish peroxidase (HRP) was electrostatically attached to the SAM-modified electrode and its electrocatalytic activity elucidated in phosphate buffer.



## **2.3 Enzymes:**

Enzymes are nature's catalyst. Like all catalysts, they increase the rate at which a reaction attains equilibrium by providing a low-activation energy reaction pathway. Most enzymes usually operate in approximately neutral pH, with mild temperatures, generate no by-products, and are highly selective. Enzyme-catalyzed reactions can be selective for one substrate or a group of substrates. They are also stereoselective and stereospecific. These are characteristics which give enzymes their analytical applications.

### **2.3.1. Factors Affecting Enzyme Activity:**

### **2.3.1.1. Enzyme and Substrate Concentration:**

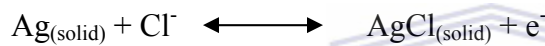
The rate of an enzyme-catalysed reaction depends on both enzyme and substrate concentrations. For a given enzyme concentration, the rate of reaction increase with increasing substrate concentration up to a point, above which any further increase in substrate concentration produces no significant in reaction rate. This is because the active sites of the enzyme molecules at any given moment are virtually saturated with substrate. The enzyme/substrate complex has to dissociate before the active sites are free to accommodate more substrate [40]. Provided that the substrate concentration is high and that temperature and pH are kept constant, the rate of reaction is proportional to the enzyme concentration.

### **2.3.1.2. Temperature and pH:**

As the temperature rises, reacting molecules have more and more kinetic energy. This increases the chances of a successful collision and so the rate increases. There is a certain temperature at which an enzyme's catalytic activity is at its greatest. The optimal temperature is usually around human body temperature (37.5 °C) for the enzymes in human cell, as well as any other reaction for analytical purposes. Above this temperature the enzyme structure begins to breakdown (denature) since at higher temperatures intra- and intermolecular bonds are broken as the enzyme molecules gain even more kinetic energy. Each enzyme works within quite a small pH range. There is a pH at which its activity is greatest (the optimal pH). This is because changes in pH can make and break intra- and intermolecular bonds, changing the shape of the enzyme, and therefore, its effectiveness.

### **2.3.2. Amperometric Detection:**

High sensitivity, selectivity, and ability to operate in turbid solutions are advantages of electrochemical biosensors. Amperometric detection is based on measuring the oxidation or reduction of an electroactive compound at a working electrode (sensor). A potentiostat is used to apply a constant potential to the working electrode with respect to a reference. A potentiostat is a simple electronic circuit that can be constructed using a battery, two operational amplifiers, and several resistors. The applied potential is an electrochemical driving force that causes the oxidation or reduction. The potential of the reference electrode is well defined through equilibrium as in the following reaction:



Provided Cl concentration is fixed, the substrate reaction produces a stable potential.

The current response can then be defined mathematically using Faraday's law:

$$I = nF(da/dt),$$

Where the current in amperes (I) represents the electrochemical oxidation or reduction rate of the analyte at the working electrode, da/dt is the oxidation or reduction rate in mols, F is the Faraday's constant, and n, the number of electrons transferred. The reaction rate depends on both the rate of electron transfer at the electrode surface and analyte mass transport. The rate of electron transfer can be accelerated by increasing the potential at which the electrode is poised. With an increase in potential, the reaction reaches the point where the rate is limited by the mass transport of reactant to the electrode. When the reaction at the electrode surface is sufficiently



fast, the concentration of the analyte at the electrode is zero and a maximum overall rate of reaction is reached. This overall rate is limited by the rate of mass transfer given by the following equation;

$$I = nAFD (dc/dx)_{y=0}$$

Where  $dc/dx$  is the flux of C (electroactive species) to the electrode surface, A is the electrode area, and D is the diffusion coefficient. The rate of mass transport to the electrode surface depends on the bulk concentration of analyte, the electrode shape and area, and diffusion and convection conditions.

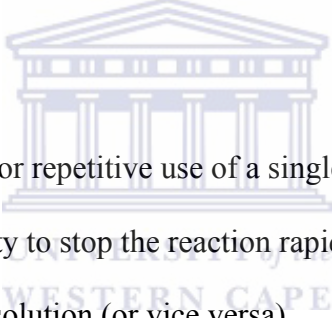


## **2.4. Immobilization Techniques:**

The term “immobilized” means unable to move or stationary. When immobilizing an enzyme to a surface, it is most important to choose a method of attachment that will prevent loss of enzyme activity by not changing the chemical nature or reactive groups in the binding site of the enzyme. In other words, attach the enzyme but do as little damage as possible. Considerable knowledge of the active site of the enzyme will prove helpful in achieving this task. It is desired to avoid reaction with the essential binding site group of the enzyme. Alternatively, an active site can be protected during attachment as long as the protective groups can be removed without loss

of enzyme activity. In some cases, this protective function can be fulfilled by a substrate or a competitive inhibitor of the enzyme.

The surface on which the enzyme is immobilized is responsible for retaining the structure of the enzyme through hydrogen bonding or the formation of electron transition complexes. These links will prevent vibration of the enzyme and thus increase thermal stability. The microenvironment of surface and enzyme has a charged nature that can cause a shift in the optimum pH of the enzyme of up to 2 pH units. This may be accompanied by a general broadening of the pH region in which the enzyme can work effectively, allowing enzymes that normally do not have similar pH regions to work together. There are a number of advantages to attaching enzymes to a solid support;

- 
- Multiple or repetitive use of a single batch of enzymes
  - The ability to stop the reaction rapidly by removing the enzyme from the reaction solution (or vice versa)
  - Enzymes are usually stabilized by bounding
  - Product is not contaminated with the enzyme (especially useful in the food and pharmaceutical industries)
  - Analytical purposes - long half-life, predictable decay rates, elimination of reagent preparation.

#### **2.4.1. Cross-linking:**

Enzyme stabilization is one of the major challenges in the biocatalytic optimization process. Immobilization of enzymes has been achieved by intermolecular cross-linking of protein, either to other proteins or to functional groups on an insoluble support matrix. Cross-linking an enzyme to itself is both expensive and insufficient, as some of the protein material will inevitably be acting mainly as a support; hence, an enzyme support is indispensable. Enzymes have to be used at higher temperatures, shear rate and organic solvent environments for the production of pharmaceuticals, agro chemicals, consumer care products etc. From an economic perspective, immobilization brings down the cost of the process in that the enzyme can be reused [41]. The short coming here is that the catalyst can be diluted, unstable at higher temperatures and low activity loading on the support [42].

Cross-linking of enzymes bring about both stabilization and immobilization of enzyme without dilution of activity. Cross-linked enzyme crystals are prepared by controlled precipitation of enzymes into micro crystals followed by cross-linking using bifunctional reagents to form strong covalent bonds between free amino acid groups in the enzyme molecules. In cross-linking enzyme crystals, the lattice interactions in the enzyme crystal when fixed by inter- and intramolecular chemical cross-links provide additional physical and thermal stability [43].

This method has been used for the immobilization of polyphenol oxidase (PPO) from edible mushroom (*Agaricus bisporus*). The effect of incorporating two different sets of monomers such as glycidyl methacrylate (GMA) and allyl glycidyl ether (AGE) and the effect of cross-linking agent ethylene glycol dimethacrylate (EGDM) with varying cross-link densities on binding and expression of mushroom PPO immobilization was studied. The effect of porogen viz. cyclohexanol and hexanol on PPO immobilization was studied. It was found that AGE copolymers with hexanol as a porogen gave higher binding and expression of PPO activity than

GE polymers. Cross-linking of amino groups of enzyme with 5% glutaraldehyde for 6 h gave stable binding of PPO on AGE-75 (Hex) polymer with a storage half-life of approximately 25 days. With optimum conditions, AGE-75 (Hex) polymer gave 70.3% of activity yield while percent retention of PPO activity was found to be 83.5%. Immobilized PPO showed a broader pH, higher temperature and excellent storage stability [44].

#### **2.4.2. Covalent Binding:**



The most intensely studied of the insolubilization techniques is the formation of covalent bonds between the enzyme and its support. When trying to select the type of reaction by which a given protein should be insolubilized, the choice is limited by the fact that the binding reaction must be performed under conditions that do not cause loss of enzymatic activity, and the active site of the enzyme must be unaffected by the reagents used.

The functional groups of proteins suitable for covalent binding under mild conditions include

- The alpha amino groups of the chain and the epsilon amino groups of lysine and arginine
- The alpha carboxyl group of the chain end and the beta and gamma carboxyl groups of aspartic and glutamic acids,
- The phenol ring of tyrosine

- The thiol group of cysteine
- The hydroxyl groups of serine and threonine

Reactions have been designed which couple with functional groups on the protein other than the amino and phenolic residues. Aminoethyl cellulose has been coupled to the carboxylic acid residues of enzymic protein in the presence of carbodiimide, and thiol residues of a protein have been oxidatively coupled to the thiol groups of a cross-linked copolymer of acrylamide and N-acryloyl-cystein.

It is possible in some instances to increase the number of reactive residues of an enzyme in order to increase the yield of insolubilized enzyme and to provide alternative reaction sites to those essential for enzymic activity. As with cross-linking, covalent bonding should provide stable, insolubilized enzyme derivatives that do not leach enzyme into the surrounding solution. The wide variety of binding reactions, and insoluble carriers with functional groups capable of covalent coupling, or being activated to give such groups, makes this a generally applicable method of insolubilization, even if very little is known about the protein structure or active site of the enzyme to be coupled.

Soybean and horseradish peroxidases (SBP and HRP) have been immobilized on glutaraldehyde-activated aminopropyl glass beads with activities of 74% and 78.5%, respectively, of the corresponding free enzymes and together with their high protein content, make them good catalysts for the enzymatic elimination of phenol from aqueous solutions in the presence of hydrogen peroxide [45].

### **2.4.3. Physical Adsorption:**

Adsorption of an enzyme onto a solid is probably the simplest way of preparing immobilized enzymes. The method relies on non-specific physical interactions between the enzyme protein and the surface of the matrix, brought about by mixing a concentrated solution of enzyme with the solid.

A major advantage of adsorption as a general method of insolubilizing enzymes is that usually no reagents and only a minimal of activation steps are required. As a result, adsorption is cheap, easily carried out, and tends to be less disruptive to the enzyme protein than chemical means of attachment, the binding being mainly by hydrogen bonds, multiple salt linkages, and Van der Waal's forces. In this respect, this method bears the greatest similarity to the situation found in biological membranes in vivo and has been used to model such systems.

Because of the weak bonds involved, desorption of the protein resulting from changes in temperature, pH, ionic strength or even the mere presence of substrate, is often observed. Another disadvantage is further non-specific adsorption of other proteins or other substances as the immobilized enzyme is used. This may alter the properties of the immobilized enzyme or, if the substance adsorbed is a substrate for the enzyme, the rate will probably decrease depending on the surface mobility of enzyme and substrate. Stabilization of enzymes temporarily adsorbed onto a matrix has been achieved by cross-linking the protein in a chemical reaction subsequent to its physical adsorption.

The behavior of horseradish peroxidase (HRP), immobilized onto hybrid particles of poly(methylmethacrylate) (PMMA) and carboxymethylcellulose (CMC) has been studied by spectrophotometry. The adsorption isotherm showed an initial step and an adsorption plateau. HRP adsorbed irreversibly onto PMMA/CMC particles; the adsorption isotherm showed an initial step and an adsorption plateau. The enzymatic activity of free HRP and immobilized HRP

(plateau region) was monitored with spectrophotometry as a function of storing time. Upon adsorbing HRP there was little (up to 20%) or no reduction of enzymatic activity compared to that for the free enzyme in solution [46].

#### **2.4.4. Behavior of Immobilized Enzymes:**

It is important to understand the changes in physical and chemical properties which an enzyme would be expected to undergo upon immobilization if the best use is to be made of the various immobilization techniques available. Changes have been observed in the stability of enzymes and in their kinetic properties because of the microenvironment imposed upon them by the supporting matrix and by the products of their own action.

#### **2.4.5. Stability of Immobilized Enzymes:**

The stability of the enzymes might be expected to either increase or decrease on immobilization, depending upon whether the carrier provides a microenvironment capable of denaturing the enzymic protein or of stabilizing it. Inactivation due to autodigestion of proteolytic enzymes should be reduced by isolating the enzyme molecules from mutual attack by immobilizing them on a matrix. It has been found that enzymes coupled to inorganic carriers were generally more stable than those attached to organic polymers when stored at 4 or 23 °C. Stability due to denaturing agents may also change after immobilization

#### **2.4.6. Kinetic Parameters of immobilized enzymes:**

Changes in activity of enzymes due to the actual process of insolubilization have not been studied to a large extent. There is usually a decrease in specific activity of an enzyme upon insolubilization, and this can be attributed to denaturation of the enzymic protein caused by the coupling process. Once an enzyme has been insolubilized, however, it finds itself in a microenvironment that may be drastically different from that existing in free solution. The new microenvironment may be a result of the physical and chemical character of the support matrix alone, or it may result from interactions of the matrix with substrates or products involved in the enzymatic reaction.

The Michaelis constant has been found to decrease by more than one order of magnitude when substrates of opposite charge to the carrier matrix was used. Again, this only happened at low ionic strengths, and when neutral substrates were used. The electrostatic potential was calculated by insertion of the Maxwell-Boltzmann distribution into the Michaelis-Menton equation using the changes in Michaelis constant, and good agreement was obtained with the value for the electrostatic potential calculated from the pH-activity shifts (see later).

The diffusion of substrate from the bulk solution to the microenvironment of an immobilized enzyme can limit the rate of the enzyme reaction. The rate at which substrate passes over the insoluble particle affects the thickness of the diffusion film, which in turn determines the concentration of substrate in the vicinity of the enzyme and hence the rate of reaction.

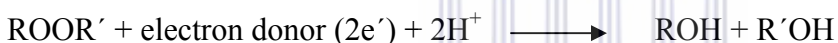
The effect of the molecular weight of the substrate can also be large. Diffusion of large molecules will obviously be limited by steric interactions with the matrix, and this is reflected in the fact that the relative activity of bound enzymes towards high molecular weight substrates has been generally found to be lower than towards low molecular weight substrates. This, however,



may be an advantage in some cases, since the immobilized enzymes may be protected from attack by large inhibitor molecules.

### **2.4.7: Peroxidases:**

Peroxidases are a large family of enzymes which catalyze typically a reaction of the form:



For many of these enzymes the optimal substrate is hydrogen peroxide, but others are more active towards organic hydroxides such as lipid peroxides. Peroxidases can contain a heme in their active sites, or redox-active cysteine or selenocysteine residues. The nature of the electron donor is very dependent on the structure of the enzyme. For instance, horseradish peroxidase can use a variety of organic compounds as electron donors and acceptors. It has an accessible active site and many compounds can reach the site of the reaction. On the contrary, for an enzyme such as cytochrome c, the compounds that donate electrons are very specific, because the active site is much closer.

Horseradish peroxidase has been electrostatically attached to a self-assembled monolayer of a thiolato Schiff base complex on gold in the present study as a representative system for the investigation of the structure, dynamic and thermodynamic properties of the peroxidase family

and especially for elucidating their biological behaviors to catalyze oxidation of substrates by hydrogen peroxide. The resulting self-assembled monolayer provides a favorable microenvironment for the enzyme (HRP) to realize direct electron transfer and to retain their bioactivity.

### **2.5. Self-assembled Monolayer (SAMs):**

Bare surfaces of metals and metal oxides tend to adsorb adventitious organic materials readily because these adsorbates lower the free energy of the interface between the metal or metal oxides and the ambient environment. These adsorbates also alter interfacial properties and can have a significant influence on the stability of metals and metal oxide. The organic material can act as a physical or electrostatic barrier against aggregation, decrease the reactivity of the surface atoms, or act as an electrically insulating film. Surfaces coated with adventitious materials are however not well defined; they do not present specific chemical functionalities and do not have reproducible physical properties. Examples such as conductivity, wettability, or corrosion resistance amongst others [47].

A self-assembled monolayer (SAM) provides a convenient, flexible and simple system with which interfacial properties of metals can be tailored. SAMs are organic assemblies formed by the adsorption of molecular constituents from solution or the gas phase onto the surface of solids or in regular arrays on the surface of liquids (in the case of mercury and probably other liquid metals and alloys). The adsorbates organize spontaneously into crystalline or semi-crystalline structures. The molecules or ligands that form SAMs have a chemical functionality, or “headgroup”, with a specific affinity for a substrate; in most cases the headgroup also has a high

affinity for the surface and displaces adsorbed adventitious organic materials from the surface. Table 2.2 highlights some examples of commonly used headgroups with the most extensively studied class of SAMs being that derived from the adsorption of alkanethiols on gold, silver, copper, palladium, platinum, and mercury [48, 49]. The high affinity of thiols for the surfaces of noble and coinage metals makes it possible to generate well-defined organic surface with useful and highly alterable chemical functionalities displayed at the exposed interface [50].

**Table 2.2: Examples of headgroups and substrates used in forming SAMs on metals, Oxides and Semiconductors:**

<b>Ligand</b>	<b>Substrates</b>
ROH	Fe <sub>x</sub> O <sub>y</sub> , Si-H, Si
RCOO <sup>-</sup> /RCOOH	α-Al <sub>2</sub> O <sub>3</sub> , Fe <sub>x</sub> O <sub>y</sub> , Ni, Ti/TiO <sub>2</sub>
RCOO-OOCR	Si(111):H, Si(100):H
Ene-diol	Fe <sub>2</sub> O <sub>3</sub>
RNH <sub>2</sub>	FeS <sub>2</sub> , Mica, Stainless Steel316L, CdSe
RCN	Ag, Au
RSH	Ag, Ag <sub>90</sub> Ni <sub>10</sub> , Au, AuAg, AuCu,Ni, PbS
RSAc	Au
RSSR'	Ag, Au, CdS, Pd

**2.5.1.**  
**Prepar**  
**ation**  
**of**  
**SAMs:**  
 The  
 tradition  
 al  
 method  
 of SAM

preparation focused largely on the assemblies formed by the adsorption of organosulfur compounds from solution or the vapor phase onto planar metal substrates of gold and silver [51-52]. These studies used three types of organosulfur compounds: alkanethiols ( $\text{HS}(\text{CH}_2)_n\text{X}$ ), dialkyl sulfides ( $\text{X}(\text{CH}_2)_m\text{S}-\text{S}(\text{CH}_2)_n\text{X}$ ), ( $\text{X}(\text{CH}_2)_m\text{S}(\text{CH}_2)_n\text{X}$ ), where  $n$  and  $m$  are the number of methylene units and X represents the endgroups of the alkyl chain ( $-\text{CH}_3$ ,  $-\text{OH}$ ,  $-\text{COOH}$ ). These experiments established many of the basic structural characteristics of these systems (surface structure, chain organization and orientation), practical protocols for SAM preparation (concentrations, length of time for immersion, solvents, and temperature), and details of the thermodynamics and kinetics of SAMs.

The most common protocol for preparing SAMs on gold, silver, palladium, mercury, and other materials (Table 2) is immersion of a freshly prepared or clean substrate into a dilute ( $\sim 1-10$  mM) ethanolic solution of thiols for  $\sim 12-18$  h at room temperature. This procedure is widely used and originates from early studies of SAMs; the experimental studies resulted from a combination of studies designed to optimize the reproducibility of the SAMs produced and convenience [53]. Dense coverage of adsorbates are obtained quickly from millimolar solutions (milliseconds to minutes), but a slower reorganization process requires time on the order of hours to maximize the density of molecules and minimize the defects in the SAM. There are however a number of experimental factors that can affect the structure of the resulting SAM and the rate of formation: solvent, temperature, concentration of adsorbate, immersion time, purity of the adsorbate, concentration of oxygen in solution, cleanliness of the substrate, and chain length (more generally, structure of the adsorbate).

Most experimental conditions for the preparation of SAMs yield organic interfaces with reproducible and desired functional behaviors. These characteristics are acceptable for some

applications of SAMs, but fundamental studies of certain materials property such as wettability, corrosion, tribology, and charge-transfer processes require an understanding of how to minimize defects in SAMs and maximize order in these systems. The effects that some parameters, such as immersion time, concentration of adsorbate, and chain length, have on the properties of the SAMs are known to a small degree, but less is known about others; like choice of solvent and temperature amongst others. We now look at some of the important factors that are of utmost importance in SAM formation.

### **2.5.2. The Role of Solvents in SAM Preparation:**

The most widely used solvent in SAMs preparation is ethanol. The limiting mass coverage and wettability of SAMs formed from solutions of alkanethiols comprising solvents other than ethanol (tetrahydrofuran, dimethylformamide, acetonitrile, cyclooctane, toluene) do not vary significantly from those formed from ethanolic solutions [53]. At least four other factors also contribute to the widespread use of ethanol; (i) it solvates a variety of alkanethiols with varying degrees of polar character and chain length. (ii) it is inexpensive (iii) its availability in high purity and (iv) its low levels of toxicity.

The effects of the choice of solvent on the kinetics of formation and the mechanism of assembly are complex and poorly understood. The presence of a solvent adds additional parameters to the dynamic equilibrium governing the adsorption of thiols: solvent-substrate and solvent-adsorbent interactions complicate the thermodynamics and kinetics of assembly. Solvent-substrate interaction can hinder the rate of adsorption of thiols from solution because the solvent

molecules must be displaced from the surface prior to the adsorption of thiols, which are less prevalent in solution than the solvating molecules.

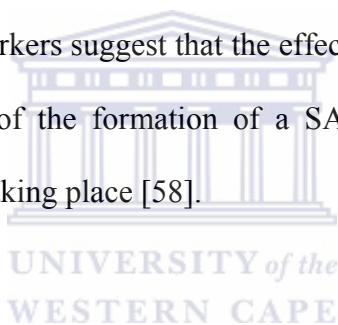
Studies suggest that the rate of formation of SAMs of alkanethiolates is faster in certain nonpolar solvents (heptane, hexane) than ethanol. The use of long hydrocarbons, such as dodecane and hexadecane as solvents reduces the rates of formation such that they are comparable to those from ethanolic solutions [54-55]. Hydrocarbon solvents may improve kinetics of formation in some cases, but the strong solvent-adsorbate interactions in these solutions impede the organization of SAMs formed from alkanethiols. Contact angle measurements together with electrochemistry suggest that SAMs formed from solutions of thiols in nonpolar organic solvents are less organized than those formed from ethanol [56].

Polar liquids are poor solvents for *n*-alkanethiols and seem to reduce the quantity of some types of defects found in SAMs (conformational arrangements, regions of missing adsorbates) and promote a densely packed monolayer. The low solubility of thiols in such solvents together with the segmental heats of adsorption for these solvents (heat associated with each additional interaction of the solvent molecules with the surface, for instance, the heat of adsorption per methylene or ROH group) probably serve to segregate the thiols at the metal surface and thus more efficiently drive the assembly process involving them. SAMs with few conformational and pinhole defects also can form from aqueous solutions containing micelles of ionic and nonionic surfactants [57]. Studies point that the role of solvent on the prototypical example of SAMs of alkanethiolates on gold indicate that the choice of solvent is clearly an important parameter in determining the resulting quality of a SAM deposited from solution, but there remains significant

challenges in developing a detailed understanding of the complex and dynamic interactions that occur between the solvent, surface, and adsorbates during the formation process.

### **2.5.3 Effect of Temperature on SAMs formation:**

Forming SAMs at temperatures above 25 °C can improve the kinetics formation and reduce the number of defects in them [58]. Elevated temperatures increase the rate of desorption for adventitious materials and solvent molecules physisorbed on the surface of the substrate and make it possible for the system to cross activation barriers for processes such as chain reorganization and lateral rearrangements of the adsorbates more easily than at room temperature. Uosaki and co-workers suggest that the effect of temperature is particularly relevant during the first few minutes of the formation of a SAM when most of the adsorption and reorganization of the SAM is taking place [58].



### **2.5.4. Concentration and Immersion Time:**

These two parameters are inversely related: low concentration of thiols in solution require a longer immersion time. For SAMs formed from alkanethiols on gold, the typical surface density of molecules (where maximum coverage is obtained) is approximately  $4.5 \times 10^{14}$  molecules/cm<sup>2</sup>, implying the minimum concentration for forming a dense SAM is approximately 1 μM or  $6 \times 10^{14}$  molecules/cm<sup>3</sup>. In practice, SAMs formed by immersion for a week in solutions with

concentrations at or below 1  $\mu\text{M}$  do not exhibit the same physical properties as those formed from more concentrated solution [53]. The amount of impurities or other sulfur-containing compounds also can complicate the use of extremely dilute solutions to form SAMs.

Spectroscopic techniques together with experimental findings suggest that the average properties of SAMs formed from *n*-alkanethiols (wettability, mass coverage, and to a larger extent, the structure deduced by (RAIRS)) do not change significantly when exposed to  $\sim 1$  mM solutions of thiols for more than 12-18 h. Electrochemistry [59], STM and RAIRS [60] indicate, however that, that the structure of SAM can continue to evolve over immersion times of  $\sim 7$ -10 days. These results suggest that the coverage of the surface increase with extended immersion times and suggest two consequences: (i) the conformational defects in the alkane chains decrease and (ii) the number of pinhole defects in the SAMs decrease. The typical time allowed for formation (12-18 h) is conveniently experimentally, but for some applications, formation over many days can improve the reproducibility of subsequent experiments that use the SAM, for instance, studies of electron transfer through SAMs [59].

### **2.5.5. The Purity of Thiol Solution:**

Common impurities derived from thiols are disulfides, an oxidation product. Experiments suggest that trace amounts of these materials ( $< 5\%$ ) do not necessarily impede the formation or alter the structure of the SAM. The disulfides usually are, however, less soluble than their thiol precursors and the reduced solubility can result in physisorption of these materials and alteration of the physical properties of the SAM. Oxidized, polar contaminants (sulfonates, etc.) can be removed by percolating the thiols over activated, neutral alumina prior to use [61].



### **2.5.6. Why a Clean Substrate?**

The surfaces on which a SAM forms and the physical object supporting that surface is often referred to as the “substrate”. Types of substrates range from planar surface (glass or silicon slabs supporting thin films of metal, metal foils, single crystals). Planar structures are widely used for characterizing the structure-property relationships of SAMs because they are easy to prepare, convenient, and compatible with a number of techniques for surface analysis and spectroscopic/physical characterization such as reflectance absorption infrared spectroscopy (RAIRS) [62], X-ray photoelectron spectroscopy (XPS) [63], X-ray diffraction, nuclear magnetic resonance spectroscopy (NMR) and electrochemistry [64] amongst others.

The criteria and method of preparation of SAM is a function of what the SAM is intended for. For example, polycrystalline films are sufficient for many applications amongst which are etch resists, templates for crystallization and model surfaces for biological studies. Owing to the high sensitivity of the above mentioned characterization techniques, the formation of SAMs on substrates that are handled in a laboratory atmosphere is essentially an exchange process. The thiols must displace whatever adventitious materials adsorbed onto the substrate prior to immersion in a thiol solution. The assumption made here is that the thiols are in fact able to displace the miscellaneous adsorbates already present. Displacement with thiols first requires desorption of the contaminants and impurities; the rate of desorption of the contaminants must, therefore, affect the kinetics of formation. SAMs have reproducible materials property when formed on substrates that are immersed into solutions of thiols within one hour of preparation or cleaned with strongly oxidizing chemicals (“piranha” solution- $\text{H}_2\text{SO}_4:\text{H}_2\text{O}_2$ ) or oxygen plasmas. Exposure to ambient conditions for prolonged times seems to allow adsorption of materials that are not easily displaced in the typical time allowed for the formation of SAMs.

### **2.5.7. Rationale for the Choice of Gold as Standard:**

Gold forms well, though not uniquely good SAMs and it is historically the most the most studied. In fact, for many applications gold may not be the best substrate. For the purpose of this study, together from the economic perspective, the following arguments can be advance for our choice of gold as a good substrate for studying SAMs:

- Gold is easy to obtain, both as a thin film and as a colloid. It is straightforward to prepare thin films of gold by physical vapor deposition, sputtering, or electrodeposition.
- Gold is exceptionally easy to pattern by a combination of lithographic tools (photolithography, micromachining, etc) and chemical etchants.
- Gold is a reasonably inert metal: it does not oxidize at temperatures below its melting point; it does not react with atmospheric oxygen; it does not react with most chemicals. These properties make it possible to handle and manipulate samples under atmospheric conditions instead of Ultra High Vacuum (UHV) conditions, which is of great practical convenience for conducting experiments that require “dirty” conditions like in cell biology and environmental pollution monitoring experiments. It binds thiols with high affinity with no unusual reactions.
- SAMs formed from thiols on gold surfaces are stable for periods of days to weeks when in contact with a complex liquid media commonly encountered in environmental analysis.

### **2.5.8. Nature of the Metal-SAM Interface:**

SAMs of practical applications are formed at the reactive interface, that is, the adsorbate and the substrate are transformed to some degree due to the reactions that lead to the formation of the

SAM. The chemistry involved for the chemisorptions of thiols on gold is straightforward but remains the most enigmatic. Because gold does not form a surface oxide (as for instance, does silver), the formation of SAMs from thiols is not complicated by chemistries that might be required to displace or reduce surface oxides, but the details regarding the nature of the metal-sulfur bond and the special arrangement of the sulfur groups on the underlying gold lattice are still unclear.

Little is known about the reactions for forming SAMs from organosulfur compounds on other metals, such as palladium, silver, copper, and mercury. Each metal has a different structural surface chemistry and consequently different reactivity towards organosulfur compounds. These differences impact significantly on the assembly process leading to a variety of structural motifs that are distinct for each SAM. Structural details of the interface between these metals and the monolayer are only understood in qualitative terms at a level that makes it possible to rationalize many details seen in organization of the organic groups they support. Consideration of bonding arrangement for several metal-sulfur interfaces for a representative does suggest however, a common reasoning: the molecules comprising the SAM tend to adopt structural arrangements that are similar to simple adlayer structures formed by the element sulfur on metal [65, 67].

### **2.5.9. Thermodynamic Analysis of the Gold-Thiolate Bonds:**

The formation of a thiolate requires the chemical activation of the S-H bond of the thiol or the S-S bond of the disulfide. The energetics involved on this bond activation vis-a-vis bond energy that directly anchors the adsorbate molecules of the SAM to the gold substrate were first examined using temperature-programmed desorption as a kinetic measure of the SAM binding energy. Dubois et al. established that the desorption of dimethyl disulfide on Au occurs

dissociatively [68]. The reaction being fully reversible, and re-combinative desorption of the disulfide is an active process with a barrier lying near 30 kcal/mol. This energy suggests that a fairly significant degree of charge transfer to sulfur must occur in the thiolate, an inference that has been based on theoretical calculations [69]. Scoles and co-workers also investigated the bonding energies of various organosulfur adsorbates on gold and their studies suggest, for the case of SAMs involving thiolate structures, bonding energies similar to those cited above [70]. Other kinetic treatments reveal the complex nature of the thermodynamics of the metal-sulfur bonding interactions. Whitesides *et al.*, Liu and co-workers both reported the results of desorption experiments that employed SAMs immersed in solvent [53]. The kinetics of these processes can be modeled using conventional rate equations, and these models suggest barriers for the desorption process that are somewhat lower than the values obtained from desorption rate measurements made in UHV (~20-25 kcal/mol). Schlenoff *et al.* used electrochemical measurements to provide a detailed analysis of the thiol/thiolate/disulfide bond energies and desorption barriers for SAMs on gold [71]. Interestingly, the barrier for the bimolecular re-combinative desorption of an alkanethiolate from a SAM on gold in the form of a dialkyl disulfide is ~15 kcal/mol, approximately a factor of 2 less than that deduced from the gas-phase studies. Worth noting is the fact that the two energies are not directly comparable given that one also contains contributions from the heats of dissolution of the adsorbate as well as the heat of immersion of the substrate in the solvent. The segmental heat of interaction of a hydrocarbon on gold is ~1.5 kcal/mol for a methylene group. In this light, the range of values appear to be one that follows directly from the different forms of measurements used to assess the strength of the Au-S bonding interaction. As vacuum measurements are most easily interpreted, it is reasonable to believe that the Au-S bond that anchors the SAM is, in fact, a reasonably strong one; a

hemolytic Au-S bond strength on the order of ca. -50 kcal/mol, based on the known S-S hemolytic bond strength of a typical dialkyl disulfide (~62 kcal/mol) [72].

### **2.5.10. Mechanisms of Self-assembled monolayers:**

Getting a clear and comprehensive understanding of assembly of SAMs requires a careful consideration of both kinetic and thermodynamic factors. Though the dynamics of assembly remain incompletely understood, it is clear that the process leading to the formation of SAMs involves a subtle interplay of the energetics of the metal-sulfur bonds and (typically) noncovalent lateral interactions among the organic groups. In most cases, the specific ordering of the sulfur moieties on the metal lattice defines the free space available to the organic components. The organization of the organic layer results from maximizing the attractive lateral interactions (van der Waals, hydrogen bonding) within the geometric constraints imposed by the structure of the adlayer. The organic groups, however, can also restrict the density of coverage: steric crowding of the organic groups can limit the arrangement of the sulfur atoms to one that is less dense than that exhibited by the elemental sulfur on a given substrate (for instance, the  $(\sqrt{3} \times \sqrt{3})R30^\circ$  structure for sulfur on gold) Fig. 2.2

A typical example of SAMs of *n*-alkanethiolates on gold demonstrates the balance between the structure of the adlayer and the lateral interactions that stabilize the assembly: the metal-sulfur interaction drives the assembly to the limiting case where the gold surface is covered by a  $(\sqrt{3} \times \sqrt{3}) R30^\circ$  overlayer of thiolates, but the attractive lateral interactions promote the secondary organization of the alkane chains that defines the fine details of the  $c(4 \times 2)$  super lattice structure. The chain-chain interactions contribute ~1.0 kcal/mol of stabilization to the SAM for

each methylene group in the chain [63]. The remaining energy dictating the organization of the SAM results from the metal-sulfur bonding.

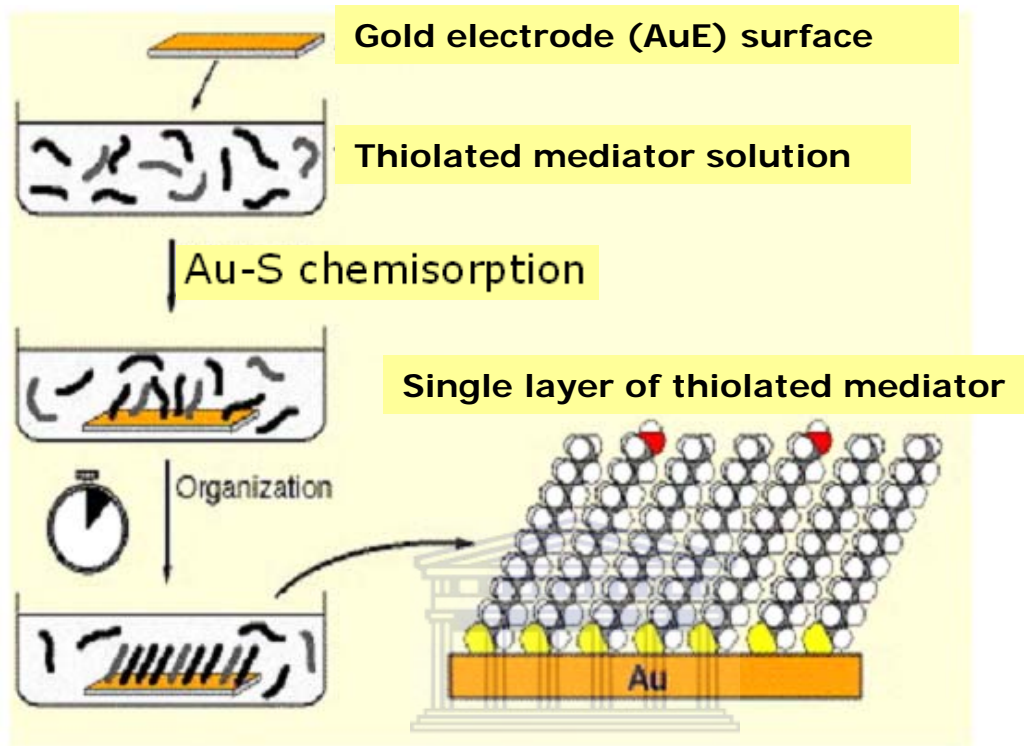


*Fig.2.2: A diagrammatic illustration of the mechanism of self-assembled monolayer formation. The initial adsorption is fast (seconds) while the final (organization) phase takes >15 h.*

### **2.5.11. Defects found in SAMs:**

The fact that SAMs adopt adsorbed structures that are directed by the thermodynamics of a reasonably complex chemisorption process only provides in theory a convenient access to highly ordered interfaces with molecular and aggregate structures that can be varied by principle of rational design. SAM structures are generally “believed” to have little defects. As a matter of fact, they are substantially more complex than the highly ordered arrangements that are commonly assumed. The causes of defects in SAMs are both intrinsic and extrinsic: external factors, such as cleanliness of the substrates, and purity of the solution of the adsorbate, are responsible for some defects in SAMs, but some result simply because SAMs are, in fact, dynamic systems with complex phase behaviors.

The substrates on which SAMs form are replete with many structural defects. The substrate which has been a bench mark, gold, presents a grain structure characterized by dense arrangements of intergrain boundaries, faceting, occlusions, twins, and other gross structural irregularities. Even in samples with strong textures, misalignments are common as are other low-index crystallographic textures. All metal substrates also have a varying density of atomic steps, and these in turn impact the structures and defects content of SAMs as depicted by numerous STM studies [73].

### **2.5.12. Rationale for SAMs Modification:**

Simple functionalities (-OH, COOH) are often adequate for studies of properties relevant to materials science such as wettability, friction, adhesion and corrosion resistance. Modifying SAMs after formation are crucial for the development of surfaces that present large, complex ligands and molecules needed for biology, biochemistry and as well as those involved in environmental analysis. The synthesis of functionalized thiols is often laborious and difficult even for simple molecules, and for SAMs comprising alkanethiols linked to a peptide, protein, carbohydrate, or other biomolecules, synthesis can provide a major challenge. Early strategies adopted for functionalizing organic films supported on electrodes for electrochemistry and on solid-phase materials used for chromatography [74]. Modification of the exposed surface of the SAM after formation offers several advantages:

- It uses common synthetic procedures and thus simplifies the preparation of the functionalized surface.
- It enables the incorporation of ligands into SAMs that are not compatible with thiols or the synthetic methods for preparing them.
- It can generate multiple samples with different types of ligands in a short period of time, since SAMs are easy to prepare.
- It preserves the ordered underlying structure of the SAM.
- An important economic advantage of modifying the SAM after formation is that the amount of ligand required for immobilization is very small ( $<1 \mu\text{M}$ ). This



characteristic is especially important for linking biological ligands that may be in short supply to the surface.

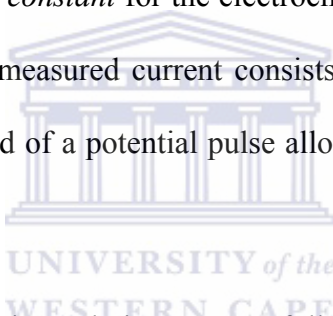
It will also be noted here that there are also some disadvantages of SAM surface modification, vis-a-vis:

- The extent of surface coverage is unknown
- The reactions can produce a mixture of functional groups on the surface.



## **2.6. Pulse Voltammetric Techniques:**

The basis of all pulse techniques is the difference in the rate of the decay of the charging and the faradaic currents following a potential step (or "pulse"). The charging current decays exponentially, whereas the faradaic current (for a diffusion-controlled current) decays as a function of  $1/(\text{time})^{1/2}$ ; that is, the rate of decay of the charging current is considerably faster than the decay of the faradaic current. The charging current is negligible at a time of  $5R_uC_{dl}$  after the potential step ( $R_uC_{dl}$  is the *time constant* for the electrochemical cell, and ranges from  $\mu\text{s}$  to  $\text{ms}$ ). Therefore, after this time, the measured current consists solely of the faradaic current; that is, measuring the current at the end of a potential pulse allows discrimination between the faradaic and charging currents.



The important parameters for pulse techniques are as follows:

- Pulse amplitude is the height of the potential pulse. This may or may not be constant depending upon the technique.
- Pulse width is the duration of the potential pulse.
- Sample period is the time at the end of the pulse during which the current is measured.
- For some pulse techniques, the pulse period or drop time must also be specified. This parameter defines the time required for one potential cycle, and is particularly significant for polarography (i.e., pulse experiments using a mercury drop electrode), where this time corresponds to the lifetime of each drop (i.e., a new drop is dispensed at the start of the

drop time, and is knocked off once the current has been measured at the end of the drop time (the end of the drop time coincides with the end of the pulse width).

A number of different pulse techniques are available on the epsilon, BAS 50, BAS 100, which differ in their potential pulse wave forms, the number of sampling points, and whether a solid electrode (voltammetry) or a mercury drop electrode (polarography) is used. Some of which are discussed below. The discrimination against the charging current that is inherent in these techniques leads to lower detection limits (when compared to linear sweep techniques), which makes these techniques suitable for quantitative analysis.

### **2.6.1. Cyclic Voltammetry (CV):**

A simple potential that is often used in electrochemical experiments is the linear wave form. The potential is continuously changed as a linear function of time; the rate of change of potential with time is referred to as the scan rate ( $\nu$ ). The simplest technique that uses this wave form is linear sweep voltammetry. The potential range is scanned in one direction, starting at the initial potential and finishing at a final potential. A more commonly used variation of the technique is cyclic voltammetry, in which the direction of the potential is reversed at the end of the first scan. Thus, the waveform is usually of the form of an isosceles triangle. This has the advantage in that the product of the electron transfer reaction that occurred in the forward scan can be probed again in the reverse scan. In addition, it is a powerful tool for the determination of formal redox potentials, detection of chemical reactions that precede or follow the electrochemical reaction and evaluation of electron transfer kinetics.

This can be explained with the use of a complex wave form composed of two isosceles triangles. The voltage is first held at the initial potential where no electrolysis occurs and hence no faradaic current flows. As the voltage is scanned in the positive direction, so the reduced compound is oxidized at the electrode surface. At a particular set value, the scan direction is reversed and the material that was oxidized in the outward excursion is then reduced. Once the voltage is returned to the initial value, the experiment can be terminated. A further voltage excursion takes place to more negative (more reducing) values. This may be useful in probing for other species present in the sample or for investigating any electroactive products formed as a result of the first voltage excursion.

The current at the working electrode is measured under diffusion-controlled, mass transfer conditions. The important parameters for a cyclic voltammogram (Fig. 2.3) are the magnitudes of the anodic peak current ( $i_{p,a}$ ), the cathodic peak current ( $i_{p,c}$ ), the anodic peak potential ( $E_{p,a}$ ), the cathodic peak potential ( $E_{p,c}$ ) and the formal potential ( $E^0$ ).

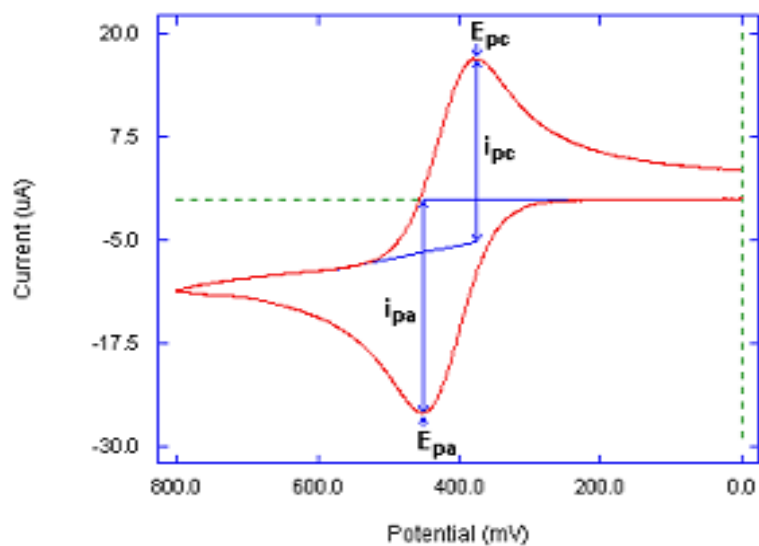


**Fig.2.3: A typical cyclic voltammogram showing anodic ( $E_{p,a}$ ) and cathodic ( $E_{p,c}$ ) peaks, together with anodic ( $i_{p,a}$ ) and cathodic ( $i_{p,c}$ ) peak currents.**

If the system is reversible, the formal potential ( $E^{\circ}$ ) will be the average of the peak potentials of the anodic ( $E_{p,a}$ ) and cathodic ( $E_{p,c}$ ) peak potentials [75];

$$E^{\circ} = (E_{p,a} + E_{p,c}) / 2 \quad (1)$$

The number of electrons transferred ( $n$ ) can be determined from the separation of the peak potentials [75]

$$\Delta E_p = E_{p,a} - E_{p,c} = 0.059 / n \quad (2)$$

Alternatively, the number of electrons can also be obtained from Tafel plots. These are produced by plotting the current versus the potential, of the area of the curve over which the reaction is occurring and with the Tafel equation;

$$\text{Log } I = \log I_0 + (\alpha_{\text{A}}nF / 2.3RT)\eta \quad (3)$$

for the anodic peaks where  $I$  is the current and  $\alpha$  the transfer coefficient.

Performing cyclic voltammograms at varying scan rates, the diffusion coefficient (which is an indication of the rate at which the electroactive species is diffusing through the solution to and from the electrode surface) can be calculated from the Randles-Sevcik expression:-

$$i_p = 2.686 \times 10^5 n^{3/2} C_{\text{ox}} D^{1/2} \nu^{1/2} A$$

$i_p$  = peak current (A)

$C_{\text{ox}}$  = concentration of oxidized species ( $\text{mol cm}^{-3}$ )

$\nu$  = scan rate ( $\text{Vs}^{-1}$ )

$n$  = number of electrons transferred

$A$  = area of the working electrode

$D$  = diffusion coefficient

Cyclic voltammetry is a technique of choice is commonly used, since it provides a fast and simple method for initial characterization of a redox-active system. In addition to providing an estimate of the redox potential, it can also provide information about the rate of electron transfer

between the electrode and the analyte, and the stability of the analyte in the electrolyzed oxidation states (e.g., do they undergo any chemical reactions) [76].

### **2.6.2. Differential Pulse Voltammetry (DPV):**

This technique is comparable to normal pulse voltammetry in that the potential is also scanned with a series of pulses. However, it differs normal pulse voltammetry in that each potential is fixed, of small amplitude (10 to 100 mV), and is superimposed on a slowly changing base potential (Fig. 2.4). Current is measured at two points for each pulse, the first (1) just before the application of the pulse and the second (2) at the end of the pulse. These sampling points are selected to allow for the decay of nonfaradaic (charging) current. The difference between current measurements at these points for each pulse is determined and plotted against the base potential.

This technique is used for the electrochemical elucidation of any species that appear at the surface of the electrode in the scanning process since each redox species generates an individual symmetrical peak. Differential pulse voltammetry together with CV can be used to estimate the formal potential ( $E^0$ ) of a redox couple. The formal potential is important for the electrochemical characterization of complexes and identification of redox processes attributed to other electroactive species other than the complexes (e.g. ligand).

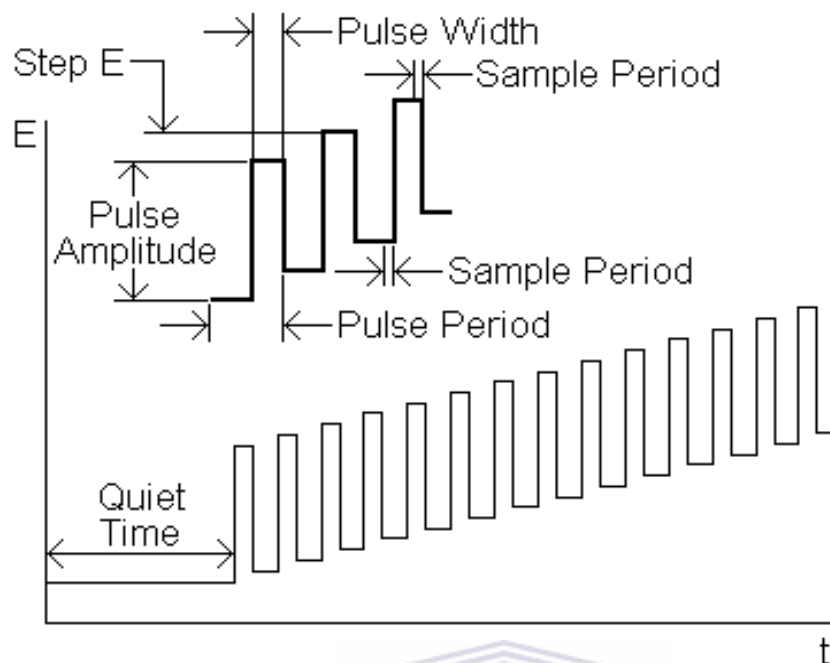
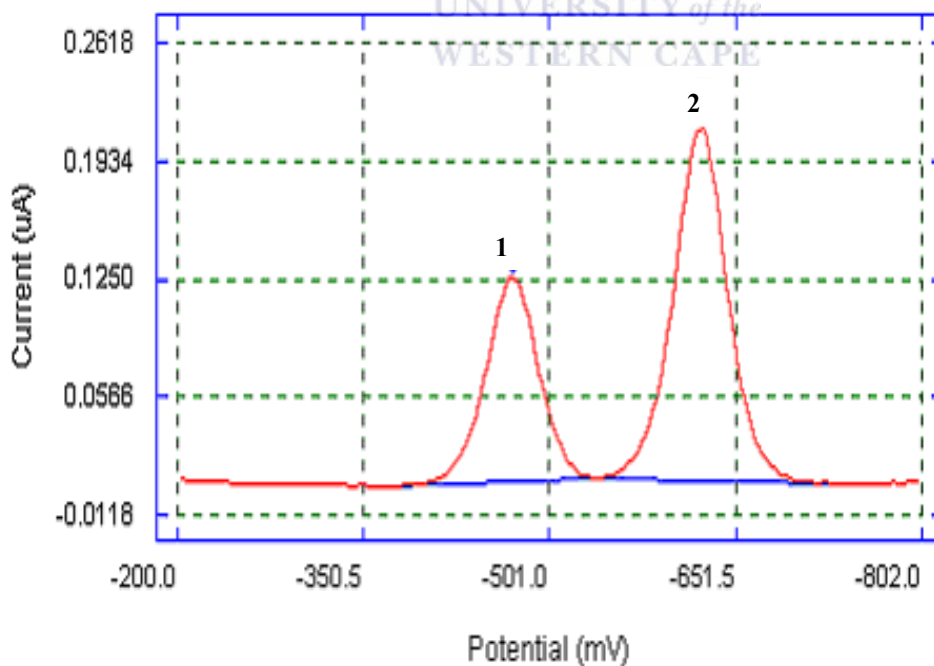


**Fig.2.4: Potential wave form for differential pulse voltammetry**



**2.6.3.**

**Fig.2.5: A typical differential pulse voltammogram**

***Osteryoung Square***



### **Wave Voltammetry (OSWV):**

The potential wave form for Osteryoung square wave voltammetry (OSWV) is shown in Fig. 2.6. The potential wave form consists of a square wave of constant amplitude superimposed on a staircase wave form. The current is measured at the end of each half-cycle, and the current measured on the reverse half-cycle ( $i_r$ ) is subtracted from the current measured on the forward half-cycle ( $i_f$ ). This difference current ( $i_f - i_r$ ) which is the net current is displayed as a function of the applied potential.

For a system which is reversible, the pulse causes oxidation of the species produced on the forward pulse back to the initial state. This produces the anodic current; thus the net current at the current-voltage peak is larger than either the forward or reverse current since it is the difference between the two (Fig. 2.7 ). The peak height is directly proportional to the concentration of the electroactive species. Concentration levels of parts per billion are easily detected.

OSWV is chiefly used because of the following advantages:-

- Its sensitivity is far better compared to other differential techniques.
- Voltammograms are obtained rapidly.
- Background currents are effectively discriminated against.
- Independence of the slope, position and net current of convective and mass transport effects.
- The total quantity of charge passed can be very small.

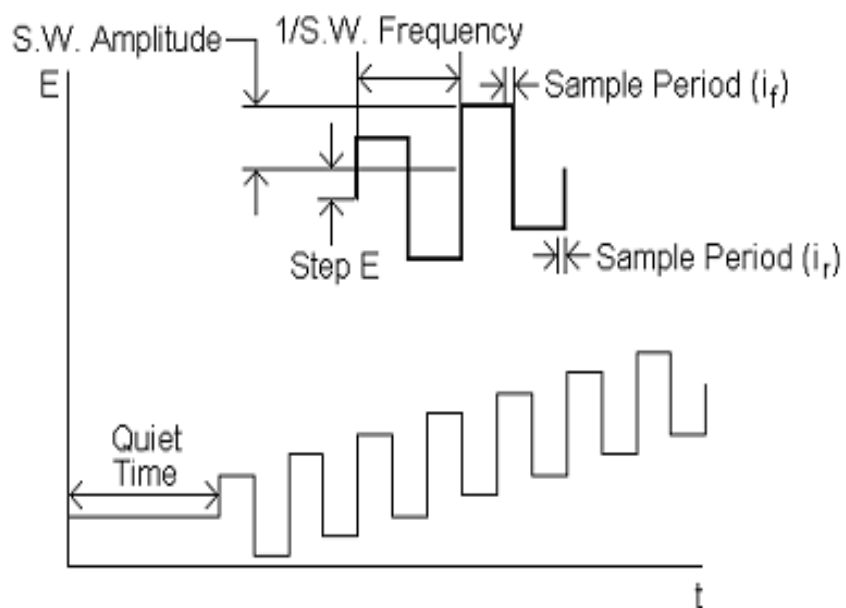


**Fig.2.6: Potential wave form for square wave voltammetry**

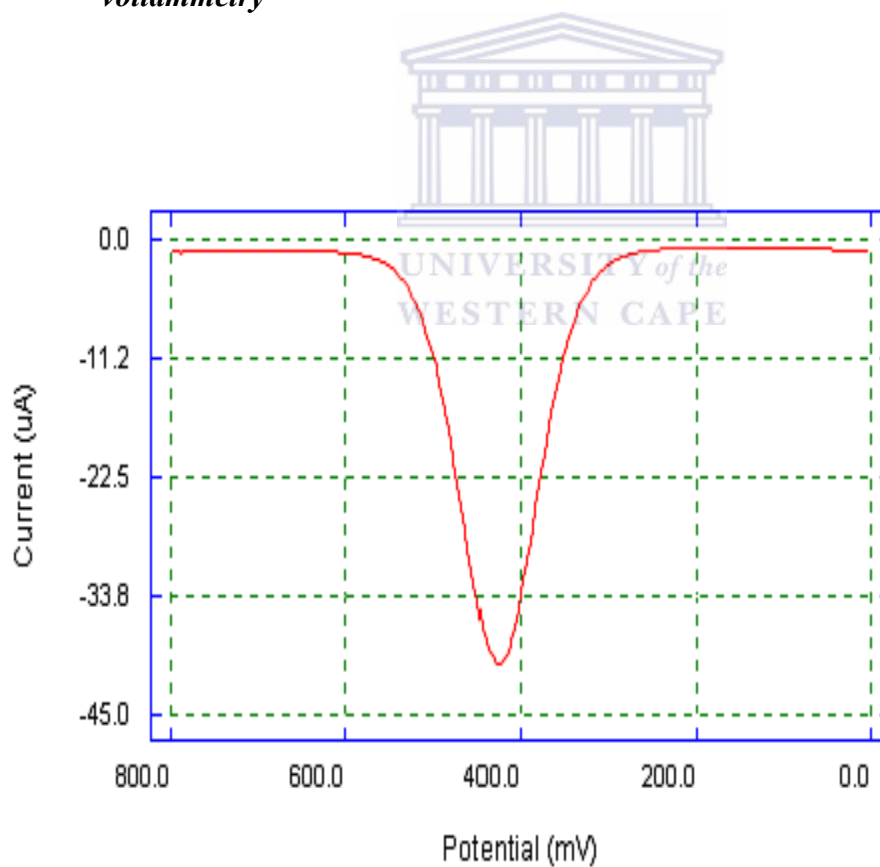


**Fig.2.7: A typical square wave voltammogram**

## **CHAPTER THREE**

### **3.1. Synthesis and characterization of cyclopentadienylruthenium (II) thiolato Schiff base complex:**

#### **3.1.1 Introduction:**

Schiff bases are typically formed by the condensation of a primary amine and an aldehyde. The resultant functional group,  $R^1HC=N-R^2$ , is called an imine and is particular for binding metal ions via the N atom lone pair, especially when used in combination with one or more donor atoms to form polydentate chelating ligands of macrocycles. (Ketones will also form imines,  $R^1R^2C=N-R^3$ , but these reactions tend to occur less readily than with aldehydes). Because of the versatility offered by this ligand donor group, together with the accessibility of ruthenium in variable oxidation states, we attempt the synthesis of a cyclopentadienylruthenium (II) thiolato Schiff base complex and its subsequent application as a mediator for horseradish peroxidase in the amperometric analysis of peroxides. Our choice of the methyl-thiolate end group is motivated by the affinity of sulfur for gold.

#### **3.2 Experimental:**

### **3.2.1 Materials:**

4-Hydroxybenzaldehyde (98%); 2-chloroethylmethyl sulphide (97%); potassium carbonate; 4-aminothiophenol; bis(cyclopentadienyl)ruthenium(II) (97%); horseradish peroxidase (HRP, 1.10U/mg, P6782); 30% (v/v) hydrogen peroxide solution, cumene hydroperoxide (98%), *tert*-butylehydroperoxide (99%), were purchased from Sigma-Aldrich. All other reagents were of analytical grade and were used as obtained from suppliers without further purification. Solvents were refluxed over an appropriate drying agent; dichloromethane over phosphorus pentaoxide, acetone over anhydrous calcium chloride and toluene over pressed sodium lumps, distilled and degassed prior to use. All organic and organometallic synthesis was performed under nitrogen with the use of standard Schlenk techniques.



### **3.2.2 Instrumentation:**

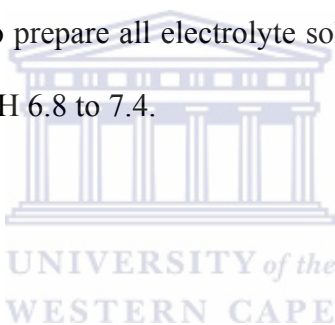
<sup>1</sup>H NMR spectra were recorded on GEMINI-200 MHz, Infrared spectroscopy (FTIR) and UV-vis was performed in the Chemistry department, University of the Western Cape (UWC). Scanning electron microscopy was done in the Department of Physics, UWC. Elemental analysis was done at The University of Cape Town (UCT) as a service.

All electrochemical analysis was performed with a Bio analytical system electrochemical analyzer (BAS100/W) software, using either cyclic voltammetry (CV) or Oyster young square wave (OSWV) voltammetric techniques. A conventional three electrode electrochemical cell was employed; gold disk working electrode, 0.02 cm<sup>2</sup> (WE), silver/silver chloride (Ag/AgCl) with a 3 M NaCl filling solution and a coiled platinum wire were used as reference and auxiliary electrodes respectively. A 20 mL electrochemical cell was used for all electrochemical experiments. A negative oxidation current was used for the display of all figures. All cyclic

voltammograms were carried out at a scan rate of 50 mV/s, unless otherwise stated. Square wave voltammograms were carried out using a step potential of 4 mV, 25 mV amplitude, and a frequency of 15Hz.

### **3.2.3 Buffers and solutions:**

Di-sodium hydrogenorthophosphate ( $\text{Na}_2\text{HPO}_4$ ) and sodium di-hydrogenorthophosphate dihydrate ( $\text{NaH}_2\text{PO}_4 \cdot 2\text{H}_2\text{O}$ ) were used in the preparation of all buffer solutions. All electrochemical experiments were carried out in phosphate buffered saline (PBS), (0.1 M phosphate, 0.137 M NaCl and 2.7 mM KCl). Unless otherwise stated. De-ionized water (Milli-Q, Millipore, Japan) purification system was used to prepare all electrolyte solutions. All experiments were carried out under an argon atmosphere at pH 6.8 to 7.4.



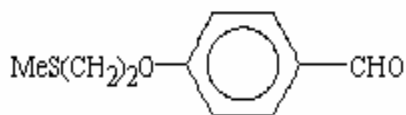
### **3.3 Methodology:**

#### **3.3.1 Synthesis of $\text{OHCC}_6\text{H}_4\text{O}(\text{CH}_2)_2\text{SMe}$ (a):**

To a solution of 4-hydroxybenzaldehyde (1.0 g, 8.19 mmol) dissolved in (50 mL) acetone in a Schlenk tube (100 mL) was added  $\text{K}_2\text{CO}_3$  (5g), followed by 2-chloroethylmethylsulphide (1.82 ml, 16.38 mmol). The reaction mixture was refluxed for 48h at 55 °C under nitrogen atmosphere. Upon cooling to room temperature, a pale orange-yellow liquid was obtained, which was chromatographed on silica gel

(230 – 400 mesh), hexane:dichloromethane (1:3) as eluent to afford the pure analytical compound with a yield of 1.42 g (88.3%).

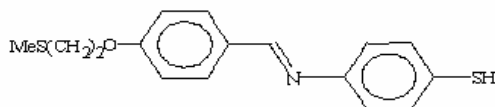
$^1\text{H}$  NMR ( $\text{CDCl}_3$ ):  $\delta$ 9.84(s,1H,CHO), 7.82 (d, 2H,  $J_{\text{HH}} = 8.8\text{Hz}$ ,  $\text{OHCC}_6\text{H}_4$ ), 6.98 (d,2H,  $J_{\text{HH}} = 8.6\text{Hz}$ ,  $\text{OC}_6\text{H}_4$ ), 4.27 (t, 2H,  $\text{OCH}_2$ ), 2.88 (t, 2H,  $\text{SCH}_2$ ), 2.22 (s, 3H,  $\text{SCH}_3$ ).



*Scheme 3.1: Chemical structure of compound (a)*

### **3.3.2 Synthesis of $\text{HSC}_6\text{H}_4\text{NC}(\text{H})\text{C}_6\text{H}_4\text{O}(\text{CH}_2)_2\text{SMe}(\text{b})$ :**

Compound (a) (0.5 ml, 2.71 mmol) and 4-aminothiophenol (0.34 g, 2.71 mmol) was dissolved in toluene (50 mL) in a Schlenk tube (100 mL). After addition of a few drops of glacial acetic acid, the reaction mixture was stirred overnight under nitrogen for 18h at room temperature. Evaporating the solvent under vacuum, a yellow residue was obtained. The product crystallized from DCM:Hexane (1:3) at  $-18\text{ }^\circ\text{C}$ . After filtration, the solid was washed with hexane and vacuum dried to afford a yellow solid. Yield = 0.39 g (47%).  $^1\text{H}$  NMR ( $\text{DMSO}-d_6$ ):  $\delta$ 8.31 (s, 1H,  $\text{C}(\text{H})\text{N}$ ), 7.88 (d, 2H,  $J_{\text{HH}}=8.1\text{Hz}$ ,  $\text{C}(\text{H})\text{C}_6\text{H}_4$ ), 7.2 (d, 2H,  $J_{\text{HH}} = 8.4\text{Hz}$ ,  $\text{NC}_6\text{H}_4$ ), 7.11 (d, 2H,  $J_{\text{HH}} 8.1\text{Hz}$ ,  $\text{OC}_6\text{H}_4$ ), 7.00 (d, 2H,  $J_{\text{HH}} = 8.5\text{Hz}$ ,  $\text{SC}_6\text{H}_4$ ), 4.22 (t, 2H,  $\text{OCH}_2$ ), 2.93 (t, 2H,  $\text{SCH}_2$ ), 2.13 (s,  $\text{SCH}_3$ ). Anal. cald. For  $\text{C}_{16}\text{H}_{17}\text{NOS}$ : C, 70.80; H, 6.32; N, 5.16%. Found C, 71.54; H, 5.38; N, 5.31%.  $\text{IR}_{\text{C}=\text{N}}$  ( $\nu = 1592.8\text{cm}^{-1}$ ) (nujol).



*compound (b)*

*Scheme 3.2: Chemical structure of*

### **3.3.3 Synthesis of $[\text{Ru}(\text{SC}_6\text{H}_4\text{NC}(\text{H})\text{C}_6\text{H}_4\text{OCH}_2\text{CH}_2\text{SMe})(\eta^5\text{-C}_2\text{H}_5)_2](\text{c})$ :**

To a suspension of bis(cyclopentadienyl)ruthenium (II) (0.051 g, 0.216 mmol) in toluene (50 mL) was added compound (b) (0.058 g, 0.216 mmol) in a 100 mL Schlenk tube. The reaction mixture was stirred at room temperature for 24 h. During this period, a yellow solid was obtained which was crystallized from DCM:Hexane, (1:3), washed repeatedly with hexane and dried in vacuum. A yellow solid was obtained. Yield = 0.022 g (44%).  $^1\text{H NMR}$  (DMSO- $d_6$ ):  $\delta$ 8.32 (s, 2H, C(H)N), 8.13 (d, 4H,  $J_{\text{HH}}=8.1$ , C(H)C $_6$ H $_4$ ) 7.82 (d, 4H,  $J_{\text{HH}} = 8.1\text{Hz}$ , NC $_6$ H $_4$ ), 7.02 (dd, 8H, SC $_6$ H $_4$ , OC $_6$ H $_4$ ), 4.51 (s, 10H, C $_5$ H $_5$ ), 4.13 (t, 4H, OCH $_2$ ), 2.97 (t, 4H, SCH $_2$ ), 2.21 (s, 6H, SCH $_3$ ). Anal calcd. For C $_{42}$ H $_{56}$ N $_2$ O $_2$ S $_4$ Ru $_2$ : C, 59.21; H, 6.41; N, 3.23%. Found C, 60.11; H, 5.15; N, 4.06%



*Scheme  
3.3:  
Chemical  
structure*

*of compound (c)*

### **3.4. Immobilization of cyclopentadienylruthenium(II)thiolato Schiff base on gold electrode:**

Before immobilisation of the cyclopentadienylruthenium(II)thiolato Schiff base self-assembled monolayer (SAM), on top of the gold electrode, a pre-treatment procedure based on the work of Willner and Rinklin [77], Schlereth et al. [78] was applied to the gold electrode. First the Au-electrode was polished with 15, 3 and 1- $\mu\text{m}$  diamond powder (BAS MF-2059) for 1min respectively, rinse thoroughly with de-ionized water and sonicated in de-ionized water for 5min, it was then immersed for 1 h in hot 2 M KOH solution. The electrode was rinsed with de-ionized water, immersed in conc.  $\text{HNO}_3$  for 10 min, and rinsed again with de-ionized water and immersed in con.  $\text{H}_2\text{SO}_4$  for 10 min, rinsed with de-ionized water. Finally the gold electrode was rinsed with the deposition solution, (DCM) and placed immediately in a solution of 1 mmol  $[\text{Ru}(\text{SC}_6\text{H}_4\text{NC}(\text{H})\text{C}_6\text{H}_4\text{OCH}_2\text{CH}_2\text{SME})(\eta^5\text{-C}_2\text{H}_5)_2]$  for 24 h at ambient temperature. Removing the Au-electrode from the deposition solution, it was rinsed with copious amounts of DCM. The counter electrode (BAS) was cleaned between each experiments by heating in a Bunsen flame. The reference electrode (BAS) was rinsed in de-ionized water between each experiment. Observation of redox activity of the SAM was preceded by a voltammetric cycle in a 0.1 M solution of NaOH between -200 mV and -600 mV vs. Ag/AgCl.

### **3.5 Immobilization of protein (HRP) on SAM:**

The SAM was transferred to a 1 mL batch cell before protein immobilization. Its surface was oxidized in 0.1 M phosphate buffer solution (pH 6.9), in the presence of HRP ( $1 \text{ mg mL}^{-1}$ ) at +700 mV vs. Ag/AgCl, at a sample interval of 500 ms, over 1500 s at a sensitivity of  $1 \times 10^{-9} \text{ A V}^{-1}$ . During this oxidation process, the enzyme became electrostatically attached to



the SAM surface. The enzyme solution was carefully recovered from the cell and stored at 4 °C for re-use.

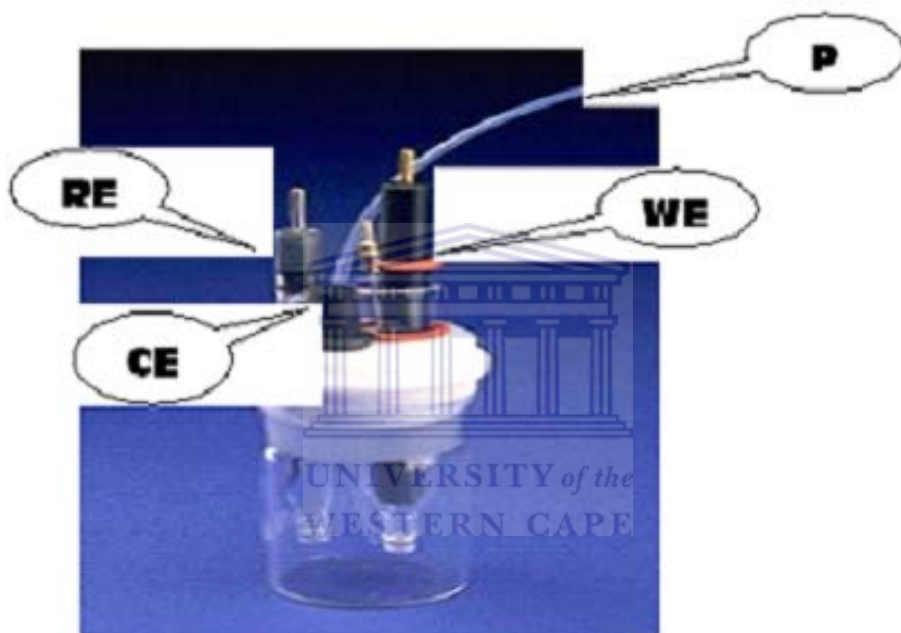


*Fig.3.1: A typical set-up of an electrochemical cell showing the working (WE), reference (RE), and counter (auxiliary (CE) electrodes and a degassing pipe (P).*

### **3.5.1 Electrochemical Characterization of cyclopentadienylruthenium(II) thiolato Schiff base complex in solution:**

Characterization of the Schiff base complex in solution was carried out using CV in  $\text{CH}_2\text{Cl}_2$  containing tetrabutylammoniumtetrafluoroborate (TBATFB 0.1 M). The concentration employed for the experiments was 2 mmol. CVs were performed between -200 mV to +800 mV and at -200 mV to +600 mV/s at a 50 mV/s scan rate respectively. These experiments were used to

evaluate the anodic to cathodic peak current ratio ( $i_{p,a}/i_{p,c}$ ), and the formal potential ( $E^\circ$ ). These experiments were also performed at varying scan rates (10 to 300 mV/s), allowing the evaluation of the Randle-Sevcik (Eq.3.1) plot to assess the quasi-reversibility of the complex.

$$i_p = (2.69 \times 10^5) n^{3/2} A D^{1/2} C \nu^{1/2} \quad \text{(Eq. 3.1)}$$

where  $i_p$  is the peak current ( $i_{p,a}$  anodic and  $i_{p,c}$  cathodic currents respectively),  $n$  is the electron stoichiometry,  $A$  the electrode surface area ( $\text{cm}^2$ ),  $D$  the diffusion coefficient,  $C$  the concentration of electroactive species ( $\text{mol dm}^{-3}$ ) and  $\nu$  the scan rate (mV/s).

### **3.5.2 Electrochemical characterization of the Schiff base complex on gold electrode:**

In order to assess the SAM's electroactivity, it required a voltammetric cycle in 0.1 M NaOH from -200 mV to +600 mV at 50 mV/s scan rate to deprotonate the methyl end group of the thiol complex. This was followed by characterization in 0.1 M phosphate buffer (pH 6.9) to interrogate the electroactivity of the SAM and subsequent enzyme immobilization.

### **3.6 Electrochemical measurements:**

The biosensor set-up was made up of Au//SAM/HRP as the working electrode, Ag/AgCl reference electrode and platinum wire counter electrode which were placed in a 5 mL phosphate buffer (pH 6.9) and connected to a BAS 100 W electrochemical work station. The Au//SAM/HRP electrode set-up was used to analyze hydrogen peroxide, cumene hydroperoxide and tert-butylhydroperoxide. All analyses were done in freshly prepared phosphate buffers. The buffers were degassed for 10 to 15 minutes and an argon "blanket" kept at the top through out

the experiments. The buffer solutions were stirred after each addition of the analyte to ensure homogeneity before analysis.

CV and OSWV experiments were used to monitor the reactions. CVs were performed at a scan rate of 5 mV/s from -200 mV to 600 mV at a sensitivity of 1  $\mu\text{A/V}$ . OSWV was also carried out at 4 mV step potential, 25 mV amplitude, 15 Hz frequency and sensitivity of 1  $\mu\text{A/V}$ . from +200 mV to -600 mV.

Calibration curves were plotted from the square wave responses of the biosensors. The hyperbolic Michaelis-Menten responses at maximum analyte concentrations were fitted to enzyme based Michaelis-Menten kinetics in accordance with the equation:

$$I = I_{\max}[\text{H}_2\text{O}_2]/([\text{H}_2\text{O}_2] + K'_m) \quad \text{Eq.3.2}$$

where  $I$  is the observed catalytic current,  $I_{\max}$  the maximum current which can be attained by the biosensor, and  $[\text{H}_2\text{O}_2]$  the bulk solution concentration of hydrogen peroxide (same for the other two organic peroxides).  $K'_m$  the apparent Michaelis-Menten constant. This can be simplified to:

$$I = (I_{\max}/K'_m)[\text{H}_2\text{O}_2] \quad \text{Eq.3.3}$$

This was used to evaluate the  $I_{\max}$  and  $K'_m$  for the sensors.



## **CHAPTER FOUR**

### **RESULTS AND DISCUSSIONS:**

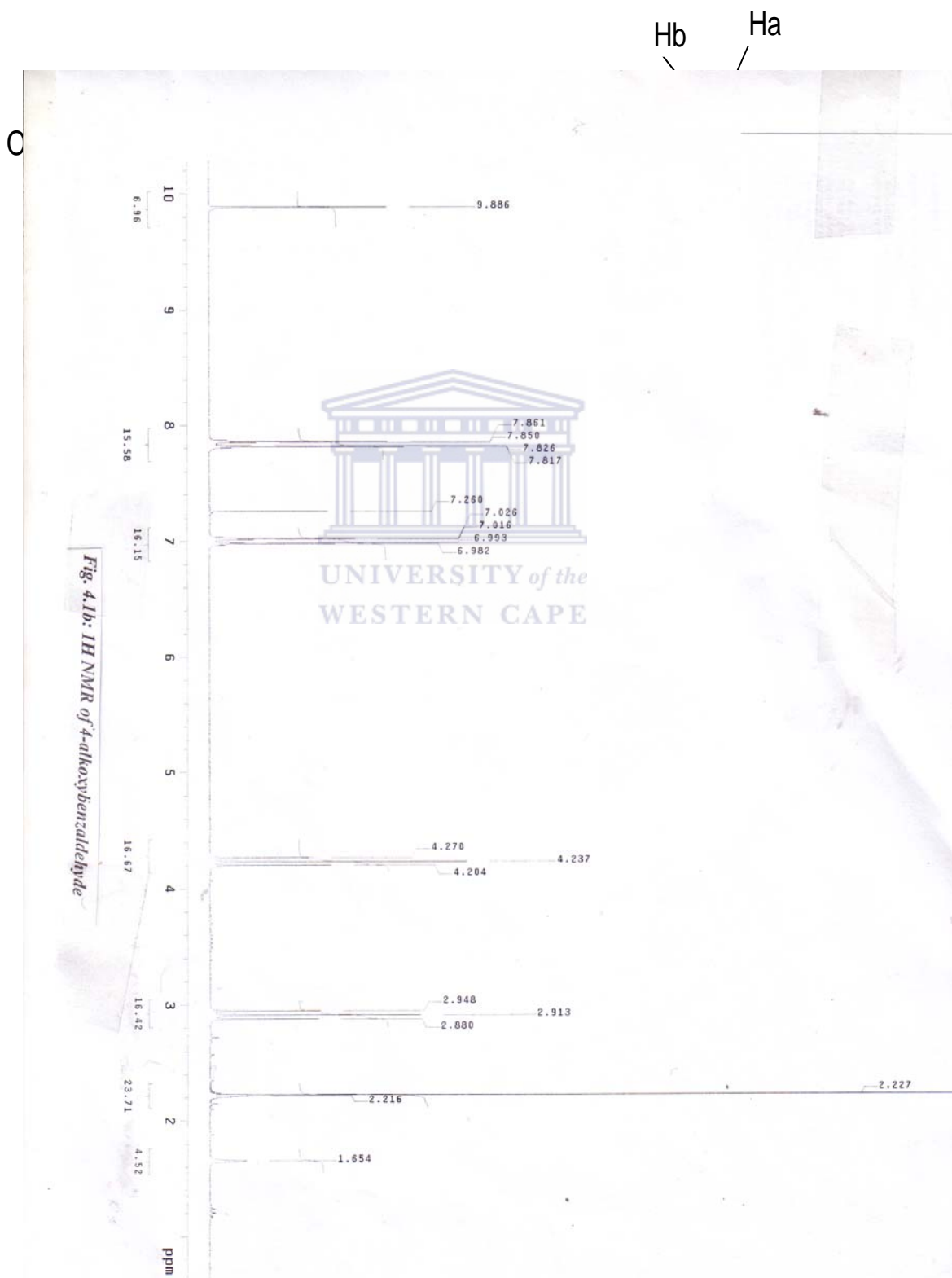
#### **4.1. Synthesis of 4-alkoxybenzaldehyde, $\text{OHCC}_6\text{H}_4\text{O}(\text{CH}_2)_2\text{SMe}$ :**

The *para*-alkoxybenzaldehyde used for the preparation of the Schiff base ligand was prepared by the Williamson reaction (Scheme 1, compound (a)). This was achieved by the reaction of 2-chloroethylmethylsulphide and 4-hydroxybenzaldehyde in refluxing acetone.

Improved yield was achieved by the use of finely ground potassium carbonate; otherwise the yield of the alkoxybenzaldehyde was low. Trace amounts of a by-product formed from the deprotonation of the carbonyl group were present as could be seen from the  $^1\text{H}$  NMR of the crude product, but the by-product was easily separated from the product by column chromatography, using a silica gel stationary phase and a  $\text{CH}_2\text{Cl}_2$ :hexane solvent mixture in a 1:3 ratio as eluent to give an analytically pure product, Eq. 4.1 (yield 88.3%). The difference in our synthetic protocol and that reported in literature; where potassium carbonate was used is in the choice of solvent. Binnemans *et al.* used butanone [78] while Scamporrino *et al.* used a mixture of toluene and water [79]. Other reaction conditions reported to effect the same reaction used potassium hydroxide in DMF or  $\text{ArSO}_2\text{Cl}$  and phenol in an ethanol:water (1:1) mixture [80-81]. In the above literature procedures the yields of the alkoxybenzaldehydes were in the range of 75 – 95%. We got a moderate yield, implying that we can use a cheaper solvent to obtain similar yield of products.

The  $^1\text{H}$  NMR (Fig.4.1b) of the analytically pure (Eq. 4.1) compound showed a prominent peak due to the carbonyl hydrogen of the **CHO** group at 9.84 ppm. This peak is typical of benzaldehyde derivatives reported elsewhere [81]. In addition, there were two sets of doublets at 6.98 ppm and 7.82 ppm due to the  $\text{H}_a$  and  $\text{H}_b$  protons respectively. The signal of the  $\text{H}_b$  proton is expected to be up field because of the shielding effect of the alkoxy chain while  $\text{H}_a$  is expected to be downfield because of the electron withdrawing nature of the carbonyl group. The simplicity in assigning the  $\text{H}_a$  and  $\text{H}_b$  is helpful in assigning the peaks of the Schiff base compound produced when the alkoxybenzaldehyde reacts with 4-aminothiophenol. The alkyl chain in the pure product gave triplets at 2.88 ppm and 4.10 ppm due to the higher electron withdrawing nature of

oxygen over sulphur ( $-\text{OCH}_2\text{CH}_2-\text{S}-$ ). A singlet at 2.19 was unambiguously assigned to the terminal methyl group ( $-\text{CH}_3$ ), Eq. 4.1.



#### **4.2. Syntheses of Schiff base ligand, $\text{HSC}_6\text{H}_4\text{NC}(\text{H})\text{C}_6\text{H}_4\text{N}_4\text{O}(\text{CH}_2)_2\text{SMe}$ :**

The Schiff base ligand was prepared by condensation of equimolar amounts of 4-aminothiophenol and the pre-formed alkoxybenzaldehyde (Eq.4.1a). This condensation reaction is the common route for imine bond formation. The product precipitated as thick yellow oil. The Analytically pure solid product was isolated by the slow diffusion of hexane into  $\text{CH}_2\text{Cl}_2$  solution at  $-18^\circ\text{C}$ . Further purification was achieved by recrystallisation from a  $\text{CH}_2\text{Cl}_2$ :hexane (1:3) mixture.

Infrared (IR) and  $^1\text{H}$  NMR spectroscopy were used to characterize the Schiff base compound isolated. IR was a simple but effective way of establishing the Schiff base formation. This was typically shown by the absence of the carbonyl peak in the aldehyde ( $1730\text{ cm}^{-1}$ ) and the appearance of an imine peak ( $1590.83\text{ cm}^{-1}$ ) (Eq. 4.2). Similar values have been reported in literature. For example the compounds N,N-bis(4-chlorobenzelidene)-2,2-diiminodiphenyl and 2-(2- $\text{Ph}_2\text{C}_6\text{H}_4\text{N}=\text{C}(\text{H})\text{C}_6\text{H}_4\text{OH}$ ) have peaks at  $1597\text{ cm}^{-1}$  and  $1614\text{ cm}^{-1}$  respectively [82]. The presence of the imine group was further confirmed by  $^1\text{H}$  NMR. The imine proton resonance occurred at 8.39 ppm, comparable to those of similar compounds synthesized by Nevondo *et al.* ( $\text{HSC}_6\text{H}_4\text{NC}(\text{H})\text{C}_6\text{H}_4\text{X}-4$ , X = F, Cl, Br, SMe and Me). In Schiff base compounds similar to ours ( $4\text{-H}_{2n+1}\text{C}_n\text{OC}_6\text{H}_4\text{NC}(\text{H})\text{C}_6\text{H}_4\text{OC}_n\text{H}_{2n+1}-4$ ) where alkyl chains replace the thiols, proton signals are found at 8.50 ppm [83], again indicating that the effect of substituent on chemical shift is generally minimal [84]. The rest of the chemical shifts helped in identifying the products. The only difference between the spectra was the integration of the signals upfield for the alkyl chain, which helped in confirming the number of protons in the chain.

The general pattern of the  $^1\text{H}$  NMR (Fig.4.1a) in the aromatic region consisted of four sets of doublets. They showed typical AB type patterns for the four protons on the two phenyl rings. The most upfield doublet was due to  $\text{H}_a$  (6.98 ppm) with the next doublet at 7.24 ppm due to  $\text{H}_e$ . The  $\text{H}_a$  and  $\text{H}_c$  protons were assigned making use of the alkoxybenzaldehyde (4.1) compound characterized earlier on and as well as compound  $\text{HSC}_6\text{H}_4\text{NC}(\text{H})\text{C}_6\text{H}_4\text{F}-4$  (7.32 ppm) [85]. The most downfield doublet is assigned to  $\text{H}_a$  while the next doublet up field was due to  $\text{H}_d$  (compared with those of the alkoxybenzaldehydes). All other signals were typical of thiol and alkyl functional groups. The resonance signal for the S-H proton was at 3.52 ppm, similar to literature values of 3.45 – 3.48 ppm for organic thiols [86].

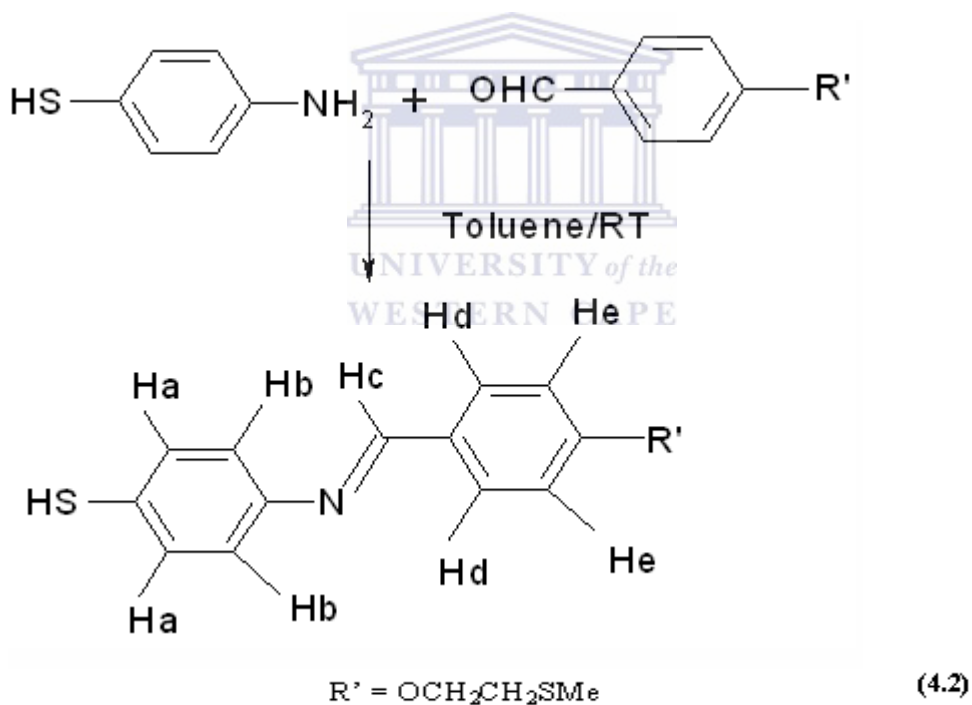
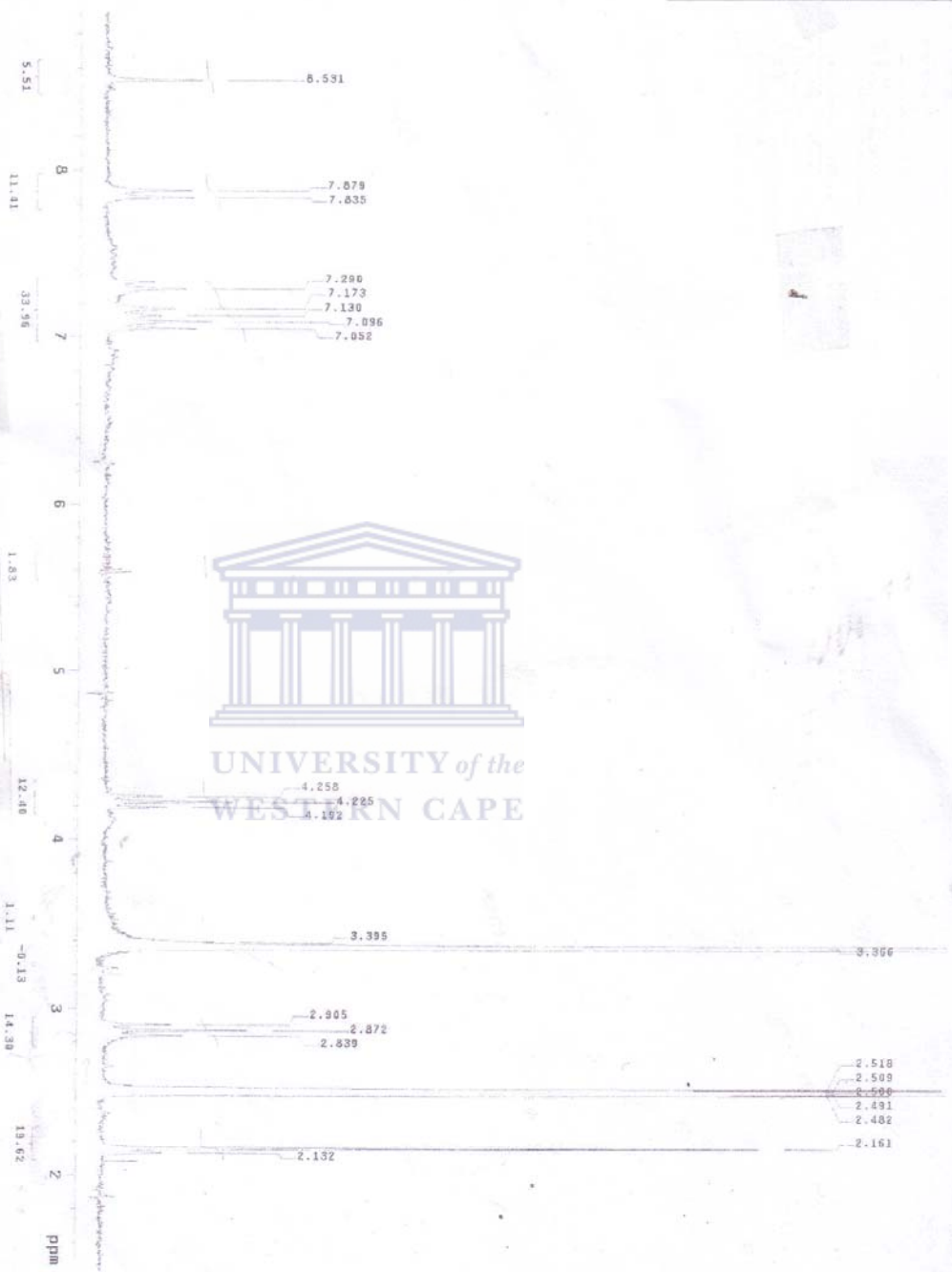




Fig. 4.1a: <sup>1</sup>H NMR of Schiff base ligand



100.0  
90  
80  
70  
60  
50  
40  
30  
20  
10  
0.0  
%T  
cm-1

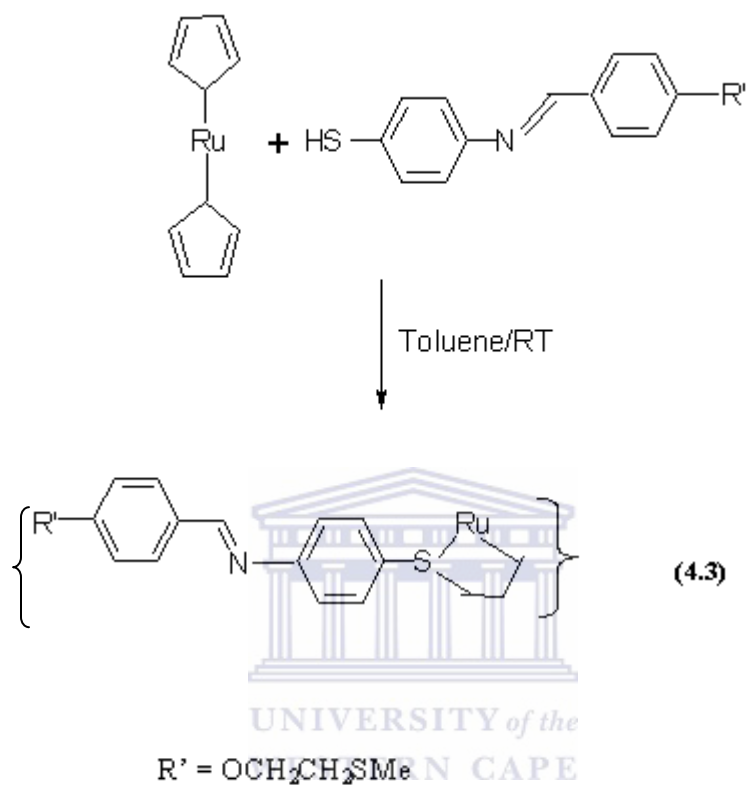
of the  
90.83 cm<sup>-1</sup>

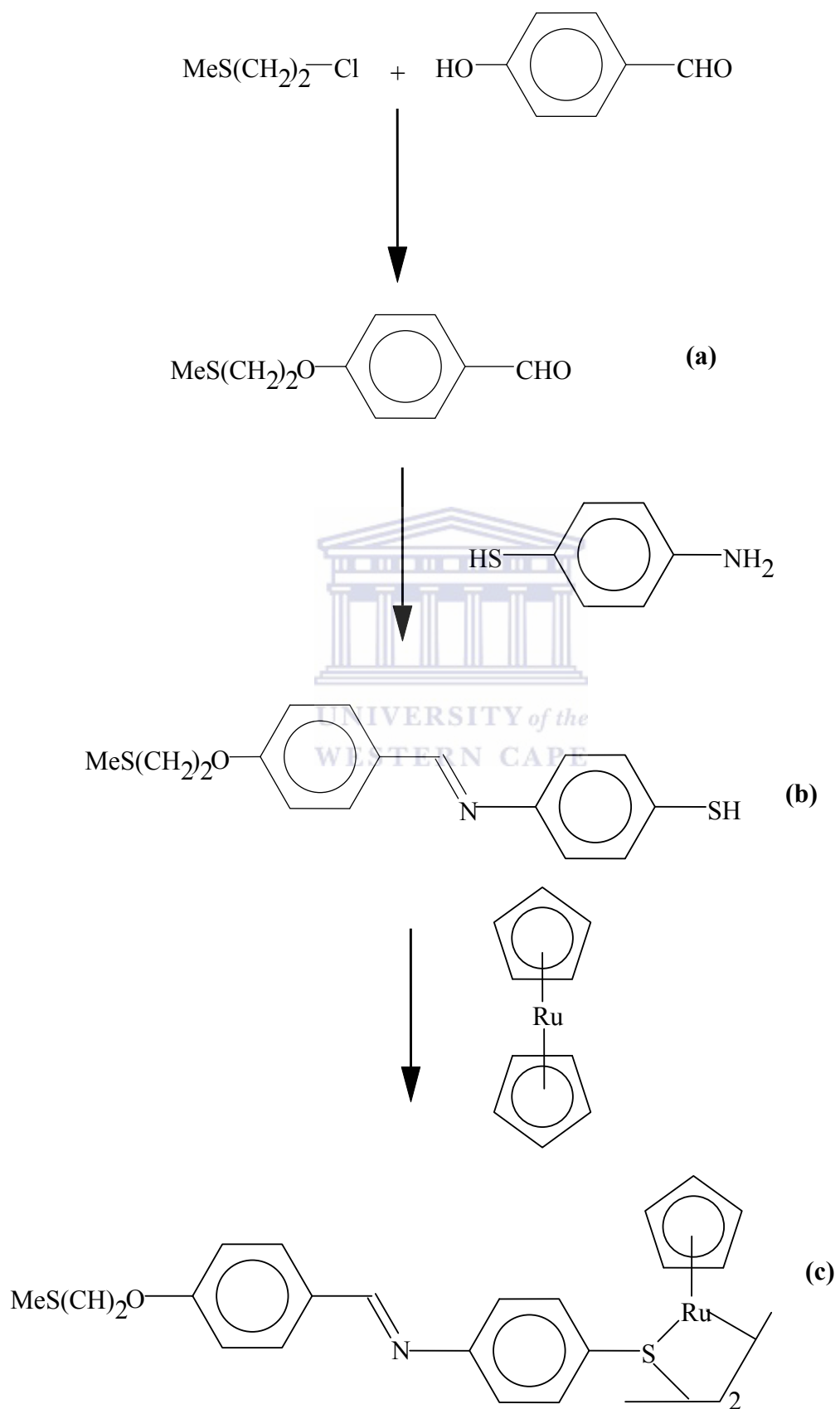
#### 4.3. Synthesis of *cyclopentadienylruthenium (II) thiolato Schiff base complex*,



The Schiff base complex was synthesized by reacting the thiol-imine ligand (Scheme 1 compound b) with bis(cyclopentadienyl)ruthenium(II), using a 1:2 ratio of reactants (Eq. 4.3). There was an immediate color change from pale-yellow to yellow on addition of the base, but the reaction was allowed to stir overnight at room temperature for complete reaction. The product was isolated by filtration and the complex re-crystallized from  $\text{CH}_2\text{Cl}_2$ /hexane at  $-18^\circ\text{C}$  to give analytically pure complex. Generally the yield was moderate (44%) with the complex being air stable under laboratory conditions and being stored in sample tubes under air for several weeks without decomposition.

The  $^1\text{H}$  NMR spectral data showed that the electronic environment of the cyclopentadienyl ring was not affected in that the thiolato resonance of the complex and those of the free ligand are very similar. The only difference was a cyclopentadienyl peak at 4.51 ppm [83]. This observation shows that the substituent on the para-position of the Schiff base ligand has no influence on the electronic environment around the ruthenium atom. Further characterisation of the complex was achieved by electrochemical methods (see below).





**4.4.** *Scheme 1. Reaction scheme for the synthesis of  $[Ru(SC_6H_4NC(H)C_6H_4OCH_2CH_2SMe)(\eta^5-C_2H_5)_2]$  complex via Williamson and Schiff base condensation reaction. Compounds (a)  $OHCC_6H_4O(CH_2)_2SMe$ , (b)  $HSC_6H_4NC(H)C_6H_4O(CH_2)_2SMe$  and (c)  $[Ru(SC_6H_4NC(H)C_6H_4OCH_2CH_2SMe)(\eta^5-C_2H_5)_2]$*

**Electrochemical characterization of cyclopentadienyl ruthenium (II) thiolato Schiff base complex in solution:**

Cyclopentadienylnickel(II)thiolato Schiff base complexes of the form  $[Ni(SC_6H_4NC(H)C_6H_4OCnH_{2n+1})(\eta^5-C_2H_5)_2]$ , ( $n = 4, 14, \text{ and } 16$ ) have been proven to exhibit ideal reversible electrochemistry, offering low positive potential values vs. the normal hydrogen electrode (NHE) [87] paving the way to be investigated for possible applications as electron transfer mediators in biosensors. Our attempt is to expand this notion to a novel cyclopentadienylruthenium(II)thiolato Schiff base complex,  $[Ru(SC_6H_4NC(H)C_6H_4OCH_2CH_2SMe)(\eta^5-C_2H_5)_2]$ , (section 2.3.3). Taking advantage of the  $\pi$ -back-bonding capability of ruthenium(II) and its accessibility in various oxidation states together with singular properties offered by the Schiff base ligands (ease of synthesise and their planarity) [88]. A cyclopentadienylruthenium (II) thiolato complex was synthesized for the formation of a novel self-assembled monolayer (SAM) on gold electrode. The redox properties of this complex were investigated under stationary conditions at a gold disc electrode under an argon “blanket”. Cyclic voltammetry (CV) in  $CH_2Cl_2$  containing TBATFB (0.1 M) was used to interrogate the redox activity of this complex owing to its high sensitivity and reproducibility. Dilute concentrations of the complex (2 mmol) were employed in all voltammetric experiments. SAM formation using a very dilute solution gives an ordered monolayer whereas a high concentration and long time (6 days) favor multiple layer formation [89]. The CV of the SAM displayed a well-defined wave assigned to the  $Ru^{III}/Ru^{II}$  redox couple. This process is observed with

characteristics of high quasi-reversibility [90]. The change in potential,  $\Delta E = (E_a - E_c)$ , where  $E_a$  and  $E_c$  are the anodic and cathodic potentials, respectively, is observed at 100 mV, with a formal potential  $E^\circ$ , of 174 mV together with a peak ratio, ( $E_{p,a}/E_{p,c}$ ) of 1.42 further attest to the quasi-reversibility of the complex. (Fig.4b). Sweeping the electrode through potentials outside its potential window can deteriorate the behavior of the system, due to the formation of oxides or hydrogen evolution at the working electrode. The purpose of sweeping the potential over a wide range was to investigate all the electrochemistry of the complex (4a). It was seen that the  $\text{Ru}^{\text{III}}/\text{Ru}^{\text{II}}$  redox electrochemistry was the only redox activity present in the complex (Fig.4a) warranting further characterisation.



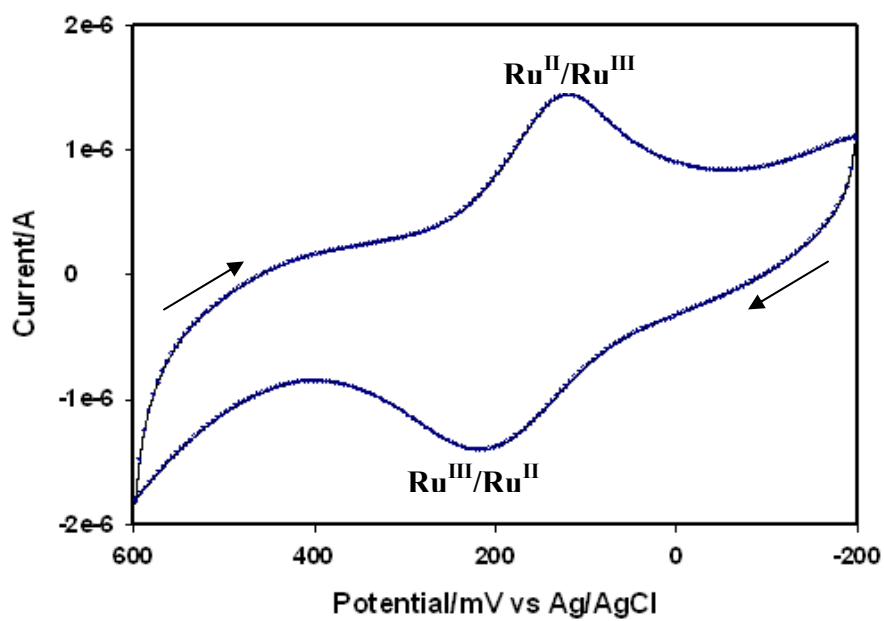
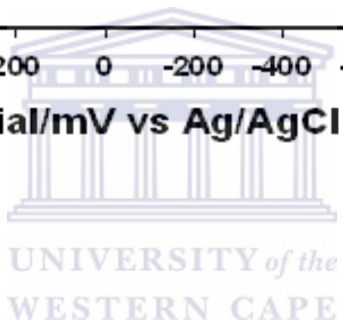
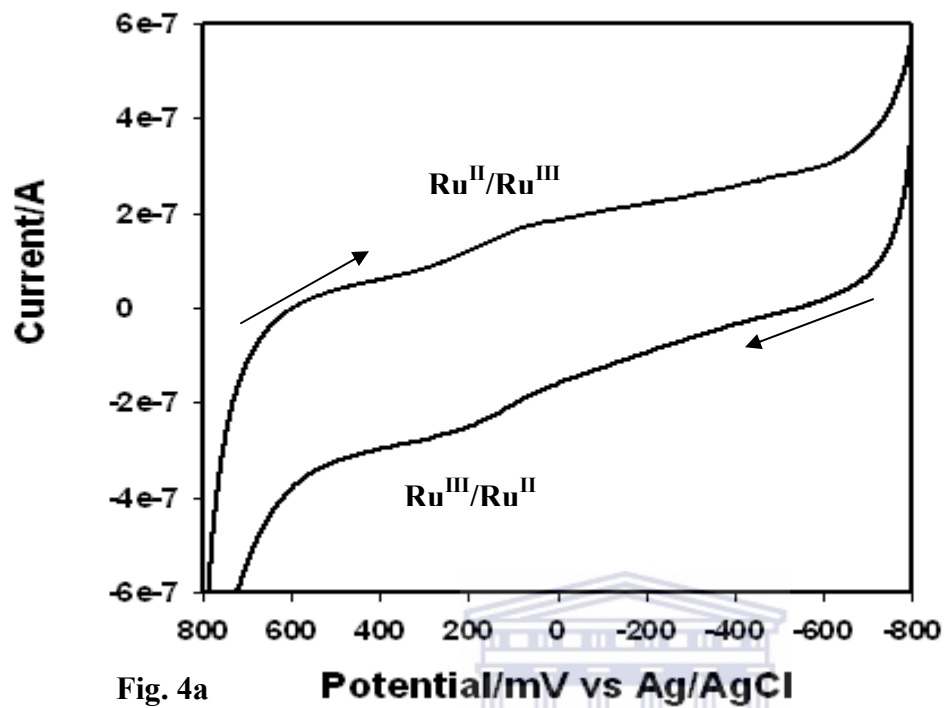


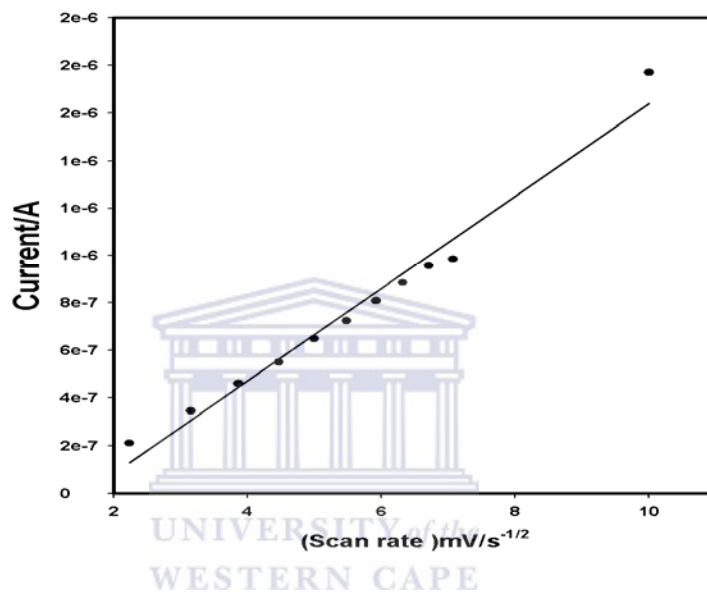
**Fig. 4a: Cyclic voltammograms of a  $2 \times 10^{-3} M$   $[Ru(SC_6H_4NC(H)C_6H_4OCH_2CH_2SME)(\eta^5-C_2H_5)]$ , on a bare gold electrode containing 0.1 M TBATFB at a potential window of (a) -800 mV/s to +800 mV/s and (b) -200 mV/s to +600 mV/s at scan rate of 50 mV/s**

(Fig

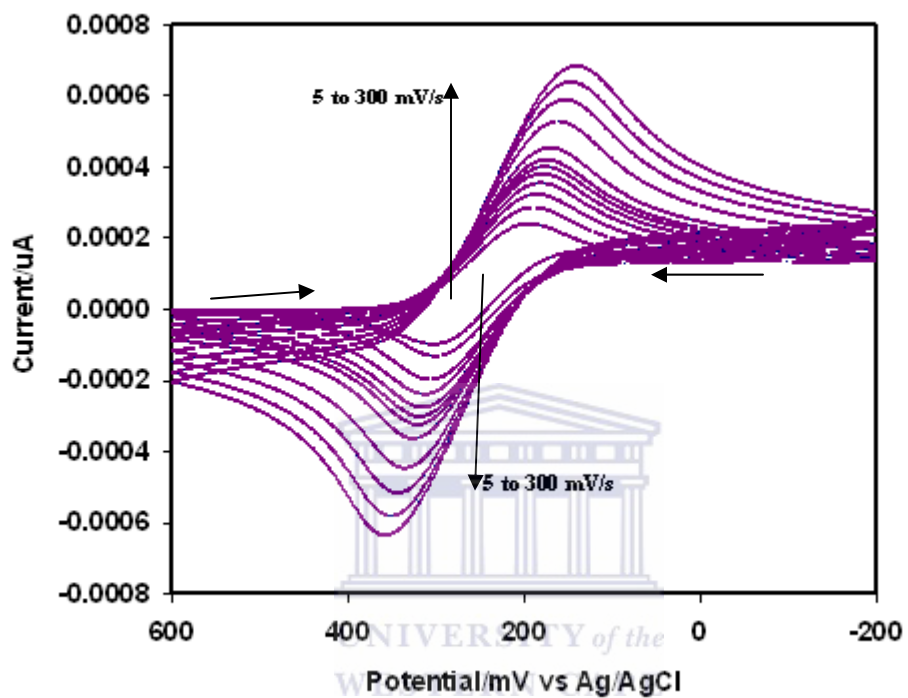
current for the

$Ru^{III}/Ru^{II}$  redox couple, with the potential held at -200 to +600 mV at scan rates ranging from 10 to 300  $mVs^{-1}$ , (Fig. 4.4b). All plots were normalized to correct for double layer-charging. The near superimposition of the plots demonstrated the quasi-reversibility of the  $Ru^{III}/Ru^{II}$  couple. The peak current was proportional to  $v^{-1/2}$  ( $r = 0.98$ ), and  $\Delta E_p$  did not change with varying scan rates. Further evidence for quasi-reversibility of the complex lie in the fact that the peak potential difference ( $\Delta E_p$ ) was 100 mV, with anodic to cathodic peak current ratio of 1.42 (Fig. 4b,  $v = 50 mVs^{-1}$ ). However, the non-zero intercept can be attributed to non-faradaic currents, reason why the complex is said to be only quasi-reversible [91]. Due to the Ru(II) thiolato Schiff base strong redox properties, together with its methyl sulfide end-group, the complex was further investigated for its possible application as an electro analytical self-assembled monolayer (SAM).





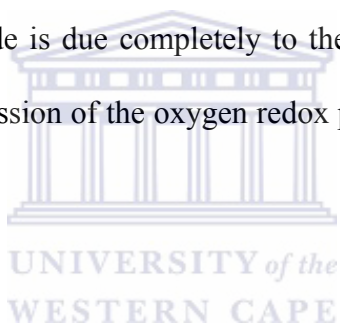
**Fig. 4.4a** Plot of  $v^{-1/2}$  vs. anodic peak current; the high correlation ( $r^2 = 0.988$ ) indicating electron diffusion limited response of the Au//SAM electrode.



*Fig.4.4b: Reversibility plots for the voltammograms of  $2 \times 10^{-3} \text{ M}$   $[\text{Ru}(\text{SC}_6\text{H}_4\text{NC}(\text{H})\text{C}_6\text{H}_4\text{OCH}_2\text{CH}_2\text{SME})(\eta^5\text{-C}_2\text{H}_5)_2$  from -200 to +600 mV/s. The scan rate was varied from 5 to 300 mV/s. All other conditions are as in fig. 4.3b. The superimpositions of the plots demonstrate the reversibility of  $\text{Ru}^{\text{III}}/\text{Ru}^{\text{II}}$  redox couple.*

#### **4.5 Characterization of $[Ru(SC_6H_4NC(H)C_6H_4OCH_2CH_2SME)(\eta^5-C_2H_5)_2]$ on gold**

In order to access the self-assembled monolayer formation on gold, PBS was used as a redox probe. The choice of the phosphate buffer was motivated by the fact that the cyclopentadienyl complex was insoluble in this buffer, offering an excellent medium (electrolyte) for studying the electrochemistry of this complex on the gold disc electrode surface. The redox behavior of this probe was completely inhibited following monolayer formation. Any redox activity observed after removing the Au-electrode is due completely to the SAM formation on gold electrode as indicated by a complete suppression of the oxygen redox peak of the probe in PBS (Fig.4.5) [87-89].



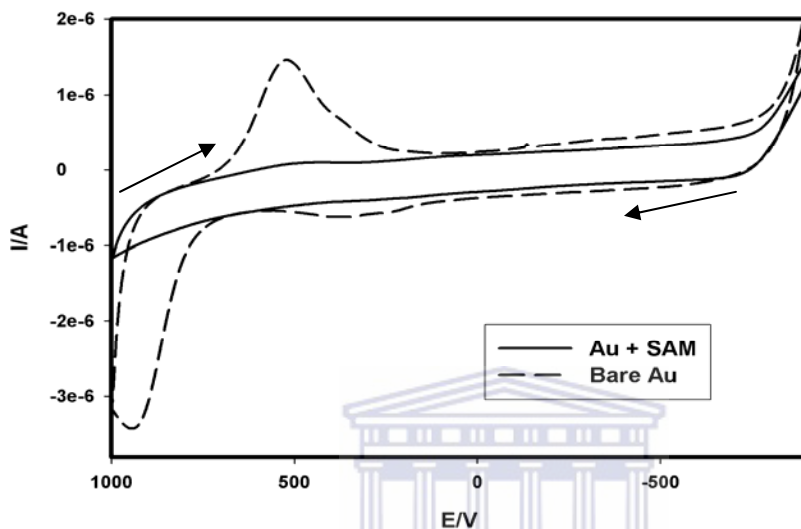


*Fig.4.5 Bare Au (broken line) and Au + SAM (smooth line) in 0.1 M PBS. SAM formation on the gold electrode was indicated by a significant suppression of the oxygen redox peak of the gold electrode. No electronic communication was observed between the Au//SAM and the solution, hence the surface of the gold electrode was completely covered by the SAM, excluding ions and water from the underlying gold electrode.*

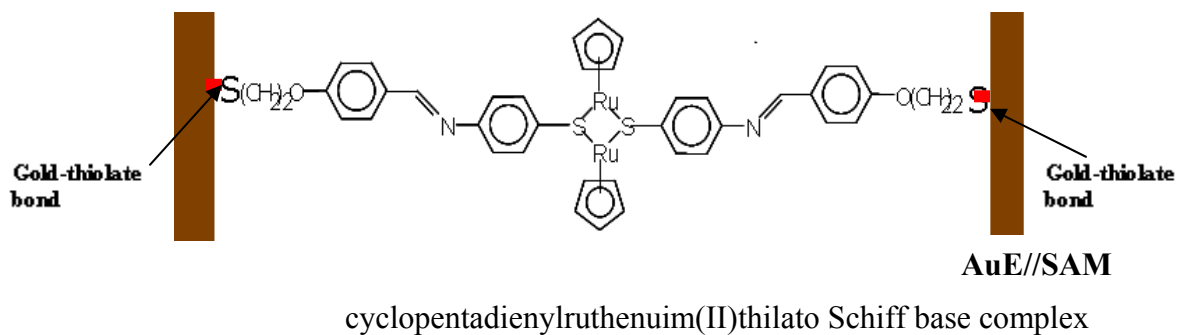


**Fig.4.5.1 Schematic representation of a single molecule, showing self-assembled monolayer formation through covalent bond formation between the thiol-end group and the gold electrode surface.**

The thiol end group of the complex was terminated by a methyl end group to avoid aggregation on the surface of gold, forming the monolayer of thiolato Ru (II) Schiff base. The SAM required a voltametric cycling in base (0.1 M NaOH) from -200 to +600 mVs<sup>-1</sup> ( $v = 50 \text{ mVs}^{-1}$ ) in order to observe any redox activity. Before cycling in base, the SAM showed little or no redox activity completely, with onset of cycling, a set of quasi-reversible peaks began to appear. As the number of cycles was increased, the areas under the anodic and cathodic peaks began to increase, reaching stability after 5 cycles (Fig 4.5.2). This implies the number of redox active molecules on the surface of the gold electrode must have been increasing. An explanation for this observation is based on the fact that the desired cleavage of the sulfur-methyl bond did not occur during the time in which the Au-electrode was left standing in the deposition solution. SAM formation had occurred but the complex was only weakly bound to the Au-electrode, via the lone pair donated by the thiol end groups. This justifies the initially observed poor electronic communication between the Ru(II) redox centres and the Au-electrode. Continued cycling after will inevitably change the conformation of the SAM as a consequence of *in-situ* generation of covalent bonding between the sulphur and Au-electrode for formation of a true SAM. This improved electronic communication between the Ru(II) centres of the complex is due to induced covalent bonding.

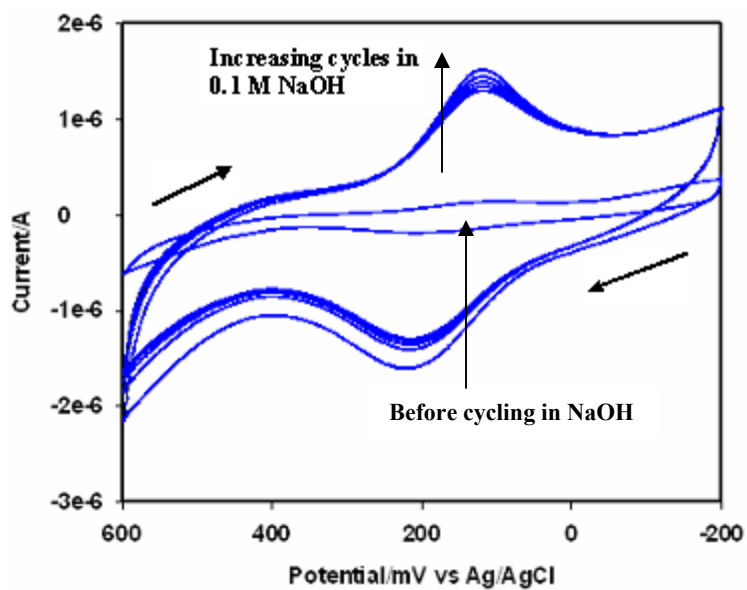
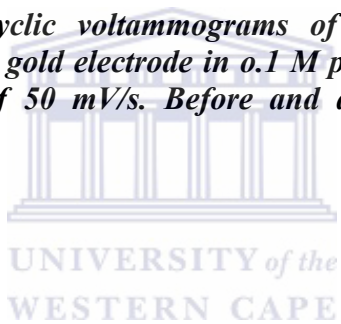


*Fig. 4.5.2: Cyclic voltammograms of the NaOH-treated SAM-modified gold electrode in 0.1 M phosphate, pH 6.9 at a scan rate of 50 mV/s. Before and after cycling in 0.1 NaOH.*



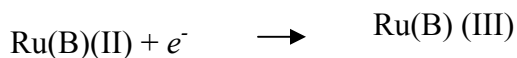
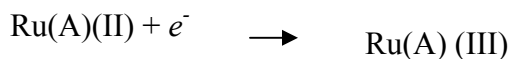
The use of bases such as  $\text{NH}_4\text{OH}$  and  $\text{NaOH}$  have also been exploited to a greater extent in deprotonating the alkyl end groups to minimize S-S bond formation [93, 94]. Other bases have also been used such as  $(n\text{-C}_3\text{H}_7)_2\text{NH}$  or dimethylaminopyridine by the same authors, but were found to be less effective in deprotonating the thiol end groups. Their method of deprotonation was by adding small amounts of the base to the SAM deposition solution; so that the deprotonation takes place in bulk solution leaving the thiol end groups free to attach to the gold substrate for conventional self-assembly. In our case, we decided to deprotonate the SAM after removal from the deposition solution, (Fig. 4.5.2) demonstrates this clearly as no electronic communication could be seen before cycling in 0.1 M  $\text{NaOH}$ . A close-packed SAM will block Faradaic processes from the electrode surface. Cycling the bare and the SAM-modified electrode in 0.1 M  $\text{NaOH}$  solution (Fig. 4.5.2) allows the evaluation of the film ion barrier factor,  $\Gamma_{\text{ibf}}$  where

$$\Gamma_{\text{ibf}} = 1 - Q_{\text{SAM}}/Q_{\text{Bare}} \quad (1a)$$

where  $Q_{\text{SAM}}$  and  $Q_{\text{Bare}}$  are the charges under the gold oxide stripping peaks for SAM-modified and bare gold electrode respectively. It can be inferred from (Fig. 4.5) that since no charge could be detected on the Au-electrode after deposition of  $[\text{Ru}(\text{SC}_6\text{H}_4\text{NC}(\text{H})\text{C}_6\text{H}_4\text{OCH}_2\text{CH}_2\text{SME})(\eta^5\text{-C}_2\text{H}_5)_2]$ , it indicates that the gold surface was completely isolated from the aqueous solution which is the source of gold oxide formation. Since no charge could be detected for the gold surface after deposition,  $\Gamma_{\text{ibf}}$  must be approximately unity indicating that the SAM provides an excellent barrier to the permeation of electrolyte species.  $\Delta E_p$  of the redox probe couple was calculated to be 89.2 mV and  $I_{p,c}/I_{p,a}$  ratio of 1.26. These are a pointer to the SAM's electrocatalytic ability to mediate electron transfer reactions of any redox couple present in

solution. Furthermore, to ascertain that the SAM layer was the only source of redox activity being observed, the anodic current ( $i_{p,a}$ ) was directly proportional to the scan rate,  $v$ , which is consistent with that expected from an electrochemical reaction involving a surface confined species ( $r^2 = 0.98$ ), uniformly distributed and non-interacting redox centres positioned at the same distance from the surface of the electrode. In the case of a reversible electron transfer reaction, it is supposed the CV peaks should be at exactly the same potential, meaning  $\Delta E_p = 0$  mV. Deviation from this ideal behavior was attributed to either the non-uniformity of the distribution centres with respect to their distances to the electrode surface, and possible interactions like electrostatic repulsion or the irreversibility of the charge transfer processes involved.

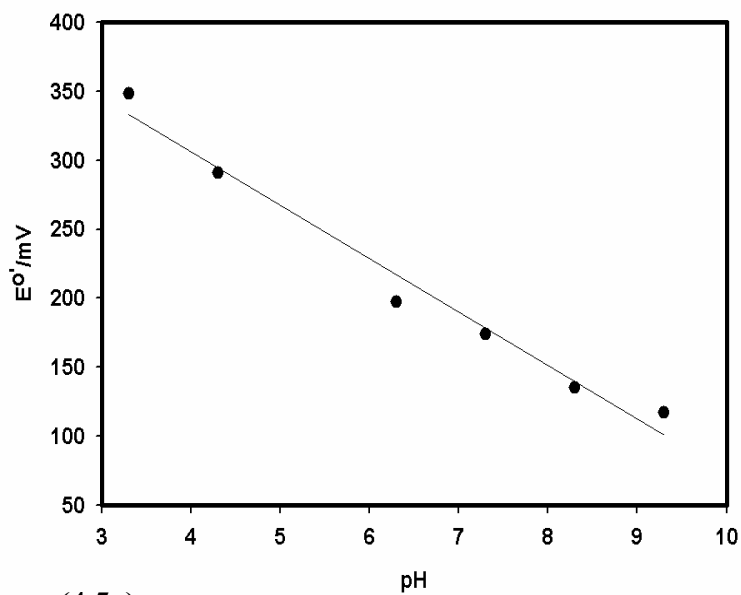
The formal potential of the SAM-modified electrode varied with pH (evaluated using OSWV in 0.1 M phosphate), (Fig. 4.5b) with a slope of about  $-34 \text{ mV pH}^{-1}$  over a pH range of 3.3 to 9.3 (Fig. 4.5a). This is close to the theoretical value of  $-29 \text{ mV pH}^{-1}$  for a two electron, one proton redox process [95]. This is in agreement with the Tafel analysis for the deduction of the number of electrons transferred for  $[\text{Ru}(\text{SC}_6\text{H}_4\text{NC}(\text{H})\text{C}_6\text{H}_4\text{OCnH}_{2n+1})(\eta^5\text{-C}_2\text{H}_5)_2]$ , ( $n = 4, 14, \text{ and } 16$ ) in bulk solution of  $\text{CH}_2\text{Cl}_2$  containing 0.1 M TBATFB. All Tafel plots gave values of approximately two for the number of electrons transferred, thus the reaction;



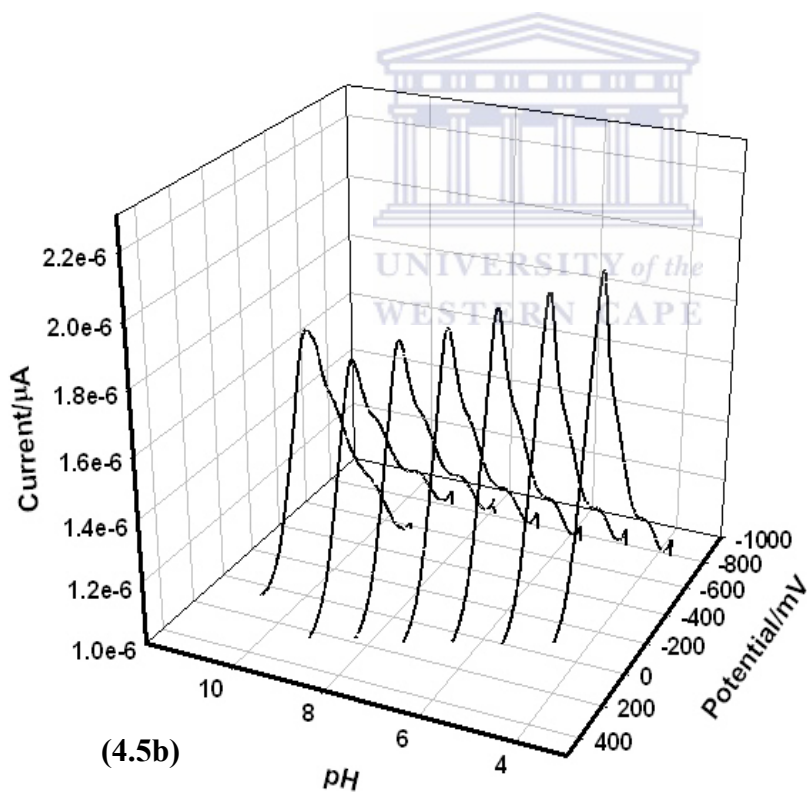


as there are two Ru(II) centres per molecule. A similar process had been observed by Ozoemena and Nyokong [96] for an iron phthalocyanine (Pc) immobilized on a gold electrode. This can be attributed to water (in acidic or neutral medium), and hydroxyl groups (in alkaline medium) coordinating to the Ru(II) centre. A pH close to neutral was chosen for this work since an enzyme is used and enzymes are pH sensitive.

Taking the number of electrons transferred to be two, the surface concentration,  $\Gamma$ , of the ruthenium redox centres was evaluated to be  $9.591 \times 10^{-11} \text{ mol cm}^{-2}$  which is reasonable compared to literature values [96, 98], which values are usually one order of magnitude higher than this. It can be deduced from Eq. 3.1 that this monolayer is effectively non-permeable to electrolyte species (implying surface coverage is relatively pin-hole free). Here we make the assumption that not all the Ru(II) groups attached to the surface of the gold electrode are electroactive. A possible reason can be that all the methyl end groups were not removed during voltammetric cycling in NaOH (Fig. 4.5b); hence electronic communication between all the molecules and the electrode surface could not occur.



(4.5a)



(4.5b)

**Fig.4.5:** (a) Plot of formal potentials vs. pH at a scan rate of  $50 \text{ mVs}^{-1}$ . pH was varied from 3.3 to 9.3 with a slope of  $-34 \text{ mV pH}^{-1}$ , demonstrating a two electron, one proton redox process. (b) OSWV voltammograms as a function of pH. The electrode was held at a constant potential of 200 mV.

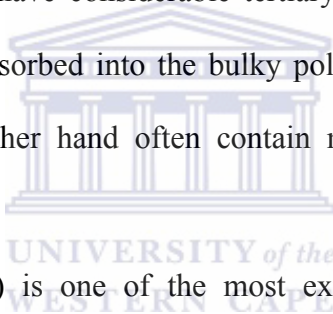
#### **4.5.1. Stability of SAM:**

The stability of self-assembled monolayer on gold was also assessed; this was studied as a function of pH and applied potential (Fig. 4.5a). The SAM showed high stability from pH 3.3 to 9.3 in the potential window -200 to + 800 mV/s. However, pH greater than 9.3, and potentials outside this window resulted in SAM desorption. This thiol derivatised self-assembled monolayer on gold electrode showed stability with no detectable desorption when stored for over a period of three weeks in phosphate buffer at pH 6.9. For the purpose of this work, a pH close to neutral is chosen for further studies, since enzymes will be used and enzymes are pH sensitive.



#### **4.6. Electrocatalytic Reduction of Peroxides at the Au//SAM/HRP-modified electrode:**

An amperometric biosensor has been developed, which incorporated the electroactive polymer, polyaniline (PANI), which undergoes redox cycling and can, couple electrons directly from the enzyme active site, to the electrode surface [71]. This was achieved by electropolymerisation of polyvinylsulphonate (PVS)-doped aniline onto the surface of a screen-printed carbon-paste electrode. Biomolecules were then doped onto the surface of the polymer by electrostatic interactions with a polymer back bone. This was used to examine the amperometric response of immobilized horseradish peroxidase (HRP) [79]. Self-assembly chemistry offers advantages over the above mentioned approach to electrode surface modification e.g polymer films, which are usually much thicker and have considerable tertiary structure leading to enzyme wastage, since the enzyme has to be adsorbed into the bulky polymer structure. Transferred Langmuir-Blogett (LB) films, on the other hand often contain many defects and can be intrinsically unstable.



Horseradish peroxidase (HRP) is one of the most extensively studied enzymes with large analytical applications in immunoassays and the development of biosensors for hydrogen peroxide monitoring. Its *in vivo* function is the prevention of oxidative damage of living cells via catalytic oxidation of a variety of electron donors using H<sub>2</sub>O<sub>2</sub> as oxidant. The usual catalytic enzyme cycle comprises three steps:

Oxidation of ferric enzyme with hydrogen peroxide forming the oxidized intermediate (Cpd I) and water:



- One-electron oxidation of a second substrate S (e.g., phenols, quinines, aromatic amines, etc.) by Cpd I leads to the formation of Cpd II and a radical product:



- Regeneration of the ferric enzyme by a molecule of substrate with liberation of a water molecule and  $\text{S}^\bullet$ .



When immobilized on the electrode surface, HRP catalyzes the reduction of  $\text{H}_2\text{O}_2$  according to (2). It is then reduced by the SAM//HRP electrode as a source of electrons with simultaneous uptake of two protons from the surrounding medium. The later reduction is referred to as a direct electron transfer process, and together with reaction (2) represents the direct bioelectroreduction of hydrogen peroxide in buffer solutions. The acceleration of the process at pHs below 7.0 was found to be the result of increased proton concentration, since proton uptake represents the rate-limiting step. The bioelectrochemical reduction of organic hydroperoxides in aqueous media proceeds through a similar catalytic cycle, which was the basis of our investigation for the development of a peroxidase-based amperometric electrode for the analysis of cumene hydroperoxide and tert-butylhydroperoxide, together with hydrogen peroxide.

#### **4.6.1 Electrocatalytic reduction of peroxides using CV at the Au//SAM/HRP-modified electrode:**

HRP was electrostatically attached to the SAM surface by application of an oxidizing potential in the presence of HRP ( $1 \text{ mg mL}^{-1}$ ), to electrostatically adsorb the enzyme onto the self-assembled monolayer on the gold electrode surface (section 3.4) [84].

In analyzing the three peroxides (hydrogen peroxide, cumene hydroperoxide and tert-butylhydroperoxide), there was a clear similarity in their electrochemistry as can be seen from the cyclic voltammograms. Figs.4.6.1, 4.6.2, and 4.6.3 depict the cyclic voltammograms of the Au//SAM/HRP-modified electrode in phosphate buffer (pH = 6.8), with (a) no peroxides present, (b)  $0.1 \text{ }\mu\text{M}$ , (c)  $0.2 \text{ }\mu\text{M}$  and (d)  $0.3 \text{ }\mu\text{M}$  peroxides under anaerobic conditions. CVs were performed after each addition, at very low scan rates ( $5 \text{ mVs}^{-1}$ ) in order to observe the fast enzyme kinetics. Irrespective of the huge background current in the CVs, the electrocatalysis of Ru(II) was observed. Although the electrocatalytic effect was not so prominent in the CVs (for cumene hydroperoxide and tert-butylhydroperoxide), an enhancement of the Ru(II) cathodic peak current was observed with the addition of these peroxides, consistent with an electrocatalytic effect [81]. The electrocatalytic effect was very prominent for  $\text{H}_2\text{O}_2$ . With the other two peroxides, it was not prominent for the anodic peak, but a small decrease in intensity was observed, confirming that the electro-produced Ru(II) was effectively consumed in the enzyme catalysis. Peak potential shifts were negligible upon addition of these peroxides.

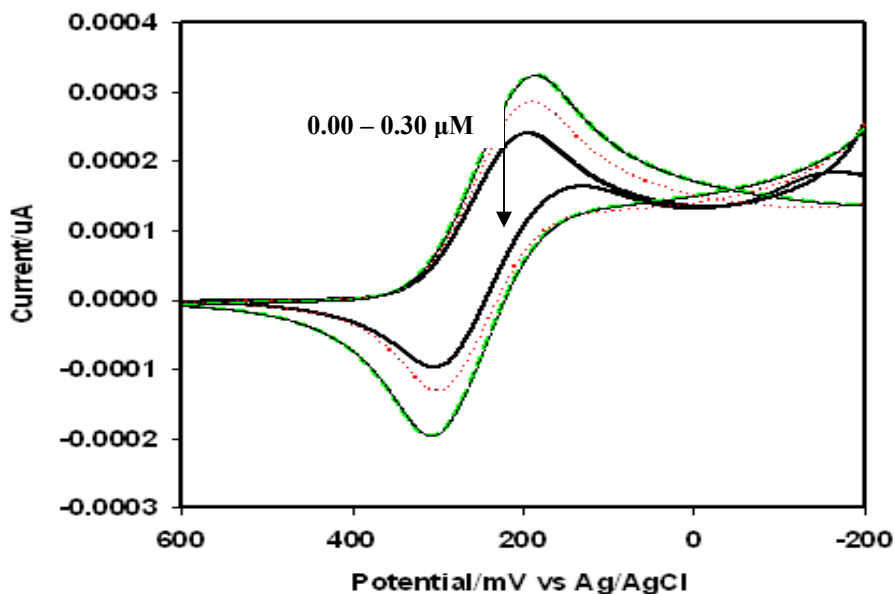


*Fig.4.6.1: Cyclic voltammograms (5 mV/s scan rate) of SAM//HRP-modified Au electrode in 0.1 M phosphate buffer, pH 6.8 for 0 mM, 0.1 μM, 0.2 μM and 0.3 μM H<sub>2</sub>O<sub>2</sub> under anaerobic conditions.*

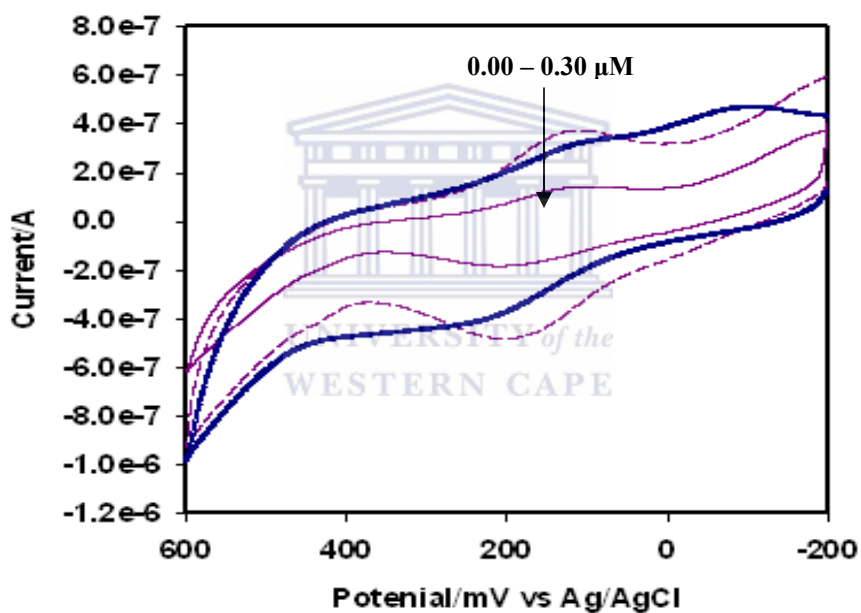


*Fig.4.6.2: Cyclic voltammograms (5 mV/s scan rate) of SAM//HRP-modified Au electrode in 0.1 M phosphate buffer, pH 6.8 for 0 μM, 0.1 μM, 0.2 μM and 0.3 μM Cumene hydroperoxide under anaerobic conditions*

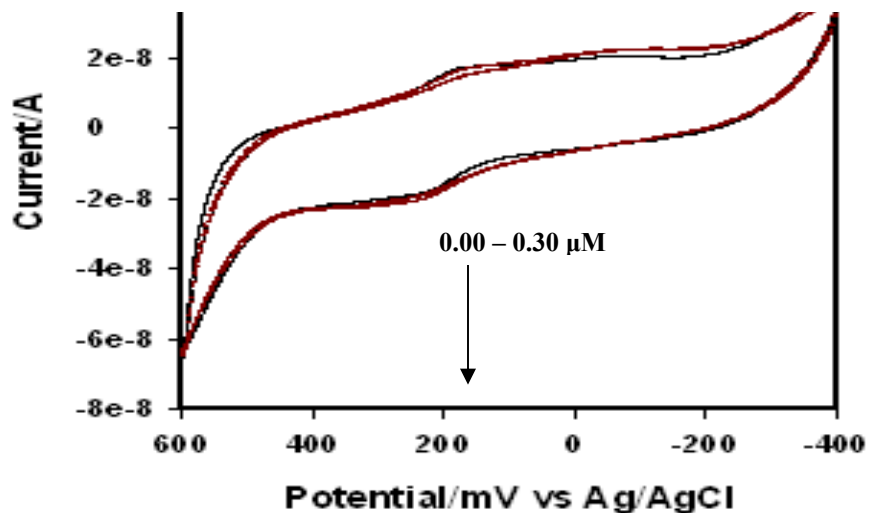


***Fig.4.6.3: Cyclic voltammograms (5 mV/s scan rate) of SAM//HRP-modified Au electrode in 0.1 M phosphate buffer, pH 6.8 for 0  $\mu$ M, 0.1  $\mu$ M, 0.2  $\mu$ M and 0.3  $\mu$ M Tert-butyl hydroperoxide under anaerobic conditions.***



#### **4.6.2 Electrocatalytic reduction of peroxides using OSWV at the Au//SAM/HRP-modified electrode:**

The same experiments (section 4.6.1) were also performed using Osteryoung square wave voltammetry. The voltammograms in Figs. 4.6.4, 4.6.5, 4.6.6 represent the net current (difference between forward and reverse currents) when the Au//SAM/HRP-modified electrode was scanned anodically. Again, the peroxides displayed similar electrochemistry with decrements in peak



heights upon addition of the peroxides being much more prominent with concomitant elimination of the high background currents observed in the CVs. The decreases in peak heights in the voltammograms of cumene hydroperoxide and tert-butyl hydroperoxide were not prominent compared with those of  $\text{H}_2\text{O}_2$ . An explanation for this observation is due to the bulky nature of the alkyl groups which can possibly block the electrocatalytic effect of the peroxides. The enhanced electrocatalytic effect observed in OSWV was attributed to the high sensitivity of the square wave technique. Thus, the electrocatalysis of the Ru(II) was verified with these results.

In order to confirm the role of horseradish peroxidase (HRP), cyclic voltammograms were carried out on a HRP-free surface. The CVs were run before and after addition of the peroxides. It was observed that there was little or no change in the cathodic peak, an increase in anodic peak current occurred (data not shown). These results are modest indicators that the SAM surface may have the ability to oxidize these peroxides. However, for the purpose of this research, it can be said that the Ru(II) complex alone cannot reduce these peroxides, and that HRP is playing an active role.

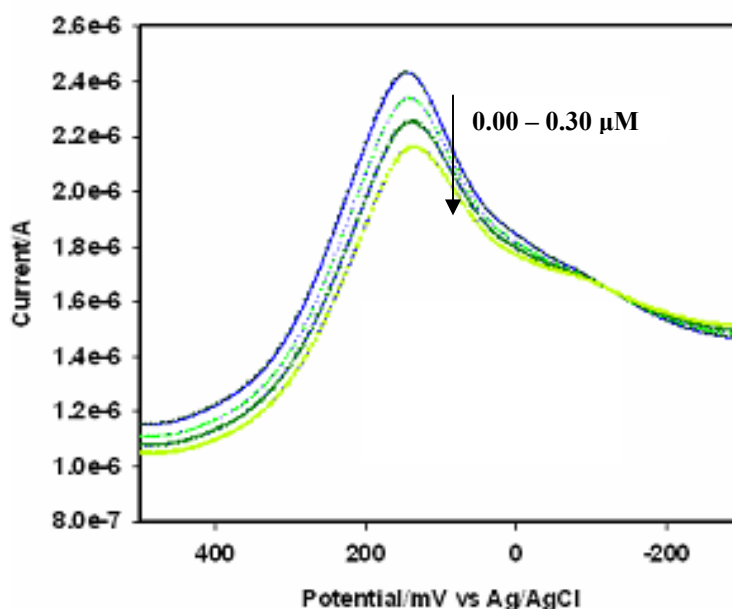


*Fig.4.6.4: OSWV (4 mV step potential, 25 mV amplitude, 15 Hz frequency) voltammograms of Au//SAM/HRP-modified electrode in 0.1 M phosphate buffer, pH 6.8 for 0.00  $\mu$ M, 0.10  $\mu$ M, 0.20  $\mu$ M and 0.03  $\mu$ M  $H_2O_2$ . Under anaerobic conditions*

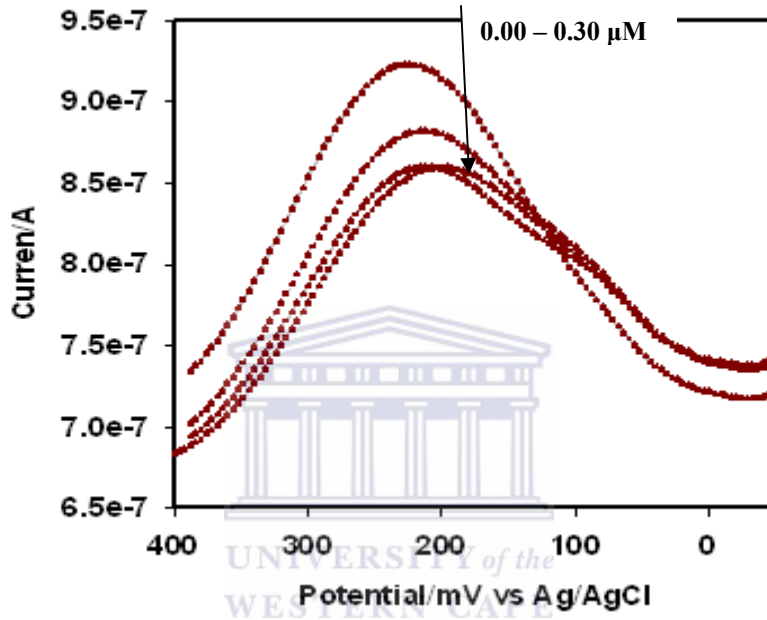


*Fig.4.6.5: OSWV (4 mV step potential, 25 mV amplitude, 15 Hz frequency) voltammograms of Au//SAM/HRP-modified electrode in 0.1 M phosphate buffer for 0.00  $\mu$ M, 0.10  $\mu$ M, 0.20  $\mu$ M and 0.30  $\mu$ M Cumene hydroperoxide under anaerobic conditions.*

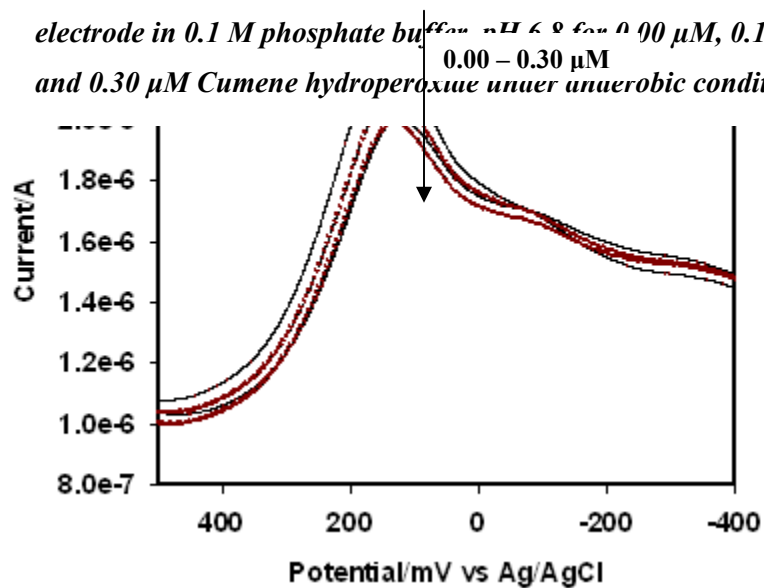


*Fig.4.6.6: OSWV (4 mV step potential, 25 mV amplitude, 15 Hz frequency) voltammograms of Au//SAM/HRP-modified electrode in 0.1 M phosphate buffer, pH 6.8 for 0.00  $\mu$ M, 0.10  $\mu$ M, 0.20  $\mu$ M and 0.30  $\mu$ M tert-butylhydroperoxide under anaerobic conditions.*



It can be said here with optimism that the two representative organic peroxides (cumene hydroperoxide and tert-butylhydroperoxide) are substrates of horseradish peroxidase as observed from the similarities of their electrochemical behavior relative to that of hydrogen peroxide as observed in the position of their cathodic peaks.

All the sensors exhibited typical Michaelis-Menten kinetics (Figs. 4.6.7, 4.6.8, 4.6.9). The limits of detection were found to be 6.45  $\mu$ M, 6.92  $\mu$ M and 7.01  $\mu$ M for hydrogen peroxide, cumene hydroperoxide and tert-butylhydroperoxide respectively, based on a signal to noise (S/N) level of 3. A linear relationship was obtained in the range 0 to 1.5  $\mu$ M (with  $r = 0.991, 0.988, 0.985$ )

respectively for the three peroxides analyzed (inset in the calibration curves). These results are stipulated in Table 4.1. The apparent Michaelis-Menten constants, (section 3.6, Eq.3.3)  $K'_m$ , was evaluated to be 27.62  $\mu\text{M}$ , 28.11  $\mu\text{M}$  and 27.92  $\mu\text{M}$  respectively, and the maximum current,  $I_{max}$ , was 5.344, 5.422 and 5.511 nA respectively.

These results are modest characteristics compared to other systems based on electrocatalytic biosensing of peroxides. For instance, enzyme electrodes based on conducting polymers display particularly high sensitivities with detection limits in the submicromolar range. Gaspar *et al* [99] have designed an impressive biosensor based on a novel polymer that reached detection limits of 25 nM for  $\text{H}_2\text{O}_2$ . The authors reported  $K_m$  and  $I_{max}$  values of 386  $\mu\text{M}$  and 91  $\mu\text{M}$ , respectively. Other groups have equally reported very sensitive peroxides biosensors based on electrocatalytic surfaces [99]. Although our novel approach is yet to reach these detection limits, it does provide advantages over other techniques in that the manner in which the SAM is prepared is an extremely versatile and simple approach for functionalizing the electrode surface. This technique can be improved upon by attempts to increase the electroactive nature of the Ru(II) molecules, and by optimizing working parameters for enzyme catalysis, such as enzyme loading on the surface of the SAM, pH and adaptation to a flow cell.

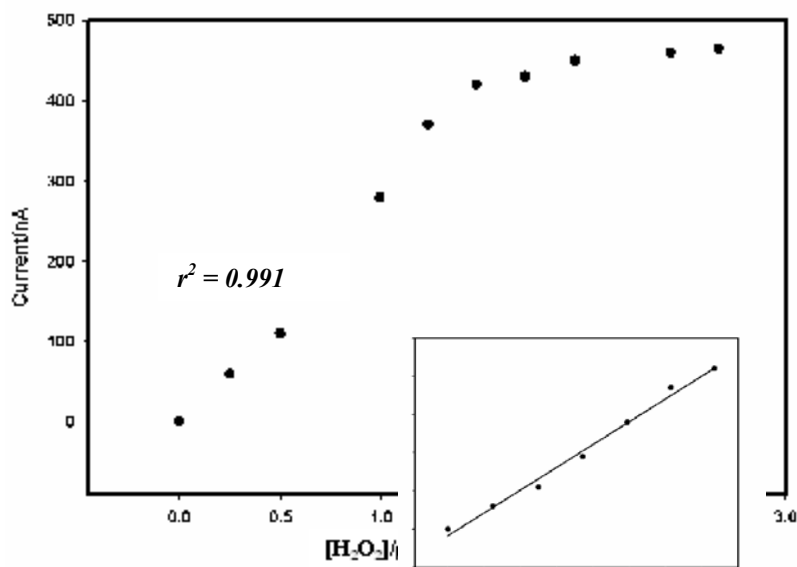


*Fig. 4.6.7: Calibration curve of hydrogen peroxide biosensor illustrating the linear range (inset) of the biosensor with a detection limit of 6.45  $\mu\text{M}$  and  $r^2 = 0.991$*

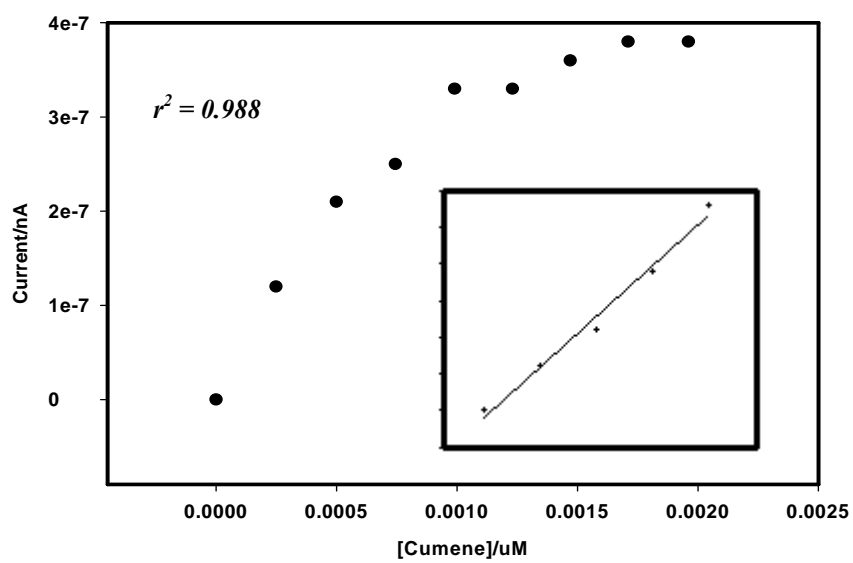


*Fig. 4.6.8: Calibration curve of cumene hydro peroxide biosensor illustrating the linear range (inset) of the biosensor with a detection limit of 6.92  $\mu\text{M}$  and  $r^2 = 0.988$ .*



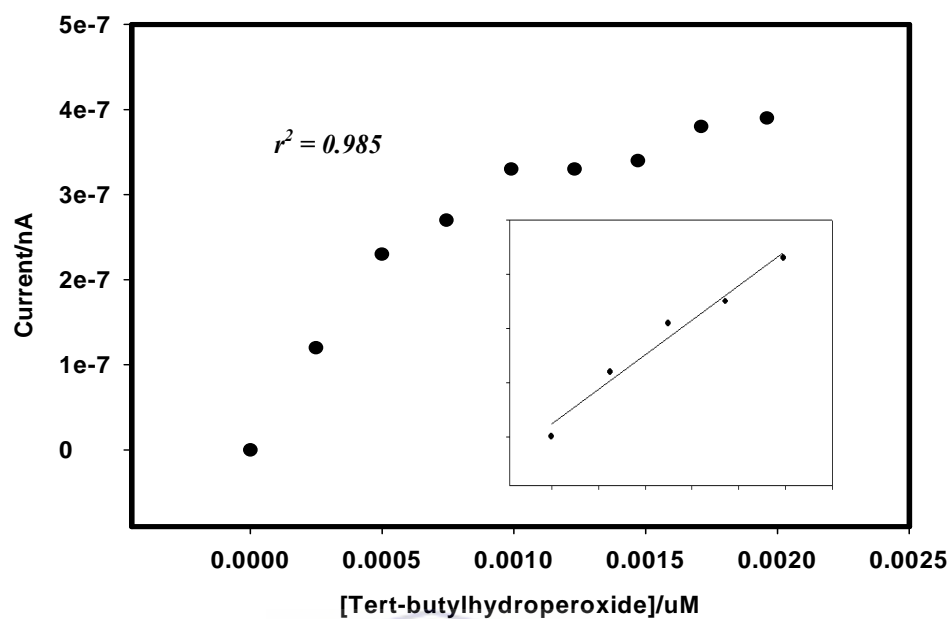


*Fig 4.6.9: Calibration curve of Tert-butyl hydro peroxide biosensor illustrating the Linear range (inset) of the biosensor with a detection limit of 7.01  $\mu$ M and  $r^2 = 0.985$ .*

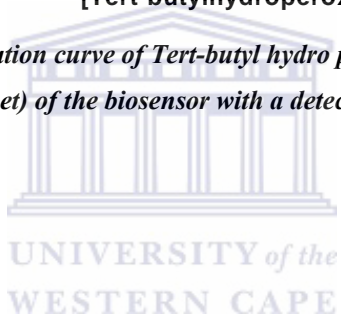


**Table 4.1: Peroxides and their respective biosensor analyses:**

<b>PEROXIDE</b>	<b><math>I_{max}</math> (nA)</b>	<b><math>K'_m</math> (<math>\mu</math>M)</b>	<b><i>DETECTION LIMIT (<math>\mu</math>M)</i></b>
<b>HYDROGEN PEROXIDE</b>	5.344	27.62	6.45
<b>CUMENE HYDROPEROXIDE</b>	5.422	28.11	6.92
<b>TERT-BUTYL HYDROPEROXIDE</b>	5.511	27.92	7.01



#### **4.8 Conclusion:**

The fabrication of a SAM of novel cyclopentadienylruthenium(II) thiolato Schiff base complex, on a gold electrode is reported for the first time to the best of our knowledge. It was found that the SAM required an activation cycle in 0.1 M NaOH before effective electron communication between the monolayer and the gold surface was achieved. It is likely that an initial scan in alkaline conditions removed the protecting methyl end groups of the Ru(II) complex, hence allowing the thiol group to covalently attach to the gold electrode surface in-situ to yield a redox active SAM. The monolayer provided effective blocking of Faradaic processes arising from gold



surface oxidation. The SAM-modified gold electrode yielded quasi-reversible electrochemistry with a formal potential of +100 mV in 0.1 M phosphate buffer, pH 6.9. The quasi-electrochemistry was attributed to the non-uniformity of the SAM monolayer, or molecular interactions between the SAM molecules themselves. The surface concentration,  $\Gamma$ , of the ruthenium redox centers was found to be  $1.591 \times 10^{-11} \text{ mol cm}^{-2}$ . The formal potential varied with pH to give a slope of about  $-34 \text{ mV pH}^{-1}$ , consistent with a two electron, one proton redox process. Further physical characterization of this SAM using methods such as electrochemical impedance spectroscopy (EIS) and transmission electron microscopy (TEM) will further reveal the fine structure of this SAM. Electrocatalytic reduction of  $\text{H}_2\text{O}_2$ , cumene hydro peroxide and tert-butylhydroperoxide at a AU//SAM/HRP-modified electrode was observed using CV and OSWV. It was observed that the electro-produced Ru(II) complex was effectively consumed in the enzyme catalysis with these voltammetric techniques. The kinetics of these sensors revealed  $K'_m$  values of 27.62  $\mu\text{M}$ , 28.11  $\mu\text{M}$ , and 27.92  $\mu\text{M}$  respectively, with corresponding  $I_{max}$  values of 5.344 nA, 5.422 nA and 5.511 nA. The limits of detection were found to be 6.45  $\mu\text{M}$ , 6.92  $\mu\text{M}$  and 7.01  $\mu\text{M}$  respectively. Attempts to increase the electroactivity of the SAM by manipulation of the surface using a mixed monolayer approach, or by alteration of the complex itself, will help improve upon working parameters of the biosensors. Optimization of the enzyme parameters will also improve the characteristics of these novel peroxidase-based biosensors. These preliminary results support the view that cyclopentadienylruthenium(II) thiolato SAMs could prove promising for developing novel electro-catalytic assemblies, especially for use in tailoring a variety of amperometric biosensor devices.



#### **4.9 References:**

1. Chidsey, C.; Bertozzi C.; Putvinski T.; Mujsce A. J. AM. Chem. Soc. **1990**, 251, 4301.
2. Chidsey, C.; Loiancono, D. Langmuir, **1990**, 6, 682.
3. Tillman, N.; Ulman, A.; Schildkruat, J.; Penner, T.L. J. AM Chem. Soc. **1998**, 110, 136
4. Allara, D.L.; Nuzzo, R.G. Langmuir, **1985**, 1, 45.
5. Lee, H.; Kepley, L.J; Hong, H.G.; Akhter, S.; Mallouk, T.E. Phys. Chem. **1998**, 92, 2597.
6. Hickman, J.J.; Zou, C.; Ofer, D.; Harvey, P.D.; Wrighton, M.S.; Laibinis, P.E.; Bain, C.D.; Whitesides, G.M. J. AM. Chem. Soc. **1989**, 111, 7271.

7. Porter, M.D.; Bright, T.B.; Allara, D.L.; Chidsey, C.E.D. *J. Am. Chem. Soc.* **1987**, 109, 9295.
8. Finklea, H.O.; Avery, S.; Lynch, M.; Furtch, T. *Langmuir* **1987**, 6, 409.
9. Xia, Y.; Zhao, X. M.; Whitesides, G. M. *Microelectron. Eng.* **1996**, 2, 255.
10. Gutmann, F.; Johnson, C.; Keeyzer, H.; Molner, j. *Charge-Transfer Complexes in Biological Systems*; Marcel Dekker: New York, **1997**.
11. Halls, J. J. M.; Friend, R. H. *Series on Photoconversion of Solar Energy* **2001**, 377.
12. Newman, D. A.; *Semiconductor Physics and Devices*; 2nd Ed. McGraw-Hill: Boston, **1997**.
13. Ertl, G.; Knoezinger, H.; Weitkamp, J. *Handbook of heterogeneous catalysis*; Wiley-VCH: Weinheim, **1997**.
14. Petrenko, V. F.; Peng, S.; *Can. J. Phys.* **2003**, 81, 387.
15. Salomon, A.; Cahen, D.; Lindsay, S.; Tomfohr, J.; Engelkes, V. B.; Frisbie, C. D. *Adv. Matter.* **2003**, 15, 1881.
16. Bard, A. J.; Abruna, H. D.; Chidsey, C. E.; Faulkner, L. R.; Feldberg, S. W.; Itaya, K.; Majda, M.; Melroy, O.; Murray, R. W.; et al. *J. Phys. Chem.* **1993**, 97, 7147.
17. Chidsey, C. E. D.; Murray, R. W. *Science (Washington, D.C.)*, **1996**, 231, 25.
18. Porter, M. D.; Bright, T. B.; Allara, D. L.; Chidsey, C. E. D. *J. Am. Chem. Soc.* **1997**, 109, 3559.
19. Chidsey, C. E. D.; Bertozzi, C. R.; Putvinski, T. M.; Mujscce, A. M. *J. Am. Chem. Soc.* **1990**, 112, 4301.
20. Tran, E.; Rampi, M.; Whitesides, G. M. *Angew. Chem., Int., Ed. Engl.* **2003**, 43, 3835.
21. Finklea, H. O.; Ravenscroft, M. S.; Snider, D. A. *Langmuir* **1993**, 9, 223.

22. Cannes, C.; Kanoufi, F.; Bard, A. J.; Langmuir **2002**, 18, 8134.
23. Kasmi, A. E.; Wallace, J. M.; Boowden, E. F.; Binet, S. M.; Linderman, R. J.; J. Am. Chem. Soc. **1998**, 120, 125.
24. J. Arnold, prog. Inorg. Chem. **1995**, 43, 353.
25. Cotton F. A.; Wilkinson, G.; Murillo, C. A.; Bochmann, M. Advanced Inorganic Chemistry, 6<sup>th</sup> Ed, John Wiley and Sons, Inc. *New York*, **1999**.
26. Liu, Y.; Qu, X.; Guo, H.; Chen, H.; Liu, B.; Dong, S. Biosens. Bioelectron. **2002**, 21, 2195.
27. Smpath, S.; Lev, O. Anal. Chem. **1996**, 68, 2015.
28. Cosnier, S. Anal. Bioanal. Chem. **2003**, 377, 507.
29. Chaki, N.K.; Vijayamohanan, K. Biosens. Bioelectron. **2002**, 17, 1.
30. Sato, Y.; Fujita, M.; Mizutani, F.; Uosaki, K. J. electroanal. Chem. 1996, 409, 145.
31. Mi-Young H.; Je- Young C.; Yoon H.C.; Kak-Sung K. *Biosens. Bioelectron.* **2002**, 17, 13.
32. Lindgren, A.; Ruzgas, T.; Gorton, L.; Csoregi, E.; Bautista, B.; Sakharov, I. Y.; Gazaryan, I.G. Biosens. Bioelectron. **2000**, 15, 491.
33. Rogers, R.K. Biosens. Bioelectron. **1995**, 10, 533.
34. Cass, A.E.G.; Davis, G.; Francis, G.; Hill, O.; Aston, W.; Plotkin, I.; Scott, L.; Turner, A. Anal. Chem. **1984**, 56, 667.
35. Bourdillion, C.; Demaille, C.; Moiroux, J.; Saveant, J.M. J. Am. Chem. Soc. **1993**, 115, 2.
36. Lever, A.B.P. Inorg. Chem. **1990**, 29, 1271.

37. Ryabov, A.D. ; Firsova, Y.N. ; Goral, V.N. ; Sukharev, V.S. ; Ershov, A.Y. ; Leijbolle, C. ; Bjerrum, M. ; Eliseev, A.V. *Inorg. React. Mech.* **2001**, 1, 8.
38. Ryabova, E. S.; Goral, V.N.; Csoregi, G.; Mattiasson, B.; Ryabov, A. D. *Angew. Chem., Int. Ed. Engl.* **1999**, 38, 80.
39. Ryabova, A. D.; Sukharev, V. S.; Alexandrova, L.; Lagadec, R.L; Pfeffer, M. *Inorg. Chem.* **2001**, 40, 6529.
40. Conn E.E.; Stumff, P.K; Brueninig G. John Wiley and Sons, **1987**, 5th Edition, pg 115.
41. Wubbolts, M.G.; Witholt, B. *Biotech. Handbook*, plenum, New York **1998**, 271.
42. Tisher, W.; Kasche, V. *Tibtech.* **1998**, 16, 35.
43. Roy, J.J.; Abraham, T.E. *Chem. Rev.* **2004**, 104, 3705.
44. Vaidya, B.K.; Karale, A.J.; Suthar, H.K; Tara Sankar, G.I.T.; Ponranthnam, S.; Nene, S. *Reactive & functional polymers* **2007**, 67, 905.
45. G'omez, L.; B'odalo, A.; G'omez, E.; Hidalgo, A.M.; G'omez, M. *Enzyme and Microbial Technology* **2006**, 39, 1019.
46. Araujo Silva, R.; Carmona-Ribeiro, A.M.; Siqueira Petri, D.F. *Journal of Biological Macromolecules* **2007**, 41, 404.
47. Adamson, A. W.; Gast, A. P. *Physical Chemistry of Surfaces*, 6<sup>th</sup> Ed. Wiley Interscience: New York, **1997**.
48. Poirier, G. E.; Pylant, E. D. *Science (Washington, D.C.)* **1996**, 272, 1145.
49. Walczak, M. M.; Chung, C.; Stole, S. M.; Widrig, C. A.; Porter, M. D. *J. Am. Chem. Soc.* **1991**, 113, 2370.
50. Bain, C. D.; Evall, J.; Whitesides, G. M. *J. Am. Chem. Soc.* **1989**, 111, 7155.

51. Troughton, E. B.; Bain, C. D.; Whitesides, G. M.; Nuzzo, R. G.; Allara, D. L.; Porter, M. D. *Langmuir* **1988**, 4, 365.
52. Bain, C. D.; Biebuyck, H. A.; Whitesides, G. M. *Langmuir* **1989**, 5, 723.
53. Ozoemena, K.; Nyokong, T. *Electrochim. Acta* **2003**, 74, 5118
54. Peterlinz, K. A.; Georgiadis, R. *Langmuir* **1996**, 12, 4731.
55. Dannenberger, O.; Wolff, J. J.; Buck, M. *Langmuir* **1998**, 14, 4679.
56. Yamada, R.; Sakai, H.; Uosaki, K. *Chem. Lett.* **1999**, 667.
57. Yan, D.; Saunders, J. A.; Jennings, G. K. *Langmuir* **2003**, 19, 9290.
58. Yamada, R.; Wano, H.; Uosaki, K. *Langmuir* **2000**, 165, 5523.
59. Chidsey, C. E. D. *Science (Washington, D.C.)* **1999**, 251, 919.
60. Terrill, R. H.; Tanzer, T. A.; Bohn, P. W. *Langmuir* **1998**, 14, 845.
61. Love, J. C.; Wolfe, D. B.; Haasch, R.; Chabynyc, M. L.; Paul, K. E.; Whitesides, G. M.; Nuzzo, R. G. *J. Am. Chem. Soc.* **2003**, 125, 2597.
62. Allara, D. L.; Nuzzo, R. G. *Langmuir* **1985**, 1, 52.
63. Bain, C. D.; Whitesides, G. M. *J. Phys. Chem.* **1989**, 93, 1670.
64. Chen, S. W.; Murray, R. W.; Feldberg, S. W. *J. Phys. Chem. B* **1989**, 102, 9898.
65. Brunetti, V.; Blum, B.; Salvarezza, R. C.; Arvia, A. J. *Langmuir* **2003**, 19, 5336.
66. Bomermann, J.; Borrmann, P.; Heiland, W. *Surf. Sci.* **1999**, 441, 107.
67. Nuzzo, R. G.; Zegarski, B. R.; Dubois, L. H. *J. Am. Chem. Soc.* **1987**, 109, 733.
68. Fischer, D.; Curioni, A.; Andreoni, W. *Langmuir* **2003**, 19, 3567.
69. Lavrich, D. J.; Wetterer, S. M.; Bernasek, S. L.; Scoles, G. J. *Phys. Chem. B* **1998**, 102, 3456.
70. Schlenoff, J. B.; Li, M.; Ly, H. J. *J. Am. Chem. Soc.* **1995**, 117, 12528.

72. Nuzzo, R. G.; Zegarski, B. R.; Dubois, L. H. J. Am. Chem. Soc. **1987**, 109,733.
73. Poirier, G. E. Langmuir **1997**, 13, 2019.
74. Oyama, N.; Anson, F. C. J. Electroanal. Chem. Interfacial Electrochem. **1978**, 88, 289
75. Bard, A.J.; Faulkner, L. R. Electrochemical Methods; Wiley: New York, **1980** pp 204.
76. Abou Hamad, I.; Robb, D.T.; Rikvold, P.A. J. Electroanal. Chem. **2007**, 607, 61.
77. Willner, I; Rinklin A. Anal. Chem. **1994**, 66, 525
78. Schelereth, D. D.; Katz, E.; Schimdt, H.L. Electroanalysis **1995**, 62. 113.
79. Scamporrino, E.; Vittalani, D.; Mineo, P. Macromolecules **1999**, 32, 4247
80. Li, Z.; Ning, C.; Zhang, S.; Cao, S.; Zhang, D.; Zhou, Q. Macromolecules **1999**, 32, 7040.
81. Moutloali, R. M. PhD Thesis, University of the western Cape, **2003**.
82. Pinheiro, S.O.; De Souusa, J.R.; Santiago, M. O.; Idalina M.M.; Moreira, I. S. Izuaura C. N.; Diogenes, Inorg. Chem. **2006**,359, 221
83. Bard, A. J.; Faulkner, L. R.; Electrochemical methods: Fundamentals and application, Wiley, New York **1980**.
84. Houlton, A.; Silva, J.; Cunningham, D. J. Chem. Soc. Dalton Trans. **1992**, 2235.
85. Yang, X.; Stern, C.; Marks, J. J. J. Organomet. Chem. **1994**, 116, 10015.
86. Nevondo, F.A.; Crouch, A. M.; Darkwa, J. J. Chem. Soc. Dalton Trans. **2000**, 43.
87. Moutloali, R. M.; Nyokong, T.; Darkwa, J. J. Organomet. Chem. **2001**, 17,629.
88. Paul M.S. Monk Fundamentals of Electroanalytical Chemistry, Manchester Metropolitan University, Manchester, UK.
89. Chaki, N. K.; Vijayamohan, K. Biosens. Bioelectron. **2002**, 17, 1.

90. Pinheiro, S. O.; De Souusa, J. R.; Santiago, M. O.; Idalina M. C.; Moreira, I. S.; Izuaaura C.N.; Diogenes. *Inorg. Chem.* **2006**, 359, 231.
91. Campuzano, R.; Galvez, M.; Pedrero, F.; Manuel de Villena, Pingarron, J.M. *J. Electroanal. Chem.* **2002**, 526, 92.
92. Houlton, A.; Silva, J.; Cunningham, D. *J. Chem. Soc. Dalton Trans.* **1992**, 2235.
93. Tour, J.; Jones, L.; Pearson, D.; Lamba, J.; Burgin, T.; Whitesides, G.; Allara, D. *J. Am. Chem. Soc.* **1995**, 117, 9529.
94. Tour, J.; Rawlett, A.; Kazaki, M.; Yao, Y.; Jagessar, L.; Dirk, S.; Price, D; Reed, M.; Zhou, C.; Chen, J.; Wang, W.; Cambell, I. *J. Eur. Chem.* **2002**, 7, 5118.
95. Porter, M.D.; Bright, T. B.; Allara, D. L.; Chidsey, C.E.D. *J. Am. Chem. Soc.* **1987**, 109, 9295.
96. Morrin, A.; Moutloali, R.M.; Killard, A. J.; Smyth, M. R.; Darkwa, J.; Iwuoha, E. I. *Talanta*, **2004**, 64, 30.
97. Li, J.; Yan, J.; Deng, Q.; Dong, S. *Electrochim. Acta.* **1997**, 42, 92.
98. Ozoemena, K.; Nyokong, T. *Electrochim. Acta.* **2003**, 47, 5118.
99. Gaspar, S.; Popescu, I.; Gazaryan, I.; Bautista, A.; Sakharov, I.; Mattiasson, B.;Csöregi, E. *Electrochim. Acta.* **2000**, 46, 255.





UNIVERSITY *of the*  
WESTERN CAPE